UNIVERSITY OF TECHNOLOGY SYDNEY

Faculty of Engineering and Information Technology

A Comprehensive Study on Energy Management Strategy Design of an Extended-Range Electric Vehicle

A thesis submitted for the degree of

Doctor of Philosophy

Boyi XIAO

June 2022

CERTIFICATE OF ORIGINAL AUTHORSHIP

I, Boyi Xiao declare that this thesis, is submitted in fulfilment of the requirements for the award of a Doctor of Philosophy degree, in the School of Mechanical and Mechatronic Engineering/Faculty of Engineering and Information Technology at the University of Technology Sydney.

This thesis is wholly my own work unless otherwise referenced or acknowledged. In addition, I certify that all information sources and literature used are indicated in the thesis.

This document has not been submitted for qualifications at any other academic institution.

Signature: Production Note:
Signature removed prior to publication.

Date: 05-June-2022

Acknowledgments

I would like to take this opportunity to thank the following people and organizations for their assistance and support during my candidature.

I would express my deep gratitude to my supervisors Professor Nong Zhang, A.Prof. Dongbin Wei, A.Prof. JC Ji and Dr Paul Walker for their tremendously valuable suggestions, thoughtful guidance, and continuous support throughout past years. Their valuable knowledge and research attitude reshaped me and made it possible for me to continue my research career.

I would also like to thank my colleagues and friends: Jiageng Ruan, Weiwei Yang, Shilei Zhou, Tim Patten, Wenwei Mo, Yang Tian, Shengxiong Sun, Hanfei Wu, Enoch Zhao, Anna Lidfors Lindqvist and all other friends at the Faculty of Engineering and Information Technology, for their support and assistance.

Financial support for my study is provided by the University of Technology Sydney (UTS) and the Guangzhou Elite Project (GEP).

Finally, my deepest thanks go to my family. It is their love, understanding and support that accompany me so far.

Boyi Xiao

Sydney, 2022

Publications

International journals

[1] B. Xiao, J. Ruan, W. Yang, P.D. Walker, N. Zhang, A review of pivotal energy management strategies for extended range electric vehicles, Renewable and Sustainable Energy Reviews, vol. 149, 2021, 111194.

[2] B. Xiao, P. D. Walker, S. Zhou, W. Yang, N. Zhang, A Power Consumption and Total Cost of Ownership Analysis of Extended Range System for a Logistics Van, IEEE Transactions on Transportation Electrification. Vol. 8, pp. 72-81, 2022.

[3] B. Xiao, P. D. Walker, W. Yang, N. Zhang, Energy management strategy via maximum entropy reinforcement learning for an extended range logistics vehicle, Energy, 2022, 124105.

[4] S. Zhou, P. D. Walker, B. Xiao, N. Zhang, Modelling and Vibration Analysis of a Parallel Hydraulic Hybrid Vehicle, IEEE Transactions on Vehicular Technology, vol. 69, no. 10, pp. 10710-10723, Oct. 2020.

International conferences

[1] B. Xiao, P. D. Walker, N. Zhang, Performance Analysis of A Electric Vehicles Energy Flow and Regenerative Braking Strategy, Intern. Conf. on Adv. Veh. Powert. (ICAVP), 2019.

[2] B. Xiao, P. D. Walker, N. Zhang, Energy Management and Economic Analysis of an Extended Range Electric Vehicle using Scotch Yoke Boxer Engine, Intern. Conf. on Adv. Veh. Powert. (ICAVP), 2021.

Contents

List of figures

List of tables

Abbreviations

BEV - Battery Electric Vehicle

EREV - Extended Range Electric Vehicle

ERLV - Extended Range Logistics Vehicle

FCV - Fuel Cell Vehicles

HEV - Hybrid Electric Vehicle

PHEV - Plug-in Hybrids Electric Vehicles

APU - Auxiliary Power Unit

ICE - Internal Combustion Engine

ISG - Integrated Starter Generator

Li-Ion - Lithium-Ion

NiMH - Nickel-metal Hydride

SC - Supercapacitor

SOC - State of Charge

SOH - State of Health

NEDC - New European Driving Cycle

CLTC - China Light-duty Vehicle Test Cycle

WLTC - Worldwide Harmonized Light Vehicles Test Cycle

PMP - Pontryagin's Minimum Principle

MPC - Model Predictive Control

MDP - Markov Decision Process

DP - Dynamic Programming

DL - Deep Learning

DRL - Deep Reinforcement Learning

RL - Reinforcement Learning

DQN - Deep Q Network

DDPG - Deep Deterministic Policy Gradient

A3C - Asynchronous Advantage Actor Critic

TD3 - Twin Delayed DDPG

SAC - Soft Actor-Critic

BMS - Battery Management Strategy

EMS - Energy Management Strategy

CD - Charge-depleting

CS - Charge-sustaining

ESS - Energy Storage System

HESS - Hybrid Energy Storage System

HIL - Hardware in the Loop

TCO - Total Cost of Ownership

Abstract

The extensive usage of conventional internal combustion engine vehicles (ICEVs) is responsible for a large amount of greenhouse gas emissions. However, the battery electric vehicle can not substitute for the traditional vehicle due to its limited energy storage ability. To moderate this issue, the extended range electric vehicle (EREV) provides a solution by providing a satisfactory driving range and lower production cost than battery electric vehicle (BEV). An EREV is characterized by having an auxiliary power unit (APU) to provide electric power to the traction motor and the energy storage system, and its battery pack can meet a majority of pure-electric driving needs. To distinguish from the other vehicle structures, the potential of the EREV platform should be further studied/presented on a full scale, and novel control strategies can be designed to improve the power performance of the vehicle. In this thesis, a research on the development process of an extended range logistics vehicle is conducted in the automobile theory and vehicle control points of view. The research priority of the study consists of three parts: the background review and the vehicle structure design, the consumption and cost analysis and the innovation on its control strategy.

First of all, a comprehensive background investigation and literature review are conducted and discussed. The investigation systematically introduces the current developments of EREV in terms of the powertrain structure, energy management and vehicle performance, while the two key focus areas of the auxiliary power are the unit (APU) charging control and hybrid energy storage system (HESS) power management. A case analysis on a typical EREV is presented along with a general

manufacturing cost analysis for different types of vehicles, showing the EREV as one of the cheapest options for long term usage.

Secondly, an extended range mathematical platform for a logistics van is proposed. Suitable configurations for the sizing of the APU, ESS and the traction motor are selected for a standardized mid-size van. This study presents a thorough energy consumption and Total cost of ownership (TCO) analysis for an Extended range logistics van (ERLV). Both EREV and BEV mathematical models are constructed and compared, and their dynamic long-term battery degradation comparison is conducted. Dynamic programming (DP) algorithm is adopted in the energy management strategy optimization, and the global result reveals the optimal energy consumption of the EREV. Comparative results demonstrate that the ERLV has a relatively long drive distance, slower battery aging trend and cheaper TCO (6.6%) when compared to the BELV.

Thirdly, a novel auxiliary power unit (APU) charging strategy with multi-object optimization is proposed on the ERLV platform to achieve high fuel conversion efficiency while maintaining battery charging health. The state-of-the-art algorithm, Soft Actor-Critic (SAC) is applied to perform a better exploration of the possible APU behaviour, and its performance is further verified by the results of the Deep Deterministic Policy Gradient (DDPG) algorithm and DP. Three targets are selected as the RL rewards for optimization: the engine fuel rate, SOC charging trajectory, and the battery charging rate (C-rate). The comparative results show that the SAC had a 36% faster convergence speed than DDPG while providing a smoother and more stable action space. The fuel consumption with SAC also outplays DDPG by around 3%, which achieves almost 90% of the global optimization result. The

successful deployment of the SAC algorithm as an EMS indicates its standout ability in dealing with wide-range actions and states with high randomness, revealing the practical potential compared with the existing RL strategies.

Chapter 1 Introduction

1.1 Background and significance

Transportation remains one of the big carbon emitters internationally, contributing worldwide to the production of greenhouse gases. Carbon dioxide (CO_2) and other by-products like carbon monoxide (CO) are generated during fossil fuel burning [1]. According to the investigation in Figure 2.1, the extensive usage of conventional internal combustion engine vehicles (ICEVs) is responsible for more than 50% of the large amount of CO_2 emissions in 2020. To address and moderate this issue, electric vehicles have grown in popularity as alternatives. Powertrain electrification enables the use of more efficient driveline technologies, such as electric machines, and the capability to improve the fuel economy of more traditional technologies, such as combustion engines, manufacturers are allowed to apply clean and renewable energies in vehicle powertrains with reduced or zero tailpipe emissions [2]. However, limits to energy storage technologies result in BEV not being able to provide a satisfactory driving range to consumers [3]. The popularization of BEV is mainly restricted by battery storage capacity, availability of charging infrastructure, battery charging speed and the EMS design rationality. To provide a comparable range to ICEVs, a BEV will have a significantly larger battery than any form of HEV. To overcome these limitations, HEV was designed as the transition product to BEV with an effective combination of combustion engine and electric motor. HEV can be further divided into three categories based on power-split methods between motor and engine: series, parallel and series-parallel (also referred to as complex hybrids). A series HEV acquires drive torque only from its motor,

and its ICE/generator combination converts fuel to electrical energy which is then captured and stored in the battery. This type of structure has the highest power conversion efficiency but usually requires a larger energy storage system (ESS) in comparison to other HEVs. Parallel HEV is capable of receiving drive torque from both engine and motor, but it needs a power splitting transmission to couple the two power plants. This structure relies less on the motor and ESS and consequently has a smaller ESS than series HEV, although the engine may work in poor efficiency conditions during normal operations. Series-parallel HEV inherits the advantages of both series and parallel. However, its complex structure inevitably raises the manufacturing cost.

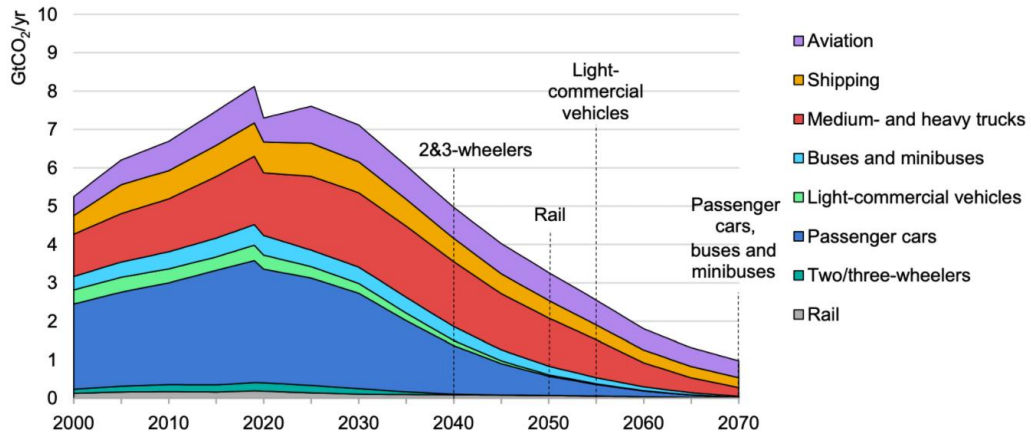

Figure 1.1 Estimation of the emission distribution to 2070 [4].

In order to maintain the driveability of the fuel-based vehicle and embrace the potential of the electric vehicles, the solution for the above matters is to bring the extended range electric vehicle (EREV) into mass production. However, the lack of structural improvement and design experience needs more frontier research to support. Model simulations and hardware tests should be conducted to test the performance of the EREV platform. This thesis includes a complete theoretical study of an EREV with respect to the energy management strategy (EMS) design.

The power flow distribution, powertrain efficiency, component degradation and total cost of ownership (TCO) of the vehicle are carefully studied and compared. Novel control algorithms are presented and installed in the EMS, and the test results can be helpful resources for the future development of the green energy industry.

1.2 Research objectives and innovations

The objectives and main contributions of this thesis are:

1. A classification and literature review for the EREV energy management is done to inspire readers.

2. An extended range system is designed and implemented on a standardized logistics vehicle model to achieve a longer driving distance and downsize the battery pack.

3. A comprehensive case analysis in terms of the EREV TCO is conducted to study the economic benefits and fuel potential.

4. Design of a global optimization method using dynamic programming to search for a balance between the optimal fuel consumption and transient battery SOC variation.

5. Conducting a battery degradation-battery loss simulation for long term usage with the power flow impacts of the APU and motor.

6. The state-of-the-art Reinforcement learning algorithm SAC and the mainstream DDPG algorithm are implemented with the model in MATLAB/Simulink environment to be trained in a variety of conditions.

7. Multi-target optimization for the Reinforcement learning environment is set, with the goal of achieving a balance between optimal fuel consumption, good APU charging speed to the battery and low damage to the battery.

8.The fuel consumption and economic benefit of the RL-based EMS is compared with the DP results to show its outstanding performance. A further case study shows the control improvements against the active-duty logistics vehicle in the market.

1.3 Presentation of this thesis

Chapter 1. The overview of the project, objectives and contributions of the thesis are introduced.

Chapter 2. An in-depth background introduction and powertrain design of the EREV are given in this chapter. The introduction and classification of the EREV energy management design are discussed in detail, and the related literature review is written from the perspectives of APU charging control and HESS power management. A case analysis is conducted on an EREV model, and an overall cost comparison for the common market vehicle types is shared.

Chapter 3. The mathematical model of an extended range logistics van (ERLV) is introduced. The detailed vehicle body model, auxiliary power unit (APU) model, motor model, and battery model are all included.

Chapter 4. An investigation of energy potential and battery degradation for an ERLV is conducted. The dynamic programming using the Bellman equation is deployed for the energy management optimization to find out the optimal fuel consumption of the extended range system whilst the battery charging is limited to a safe level. Secondly, the TCO of the target vehicle is analysed with the battery degradation predicted.

Chapter 5. This chapter shares an idea of achieve fast charging control of the vehicle battery using the APU. The study examines a multi-target energy management strategy using two Reinforcement learning algorithms to interact with the ERLV

model. Battery charging protection is considered as one of the key factor in the optimization. Improvements are made to the latest RL algorithm to further boost the performance of the APU and slow down the ESS degradation.

Chapter 6. A case study is conducted on an ERLV equipped with specially designed engines with a Scotch Yoke mechanism. Two engine prototypes with different capacities are tested with two charging strategies for feasibility analysis to explore the economic benefit.

1.4 Statement of COVID-19 impact on the research

The research projects have been impacted by the COVID-19 pandemic. Some of the co-operational Lab tests were not available.

Chapter 2 Literature review

2.1 Introduction

This chapter systematically describes the background and reviews the structure of EREV using the existing studies and references. The modern control strategies are classified based on their logical pattern, and the knowledge of the APU charging control strategy and HESS power management are discussed in detail. Furthermore, a case analysis of the EMS performance based on a commercially available model is also conducted.

2.2 System Design of Extended Range Electric Vehicle

The simplified topologic construction of an EREV can be illustrated using Figure 2.1. Thanks to the on-board chargeable battery pack, the EREV can meet a majority of pure-electric driving needs. It is also supported by a secondary onboard auxiliary power unit (APU) to recharge the battery. The wheels of an EREV are completely driven by its electric motor. The APU usually consists of a fuel combustion engine with paired generator (also known as an integrated starter generator, ISG), but recent studies pointed out that it can also be a fuel cell system that uses hydrogen (H2) to generate electricity [5-8]. In comparison with the series plug-in hybrid electric vehicle (PHEV), EREV has higher degree of electrification with mature APU-ESS sizing and well-balanced control strategy design [9]. For instance, some new types of APU are also studied. Bou Nader et al. designed a gas turbine system based on energy theory [10]. Unlike some other types of hybrid vehicles in [11-13], the drive torque of EREV is directly provided by traction motor(s), and its engine only works for fuel-to-electricity conversion in effective operating conditions. The

engine output shift is connected with the ISG, and the energy flow is converted from chemical energy to mechanical torque and finally turns into electricity. Compared with other types of hybrid vehicles, EREV can support a certain distance of all-electric driving, and its onboard APU will supply power if the battery state of charge (SOC) drops to a certain threshold or the vehicle is in high power demand. Series Plug-in hybrid electric vehicle (PHEV) can be considered a kind of EREV at a certain level [14, 15]. However, functionality such as engine configuration, charging logic of the ESS, powertrain design and relative battery size may vary [16-23]. Variants of different vehicle powertrains are tabulated in Table 2.1.

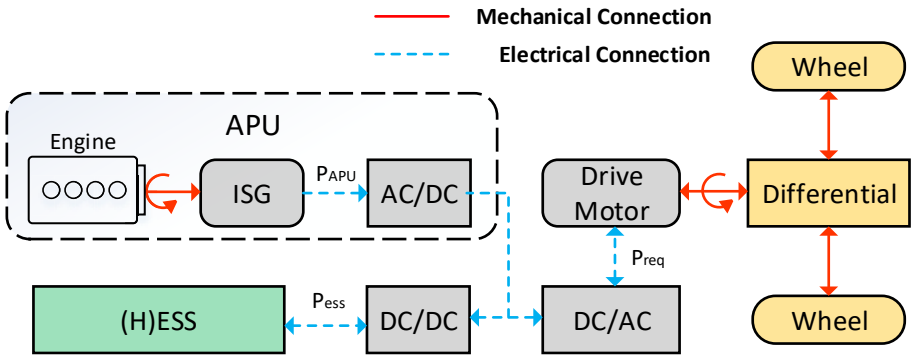

Figure 2.1 Powerflow overview of an engine-based EREV [24].

Table 2.1 Alternative vehicle configurations and comparison.

Model	Range	Engine Efficiency	Performance	Powertrain complexity	Electric Motor(s)	Transmission	Battery size
ICEV	++	+	++	+	0	1	-
BEV	+	-	++	+	1	0	+++
Parallel	++	++	+	++	1	1	+
Series	++	++	+	+	2	0	++
Series-Parallel	++	++	+	+++	2	1	+
PHEV	++	++	+	++	2	1	++
EREV	++	+++	++	+	2	0	++

In recent years, EREV has been regarded as one of the key platforms in the electric vehicle industry [25, 26]. Car manufacturers have pushed the EREV into applications, and products like Chevrolet Volt, BMW i3 REx, and Nissan e-Power

have received wide attention [27, 28]. The range extended van Ford Transit hybrid gives a solid solution to the logistics city driving, and it has a downsized engine with better fuel economy than its ICEV version [29]. A wide variety of research has been carried out with the aim of raising vehicle energy efficiency and performance through a combination of configuration studies, energy management and optimal control. Research found that the size and capacity selection for EREV energy storage system greatly influences energy management strategy [30]. Engine selection can affect how much energy the battery will conserve, and different driving patterns may also have an impact on the selection of the battery capacity. The energy management development for the EREV should be able to efficiently manage the transient power distribution and balance the capacity and performance for each component. On that account, designing an energy management strategy is critical and challenging; a programmer should balance the trade-offs between dynamics performance, fuel consumption, conversion efficiency and thermal aspect [31-33].

Some of the latest studies on EREV energy management and APU charging control optimization [34-38] have made great contributions to the field. Although these up-to-date methodologies may have acceptable efficiencies and innovative logic, there are still plenty of potential and unknown problems to be dug into through the application of these emerging technologies. To illustrate this, some researchers noticed that it was difficult to balance the energy distribution using rule-based solutions when the control system is facing different driving patterns; and there may be observable errors and unpredictable flaws, such as high computational load or use of unfitted data, when optimization-based solutions are applied to energy

management strategies [21, 39-41]. There are few references that can clearly solve or improve on these problems.

2.3 Basic operation pattern of EREV

As shown in Figure 2.2, an EREV works in two modes: Charge-depleting (CD) and Charge-sustaining (CS). Different from other HEVs, EREV can work like a BEV in CD mode. In this mode, the vehicle operation power comes from its (H)ESS, namely the combination of battery and supercapacitor (SC) packs. The ICE is turned off in this mode. Usually, CD mode will be selected when the (H)ESS maintains a high SOC or the vehicle only operates with a low power requirement. Conversely, as the SOC drops down to a certain threshold or power demand increases, the engine will usually start up to compensate for the lacking power. In this case, the electric energy from APU can power the ESS and traction motor through power converters. Moreover, studies show that the power management of HESS has a considerable influence on the APU charging control and power flow distribution [42-45]. To introduce the APU control strategy and HESS power management, the concepts of APU and HESS are presented in the following sections.

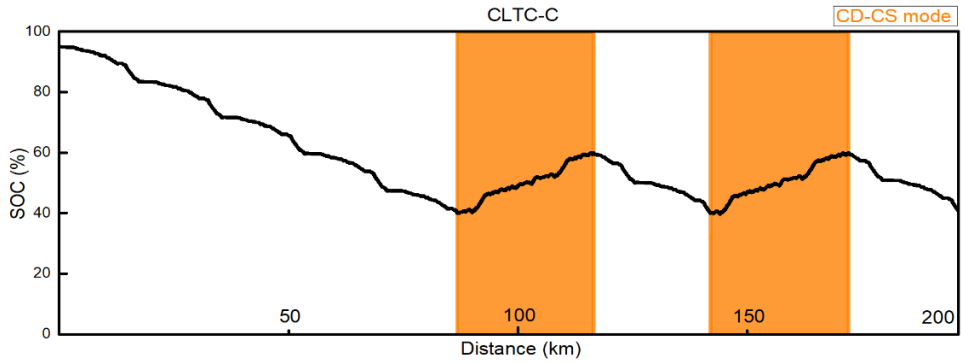

Figure 2.2 A CD-CS mode switching sample of an EREV.

2.3.1 Auxiliary power unit

The selection of an APU for EREV is determined by the vehicle design objective [46, 47]. Choosing a compatible type of engine and the ISG is rather important because an inappropriate component may increase the cost, reduce the efficiency of the system and even cause unsolvable failures.

Selecting the engine for an EREV is different from selecting for a conventional vehicle. Engine for a traditional vehicle usually requires wide-range dynamic performance and larger displacement, but it has a high fuel consumption to ensure sufficient power across the whole speed range [25]. However, the engine selection for APU is a different story. The number of engine pistons and displacement can be reduced with the degree of vehicle electrification [46]. Because the range extender is designated to provide pure electric power, smaller engines with fewer cylinders can be specially designed for EREV [48, 49]. A smaller displacement engine uses fewer materials and electric parts, which means it has a lower manufacturing and design cost than the engines for traditional vehicles [25]. In addition, as the engine does not have to run in a wide speed range, the engine for EREV can be set to operate in a high-efficiency area, and the noise and vibration can be further reduced. For instance, SYTECH ltd has designed a series of downsizing boxer engines based on the Scotch yoke mechanism for APU use [50]. The prototype is shown in Figure 2.3, while the engine is optimized to work in fixed operation points for low fuel consumption. In addition, the noise and vibration problems caused by clutch and transmission can be greatly suppressed, and the traditional transmission is no longer a compulsory part of the EREV powertrain [51, 52].

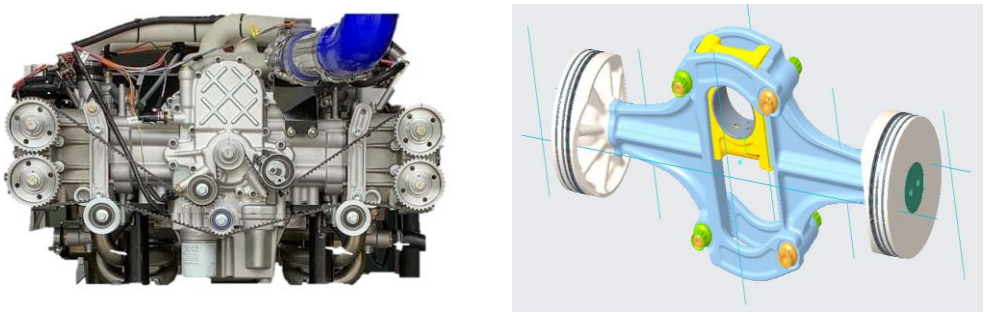

Figure 2.3 Downsize engine equipped with a Scotch yoke (a) Engine outer shell; (b) Scotch yoke mechanism.

The engine type for APU is no longer limited to the Otto cycle. The outdated 2-Stroke engine and rotary engine are now brought back to life because of their favourable operating features. In [48], a single-cylinder two-stroke gasoline engine is specially designed for electric power generation. Meanwhile, Mazda announced its new EREV project, which may adopt a redesigned rotary engine as the range extender [53]. The boxer engine can also be considered a perfect candidate for its rotary stability and reliability.

2.4 Hybrid energy storage system constitution

As a multi-energy-source vehicle, EREV requires a flexible energy storage system to handle and utilize the fluctuant electric power. The lifespan of an ESS depends on battery throughput and its working temperature, and its condition can deteriorate in cold temperature operation [54]. To mitigate the battery stress, SC can be installed to cope with the severe environment and extensive current loading. Thanks to the high power density and the charge efficiency of the SC, the APU output may have a lower negative impact on the battery state of health (SOH).

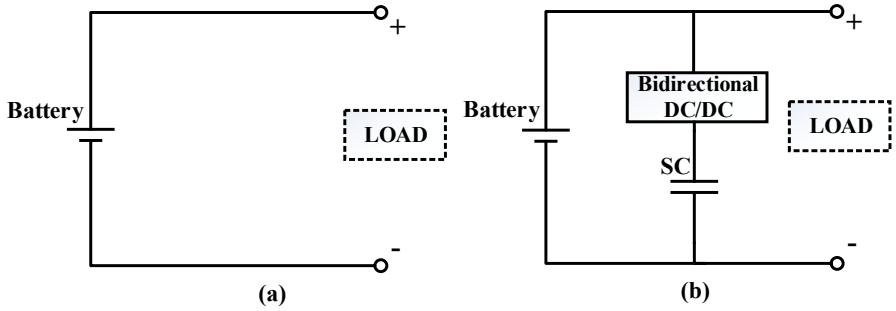

Figure 2.4 Samples of an ESS and a HESS: (a) ESS, (b) HESS [24].

Two basic configurations are available for electric energy storage, and their samples are shown in Figure 2.4. First, the baseline ESS is a battery only storage system as the most straightforward configuration. HESS has been developed to compensate for high peak discharge and improve battery lifespan. These combine SC and battery using buck/boost converters to maintain voltage stability between the battery and SC [39]. The characteristic of battery and SC are introduced as follows.

2.4.1 Battery

EREV uses a rechargeable battery pack as its electric energy storage. Its battery cell should have a high energy density (Wh/kg). Besides, the recharge life and charge efficiency should be taken into consideration as well. There are two major kinds of suitable batteries for modern electric vehicles: nickel-metal hydride (NiMH) and Lithium-Ion (Li-Ion) batteries. NiMH battery has a long lifespan of up to 2500 recharge times of 80% depth of charge [55], and it is now very affordable in the market. However, with the demand for vehicle mileage, most automotive companies adopt Li-Ion batteries in spite of the higher price cost. Li-Ion battery has the highest energy density and the best efficiency among all types of batteries [56], but rigid charging control is essential. There are two basic methods to charge a Li-Ion battery: constant voltage charging and constant current charging. When the

SOC reaches a certain threshold, the charging method should change from constant current to constant voltage to avoid overcharge and damage to the battery. In addition, the battery pack is constructed with a large number of individual battery cells, which makes it difficult to measure, calculate and balance the SOC of the whole set. The battery SOC can be calculated using this simplified formula [14]:

$$\dot{SOC} = \frac{U_{oc} - \sqrt{U_{oc}^2 - 4R_r P_{batt}}}{2Q_{bat}R_{tml}} \tag{2.1}$$

where Q_{bat} is the nominal battery capacity, R_r is the battery internal resistance, P_{batt} is the battery terminal power and U_{oc} stands for the open-circuit voltage [14]. The Li-ion battery SOC estimation technics can help to prevent the battery from overcharging and over-discharging.

2.4.2 Supercapacitor (SC)

When installing a large capacity battery pack on EVs, the cost and weight will increase significantly. However, if the battery pack size is reduced, the battery recharge rate will be increased noticeably and exacerbate the battery decrement. In addition, the lifespan of the battery will decrease quickly during high current loading. To overcome these drawbacks, SC can be the secondary power storage unit and installed in combination with the battery. The SC, as shown in Figure 2.5, has a much higher power density and a significantly longer lifespan than a Li-ion battery [44, 57]. The first application of SC in automotive powertrain was on a Mazda model in the late 1990s, and it was used to store recovered regenerative braking power for acceleration [58]. The charge of an SC is stored on its electrodes and there are no redox chemical reactions, which allows it to have a higher power density than battery [59]. In addition, it has lower internal resistance that guarantees

a higher efficiency than the battery as well. These special characteristics make SC the perfect choice for fast charging and fast discharging [60]. Regenerative braking sometimes provides a heavy current to ESS that may damage the battery [61]; installing an SC can avoid this battery damage [60]. The energy calculation equation of an SC can be described as:

$$E = \frac{1}{2} C(V_2^2 - V_1^2) \tag{2.2}$$

where E is the total usable electric energy, C is the capacity, V_2 is the charged terminal voltage, and V_1 represents the cut-off voltage. We can observe that the total electric energy of an SC is directly related to its terminal voltage.

Figure 2.5 Appearance of an SC pack [62].

Pieces of literature have presented different methods to estimate the supercapacitor SOC. For instance, Song et al. [63] regarded the SOC of the SC as a linear relation with the SC open circuit voltage V_{sc}, and they estimated the SOC by Eq. (3):

$$SOC_{SC} = \frac{V_{SC}}{V_2} \tag{2.3}$$

The operational range of the SOC is assumed in the range [0.5 - 1] because 75% of the usable SC energy *E* is discharged when the SOC drops to 0.5 [63]. On the

other hand, Li et al. [64] used the current integral equation approach to real-time estimate the SC SOC:

$$SOC_{SC}(t_1) = SOC_{SC}(t_0) - \frac{1}{E}\int_{t_0}^{t_1} I_{sc}(t)\,dt \tag{2.4}$$

where I_{sc} is the real-time current from the SC. This method has a higher requirement for the current sensor in field tests as the current varies rapidly [39].

2.5 Energy management classification

Specific control strategies should be customized to utilize the energy better and expand the ESS lifespan [65]. Therefore, EMS is employed to extend battery lifespan, raise fuel conversion efficiency and balance energy distribution [17]. The concept of EMS can be traced back to the 19 century, and it was defined as 'a plant design interrelated with power conversion components and the unique characteristics of ESS' [66]. Companies such as Bosch, Denso and BYD have applied their EMSs to their electric models [60, 67-69]. Energy management for EREV consists of three main aspects: APU charging control strategy, dynamic power management of ESS and safety detection. In this section, the APU charging control strategy and HESS power management will be mainly introduced and discussed.

Modern energy management control strategies can be systematically classified into two categories: rule-based strategy and optimization-based strategy. Their relationships are arranged in the following dendrogram.

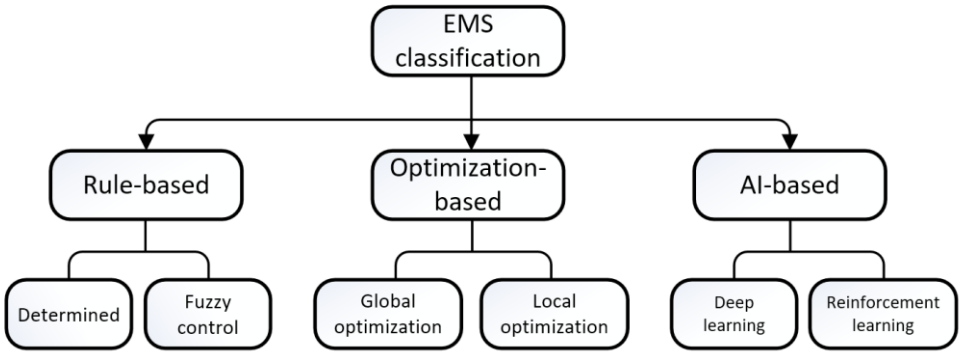

Figure 2.6 Classification of energy management strategies.

Table 2.2 Classification of energy management control strategies.

Rule-based Strategy	Optimization Strategy	AI Strategy	Literature
Close loop control	Dynamic programming	DQN	[70], [41, 71-73]
Fuzzy logic	Genetic algorithm	DDPG	[74, 75], [76-78],
Forward chaining	Model predictive control	A3C	[37], [79-81]
Look-up table	Pontryagin's minimum principle	TD3	[82], [14, 83, 84]
		SAC	[85]

Some samples for EMS are displayed in Table 2.2. Most rule-based energy management methods have an efficiency superiority when applied to a real-time electric vehicle powertrain [31]. This kind of rule is developed on the basis of intuition, human expertise, experimental results and mathematical models [86]. Generally, several datasets are collected and sent to the rule-based controller, and the controller will give out a preset output to the controlled objects [87]. This preset output can be a levelling or a weight value to minimise the control error between the desired and actual values. On/off strategy, geometric control, closed-loop control and fuzzy logic control can be considered rule-based methods [88].

Optimization is a process of mathematical evaluation to search for the best fitting solution for one or more specified objects [89]. These solutions can make the best of object performance in the exploration phase when selecting advisable variables [90]. When looking at the introduced EMS methods above, we can observe those defects which still need improvements. An optimization strategy is performed using

a specific mathematical calculation or dynamic function to minimize loss and unwanted fluctuation [69, 91-94]. These are generally computationally intensive and are performed offline with known data. In recent years, some optimization methods can be operated in real-time or through online computing, depending on their model complexity [91, 95]. For instance, scholars adopted Pontryagin's minimum principle for energy management optimization because it has a short computation time [96-98]. Methods like dynamic programming (DP) and genetic algorithm (GA) have higher potential and performance for EMS optimization and model predictive control (MPC), but they are rather complex and may need further research for implementation [5, 99]. These advanced training technologies can surely raise the efficiency of energy management and let the strategy itself adapt to the operating environment; however, some systematic study directions should be set by discipline leaders from a development perspective. In addition, some optimization methods cannot be deployed as a real-time method because they may rely on previous data, but these methods can be used as valid benchmarks to evaluate the control performance of other EMS strategies.

The AI-based EMS has attracted great attention in the past three years. The deep learning (neural network, NN) [78, 100], reinforcement learning [101-103] methods are the two main classifications of the AI-based EMS. Deep learning utilizes NN to train eigenvalue from the data, and the nodes in NN layers are arranged and given weights to the connections between them. In contrast, the RL agent works as an independent controller to interfere with the environment, and it makes decisions based on trial and adjusts itself through reward feedback. The AI EMS is known for requiring a pre-training process for the algorithm to understand the controlled

target and environment. After training, the AI EMS can be implied in real-time with a low computational load, and it is capable of handling complex control signals and data inputs. Scholars also discovered the potential of combining DL with RL to produce Deep Reinforcement learning (DRL) [104]. DRL inherits the merits from DL and RL, for instance, it holds the ability to maximize reward goals in episodes; and handle wide action space and states with the help of NN. The leap performance of the DRL was proved by defeating human experts in numerous Atari games, and is currently in commercial use for the e-sports game DOTA2 [105]. It is now testing against real-world environments that may have numerous possible actions and state inputs. In the automobile industry, DRL has unlimited potential in vehicle EMS design by feeding it with unlimited data. Thanks to the emerging vehicle-to-everything (V2X) technique, the training data for the DRL EMS can be gathered from anywhere, while the online cloud server easily handles the computational load for the RL pre-training. Since 2013, DRL algorithms such as DQN, DDPG, PPO, TD3 and SAC have been developed to improve the training quality and performance of the agent. Some early DRL algorithms utilize the Q-value to update the agent policy, which can cause instability during some training; for the model-free algorithm, the sampling efficiency is also worrying. Improvements are made to amend these issues. For instance, the experience replay solution is applied to increase the sampling efficiency, as it utilizes the previous data from the training by repeatedly selecting a random mini-batch for the policy improvement; the adding of the target networks helps supervise and stabilize the agent during training; the soft update for the target networks uses partially update with factor φ to prevent the

agent from sudden performance drop. External noise and maximum entropy techniques are also used to improve the exploration of the agent.

In the following section, two types of strategy orientations are introduced in detail. It is also worth mentioning that the energy management strategies for different components in the powertrain may restrict and influence each other. APU charging control strategy and HESS power management are crucial to EREV, and they work as the upper and lower layer of the EREV energy management [71].

2.6 APU Charging control strategy

According to the simulation and experimental results [49, 106-109], the highest efficiency of the ICE and Proton Exchange Membrane (PEM) fuel cell are around 41% and 66%, respectively. The efficiency of an engine-based APU varies with the engine speed and the output torque [110], while the efficiency of a fuel cell unit is mainly affected by its working temperature and fuel purity [111]. Considering the incomplete fuel-cell technology and the shortage of hydrogen production, adopting an engine as the range extender is currently more desirable for most EREVs. More importantly, different charging strategies should be applied on the basis of the above APU behaviours. APU charging control strategy can be classified into two types: the power demand following strategy and the optimal range strategy.

2.6.1 Power following strategy

The power following strategy usually operates based on the vehicle power demand, and it amends the APU electric output to supply most of the vehicle power requirements. During vehicle operation, the APU will supply most of the electric power to the drive motor, which means we do not need a large HESS for backup power. The simplified diagram of the power following strategy is shown in Figure

2.7. The Fuel cell (FC) extended range electric vehicles commonly adopt this type of strategy because of the flexible fuel cell discharge characteristic [112-115]. However, when it comes to combustion engine based APU, it requires an engine with a wide high-efficiency operation range [34, 116]. Moreover, due to the faster transient response of a drive motor than that of an engine, HESS should compensate for the transient power lack between APU output and actual power demand [34, 117]. The SC in HESS can suit perfectly for supporting transient power error in most cases.

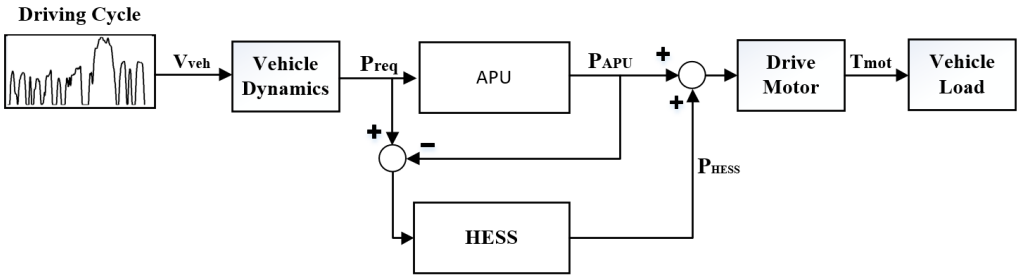

Figure 2.7 Logic diagram of a power following strategy example [24].

Before setting up the power following strategy, the power supply capacity of APU and HESS should be measured and optimized to ensure the designed system meets the actual power requirements of the vehicle [82]. Moreover, the essential requirement for this strategy is to achieve a faster control convergent speed, or the execution delay of the control strategy will cause considerable power compensation from the HESS.

Scholars have designed control strategies to follow power demand based on particular testing platforms. A fuel cell hybrid vehicle installed with HESS has applied fuzzy logic control to amend APU output power based on HESS SOC and driving need [118]. Accordingly, Barelli et al. applied a 12-hour real-world driving cycle for a fuel cell bus HESS sizing in order to have a more stabilized power

requirement estimation; the result proved that a compact fuel cell APU could provide most of the power for driving whilst the battery SOC maintains a high level [115]. Meanwhile, Simoes et al. also chose FLC for their Power following APU charging strategy [74]. Conversely, they decided to focus on selecting the best operating power range (approximately 65 - 180kW) of the fuel cell, in which the FC efficiency can be higher than 43% [74]. Nevertheless, when adopting a combustion engine and ISG as the APU, the fuel consumption may change significantly due to the variable engine operations. Zhang et al. designed a slot-PM-assisted generator that can be applied with a combustion engine under varying duties; the simulation results showed that the power density of this generator could double when compared to those of DC-excited structure [119]. Wang et al. described a new concept of EREV called Through-The-Road (TTR), and they adopted an online drive cycle/power predictions for the energy management design [120]. In this platform, the APU followed the total power demand and its output torque was kept within a high-fuel-efficiency boundary [120]. For the improvement of the traditional power following strategy, Yan et al. have introduced a fuel cell hybrid electric tram using a modified power following APU charging strategy [72]. The strategy is an online strategy that works on the basis of minimizing energy consumption and guarding the end-state SOC. Hardware in the loop (HIL) test showed that the hydrogen consumption is 8.99% lower than that using the traditional power following method [72]. In addition, Li. et al. applied different strategies using DP and pseudo-spectral optimal control to decide the power distributions of APU and battery during the CS stage [34]. Energy efficiency

improvement was also conducted in [6, 121], from which an engine ideal economy curve was selected for the APU to provide the required power to the powertrain.

2.6.2 Optimal range strategy

The optimal range strategy has the ability to maintain high APU fuel efficiency. Every engine has its optimal operating range where energy conversion efficiency is comparably high. Therefore, this strategy sets the engine to operate in some fixed optimized points or an operating range at all times. For instance, the APU in [122] operates in three operation points with high energy efficiency. Once the APU is turned on, the redundant power will be used to charge the ESS. An example logic diagram of this strategy is described in Figure 2.8.

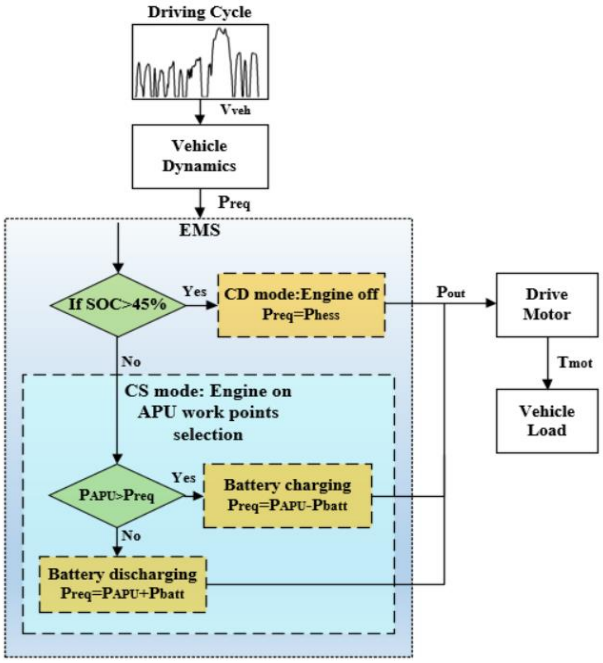

Figure 2.8 Basic logic diagram of an optimal range strategy [24].

Before choosing the appropriate engine operation range, a series of calculations should be carried out to determine the transient power requirement and the battery condition. The optimal range strategy is a nonlinear charging strategy and has a limited engine operation range. Compared with the power following approach,

there are more external data for optimal range strategy to utilize, such as motor power demand, battery SOC, current driver driving pattern, charging efficiency, etc. [6, 12, 123]. These data can give an overview to EMS and help the strategy to make decisions.

There are numerous methods of setting and choosing APU operation points, and scholars use experimental data and optimization algorithms to deduce their unique parameters [32, 124-126]. A fuzzy logic charging strategy is proposed in [67] after setting up a full Simulink vehicle model, and a HIL simulation is carried out to verify its potential. In [127], Lee has conducted a charging efficiency comparison among different generator operating points by using real-world driving cycle data, proving a charging strategy can effectively make good use of the energy by adopting better APU operation points. Chen et al. designed a power charging strategy that mainly focused on extending battery life and avoiding fuel energy losses [121]. The strategy adopted dynamic programming (DP) to extract driving pattern data. Another similar strategy focused on minimizing the fuel consumption of an extended range electric bus [128]. In [89], trajectory optimization was deployed to find optimal APU operation curves, and the engine emission was also considered for evaluation.

In recent years, scholars have introduced machine learning and mathematical optimization methods in designing optimal range strategies. These methods are better at discretising diverse data and handling complex systems in comparison with the rule-based methods. For instance, machine learning methods can adapt the system to an uncertain operating environment. In [129], a genetic algorithm was utilized for training test data from a diesel engine, and it aimed to raise engine

efficiency by optimizing injection timing. Zhao et al. investigated the efficiency of a 3-cylinder Atkinson engine and introduced an artificial neural network to the APU charging strategy [78]. The results showed that the optimized operation points of the engine could reach a high efficiency of 40.2% [78]. In reference [83], a neural network controller was designed to train data from two inputs: the battery SOC and distance to gas stations. Stefano et al. [77] applied stochastic model predictive control to identify the driver behaviour, and the engine-battery power ratio changes according to the driving style and traffic condition. Moreover, another optimal range strategy is proposed using DP and PSOC algorithms [34], and in this case, the actual power demand is selected as its analysed object.

2.6.3 Comparison of the two strategies

Generally speaking, the two APU charging strategies have their own pros and cons, which are categorized in Table 2.3. The power following strategy and optimal range strategy have their own unique pros and cons. The power following strategy allows EREV to have a smaller size ESS because its battery is mainly used for compensating the power error between APU output and vehicle required power. On the contrary, the optimal range strategy allows EREV to install a more compact engine, and the APU can be determined to turn off/on based on the ESS condition. In general, the selection of the two APU charging strategies can be made depending on the vehicle platform and travel requirements. The current research status of these strategies may assist in developing new methods in APU charging control area and constructing real-time HIL experiments.

Table 2.3 Introduction of the two APU charging classifications.

Category	Power following method	Optimal range method
Characteristics	The output power of the APU will go after the required power from the vehicle. APU will stay operating in most cases. [34]	The APU works in a certain fixed stage or an optimized dynamic range to maintain a higher energy conversion efficiency. APU may not always start if the SOC is high enough. [6, 12, 123]
Requirement	ESS should compensate the power deviation caused by engine delay. [34]	Detailed strategy should be designed to consider vehicle operation and ESS sizing[17].
Advantage	Relying less on battery, less charging loss of battery. The size of ESS can also be reduced.	Favourable fuel utilization; smaller engines can be selected. The engine can operate in low vibration conditions [65].
Disadvantage	Low energy conversion during some high-duty operations.	A higher requirement for thermal management due to frequent battery charging.

2.7 Dynamic power management for HESS

A well-designed HESS will significantly raise the energy utilizing ability of multi-power-source vehicles like EREV. For most electric vehicles, the cycle life of the Li-ion battery and its output ability determine its driving practicability. The battery usually works as the main power supplier for the EREV powertrain, but a sudden peak discharging or charging may do great harm to the battery lifespan [130, 131]. The battery's peak current range to the motor of a 2003 Honda insight was approximately 50A to 70A [44, 132], and with the fast development of electric motor technology, Li-ion battery may not be able to follow up the motor's high transient power requirement nowadays [133]. Installing SC as the secondary power storage component can help to settle this issue, and it also allows us to install a drive motor whose peak power requirement is higher than the actual battery output capability. The advantages of battery and SC can be well utilized while avoiding the disadvantages in virtue of a well-designed power management. Simulations show an 8.7% further energy consumption can be reduced in some driving cycles

by applying SC to ESS [134]. In Figure 2.9, some widely adopted topology structures of HESS are shown where the battery pack and SC are connected in parallel to the power converter [63, 67, 130, 135, 136]. However, in [42], the battery and SC can be connected in series to minimize cost and space.

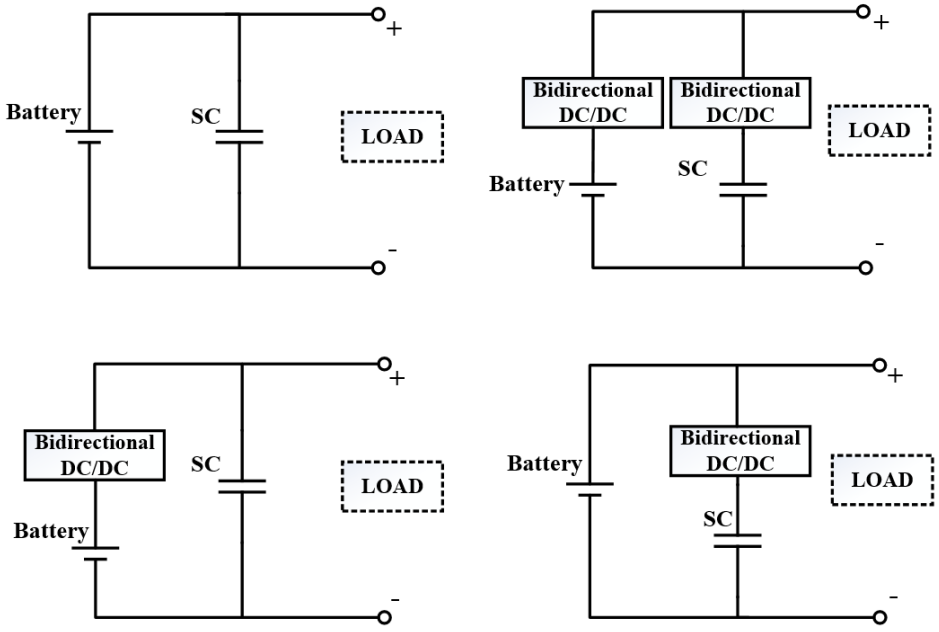

Figure 2.9 Wide-adopted topology structures of HESS.

The location to employ the bidirectional DC/DC converter significantly impacts the operating characteristics of HESS. For instance, as with the last two topologies shown in Figure 2.9, a DC/DC is connected in series with the battery/SC. The general advantage of these topologies is to minimize the component cost and mass. When the DC/DC is in series with the SC, we are allowed to make good use of the SC in a wide voltage range and vice versa (for DC/DC in series with the battery). Furthermore, two DC/DCs can be installed in series with each of the two components for higher power performance; however, this may also result in cost rising and make the system more complex.

In most cases, when the vehicle is driving at its peak performance, the engine or fuel cell will start and output power in conjunction with HESS. The available drive power of an EREV can be described as:

$$P_{veh} = P_{APU} + P_{bat} + P_{sc} \tag{2.5}$$

where P_{veh} is the total consumed power of the vehicle, P_{APU} is the output power from APU, P_{bat} and P_{sc} are the charging or discharging power of battery and SC, respectively.

It can be observed from the equation that the power output of these three components is highly complementary, which means their sizing selections have to be dynamic and should consider their performance, power density and invested cost (including component price and average fuel consumption). Furthermore, the power output of the APU should also depend on the general power requirements of the vehicle, especially when the APU is adopting the power following strategy. Studies have been put forward by taking all factors above into consideration [63, 67, 133, 137]. For instance, Raga et al. presented a comparative analysis of several HESS architectures on a fuel cell hybrid vehicle [137]. According to their analysis data, using SC is highly recommended when the vehicle is in great power need [137]. Additionally, the impact of heavy current output from a battery can be sharply mitigated with the help of SC and APU employment [67].

However, introducing secondary energy storage to EREV may also lead to many application difficulties. For instance, the sizing of Li-ion battery, SC and even APU should be optimized and the APU charging strategy will have to be redesigned [43]. Furthermore, the degree of hybridization between APU and HESS has to be re-examined in order to achieve greater balance. The fundamental system-level

requirements of HESS should be figured out before breaking down to a component level. A synthesis of mainstream HESS architectures and their power management is conducted in [137]. It was summarized in this article that there are three system-level goals for designing a HESS power management: a) avoid excessive charging/discharging of battery to extend its lifespan; b) to make good use of the SC fast charging/ discharging ability; c) to better sizing of the HESS to reduce weight and cost. Hence, we can categorize the dynamic power management design as solving a multi-objective optimization problem.

To confront this optimization problem, a general understanding of the HESS operating condition is essential. Calculations and experimental exercises should be performed afterwards, and an elementary framework for HESS can be constructed based on the vehicle powertrain requirements. The optimization contents, such as HESS sizing and charging control, are discussed in the following subsections.

2.7.1 Sizing design

The aim of the HESS sizing design is to raise the overall energy economy whilst minimizing the HESS cost and mass [43] [138]. Previous researches saw driving range demand, APU capability and chassis parameters as the main factors for HESS sizing, but the sizing design should also consider the influence of actual vehicle energy consumption [139]. Generally speaking, HESS sizing for EREVs must satisfy the energy requirement for an adequate pure-electric driving range [140]. In addition, it should also focus on extending the battery lifetime, which means the design has to take full advantage of an SC [67, 141]. However, the adoption of SC is delicate due to its high cost and low energy density. Its capacity should be sufficient to at least absorb the amount of energy from one complete regenerative

braking [61]. To illustrate, our multi-objective component sizing procedure is introduced. Some variables such as average weight, cost, space and maximum power output were first picked as future optimization objects. After that, we defined a price limitation range, and a feasible Pareto optimization is applied on it to select the best member from the candidate pool [130]. The selected members are applied to a prototype platform and compared with two other methods, while a parameter called Hybridized Cost Ratio (HCR) is presented to describe the cost ratio of HESS parts that helps find potential options [130]. A simplified flowchart of possible HESS design options screening is shown in Figure 2.10.

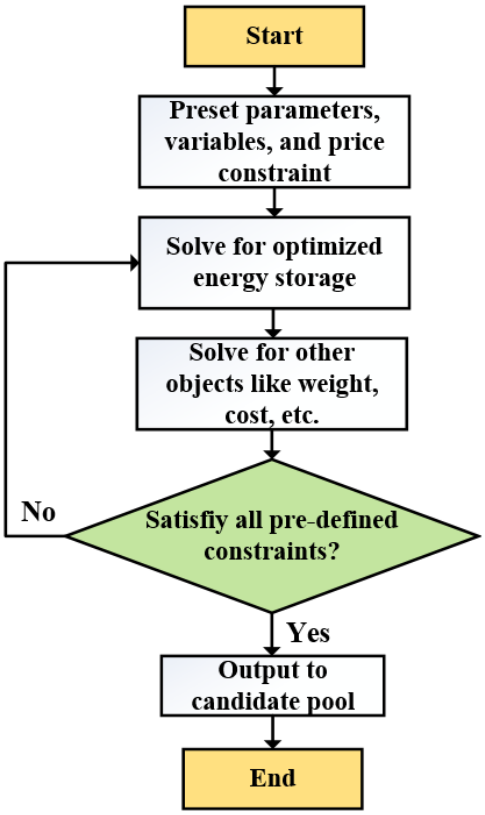

Figure 2.10 Flowchart of Possible HESS design options identification [24].

Other studies have chosen some different optimizing objects. For instance, Boundaries of power and mass for the proposed structures are defined considering the APU power output, and its SC is used to absorb the remaining power from APU

when the battery pack cannot withstand the high current [137]. Another concept called 'degree of hybridization' (DOH) was put forward in [133] which can be described as:

$$DOH = \frac{P_{req} - P_{APU}}{P_{req}} \tag{2.6}$$

where P_{req} stands for the total power demand from vehicle P_{APU} is the output power from APU. In this study, DOH was used as the main optimal object to decide the charging/discharging limitation of HESS, and it also signified the cost when putting up the EREV platform [133]. Subsequently, parameters of different components were calculated based on DOH, and a fitting check was conducted to see if these sizing parameters could satisfy the overall requirements of weight, power and cost [133]. A similar sizing solution based on weight reduction is proposed in [138] using the Ragone methodology. Sadounl et al. considered the charging rate of batteries as the main condition when using a pre-set battery capacity [142]. In [143], a dynamic calculation was proposed to estimate the battery SOC and employed a metaheuristic algorithm to determine how large the battery pack should be. However, instead of considering the combined influences of vehicle battery health management and heavy charging, the only optimal target of this paper was to minimize the total cost of the battery cell [143]. The strategy was then improved in [144] that both the battery health and total cost of the HESS were considered as the optimization goals using dynamic programming. Additionally, that reference [145] proved the SC average power output in driving simulation has a great influence on determining SC capacity. Tongzhen et al. compared three different sizing topologies on regenerative braking for hybrid vehicle powertrains, and they had discussed some other suitable application fields for these sizing topologies [146].

2.7.2 Power distribution control of HESS

For HESS, it is hard to define the power distribution to the battery and SC because of their diverse electric characteristics. Recent studies have demonstrated that SC can provide high instantaneous peak power which is several times greater than the Li-ion battery [58, 147, 148]. Greater energy efficiency for HESS can be achieved by lowering the battery current under a certain value [148]. Furthermore, considering the different charging characteristics of the Li-ion battery and SC, new energy management methods should be deployed. According to the three system-level goals for designing a HESS power management (mentioned in Section 4.2), utilizing the fast charging/discharging ability of SC to avoid battery from excessive usage is the key.

To achieve this goal, scholars are trying to provide solutions using advanced rule-based charging strategies. In the early stage, the discharging power simply came from the battery set while SC compensates [149, 150]. In most studies, the current and voltage of the battery set were monitored and restrained to reduce the impact on battery degradation [132, 148, 151], but some of the studies did not build up a battery degradation model to study the impact of battery SOH. Yang et al. [152] pointed out that battery SOH should be considered as the evaluation indicator for the HESS power management arrangement. SOH is the indicator for the remaining charge acceptance of the battery, and the cumulation of the battery loss Q_{loss} will result in the decline of SOH. An empirical formula-based Arrhenius degradation model based on Ah throughput calculation can be used to calculate the Q_{loss} with the following equation [153]:

$$Q_{loss} = A \cdot e^{-(\frac{E_{act} - B \cdot C_{rate}}{R \cdot T_{Bat}})} (A_h)^Z \qquad (2.7)$$

where Q_{loss} is the capacity loss of the battery, A is the pre-exponential factor, C_{rate} is the battery discharge rate, R is the Molar gas constant (8.314J/mol/K^{-1}) and T_{Bat} is the battery absolute temperature. Ah is the Ah-throughput and Z is the time factor. E_{act} and B represent the activation energy and correction factor of the discharge rate, respectively.

An experiment data for $LiFePO_4$ battery cell were shared in [144, 153]. The authors used the least square fit method to calibrate the parameters, where A is 0.0032 and Z is 0.824:

$$Q_{loss}(t) \approx 0.0032 \cdot e^{-(\frac{15162-1516 \cdot C_{rate}}{R \cdot T_{Bat}})} (A_h)^{0.824} \quad (2.8)$$

The battery SOH can be achieved by the cumulative formula:

$$SOH(t) = 1 - \sum_{t=0}^{t} Q_{loss}(t), \in [0,1] \quad (2.9)$$

The estimated SOH plays a critical role in extending the HESS lifespan. The optimal power management strategy should adopt battery degradation status as one of the input states or constraints for long term accuracy. For instance, Hu et al. [81] designed an MDP control considering the degradation of the FC and battery, where the SOH is used as one of the main constraints for calculating the minimum operation cost.

On the other hand, the battery SOC also has an influence on HESS power management, for example, on deciding the charging logic of the battery and SC [42]. Lukic et al. [154] suggested that the SC should be charged first until it reaches full capacity, because the SC can guarantee high discharge efficiency and large currents for future driving loads. Other studies supported that the battery and SC should be charged simultaneously to avoid providing high current directly to the

battery [155, 156], while the SOC of SC should be maintained at an appropriate level so that there is sufficient capacity to absorb/release instant power [157, 158]. These early utilizations of HESS power management were mostly rule-based that could not fully adapt to the rapid power variation of HESS [159]. The cooperation of APU and HESS was overlooked as well, which made it hard to decide how the APU should work for the best outcome [158]. More importantly, a comprehensive and great range of human expertise is needed when adopting control expert systems like fuzzy logic [67]. He et al. [67] constructed a fuzzy-based power management with a power adjustment module considering velocity as the main input. The authors pointed out that the voltage of the SC should be comparative low during high vehicle velocity, so as to make room for absorbing regenerative braking power. In [160], an all-sided ruled-based strategy is constructed for a multi-mode HESS platform. The strategy paid close attention to the voltage of the SC and battery so that a decent charge efficiency was achieved. However, the authors had to design and adjust nine complicated operation modes to make this happen.

To improve the develop efficiency and feasibility, the first optimization method was introduced to the automotive field in the early 2000s using neural networks [45]. This method was used to acquire a higher energy efficiency of the EMS for further drive range. Later on, a weighted method and a no-preference method were applied to optimize the power distribution of HESS and balance its efficiency [76]. The simulation and bench test proved the real-time control ability and wide applicability of these two methods [76]. Nguyen et al. proposed a new real-time EMS based on Pontryagin's minimum principle (PMP) method, and has compared it with strategies like filtering, λ-control and DP [97]. HIL experiments had also

been conducted and proven the PMP method has a higher ability to minimize the battery aging problem than traditional rule-based methods [97]. In [42], a power split control was installed on an HEV, and the power distribution to battery and SC was decided by a specific ratio. This ratio was calculated using meta-heuristics method and it aimed to extend the lifespan of the battery. It appears that these optimization methods are continuing to gain interest with academia and they are slowly becoming the mainstream strategy for HESS. However, according to [161], the control performance from [42] may get worse when the input predictive data change significantly, and the system efficiency will remain low during the adjustment delay. Therefore, Song et al. [159] improved the traditional MDP method with the consideration of simultaneous current injection to improve the identification accuracy of the HESS state signals. In addition, Choi et al. [161] developed a real-time optimization method considering transient load dynamics and SC voltage variation. Their method is designed to minimize both battery power magnitude and power loss. At the same time, the MDP algorithms mentioned above need on-board HIL verification and vehicle road experiment to test their ability to converge with real-world road uncertainty.

2.7.3 Existed problems and future trends

Some noticeable problems should be pointed out and solved from the studies above. For instance, the coordination control of APU and RBS is rarely brought up. When APU and RBS are both operating, this abrupt power from them should be handled and absorbed by the HESS. However, the combined current will be excessive, which may threaten the lifespan of the HESS. A proper strategy toward this problem should be discussed in the future. Secondly, tests on HESS thermal effects should

be included for HESS power management. Studies show the operating temperature of SC will also affect the efficiency as a large amount of heat can be generated under heavy cycles [162, 163]. The battery operating temperature will also affect the battery efficiency, and more seriously, the battery health [148]. As a result, a battery degradation model is required to study their correlation, and the SOH of a battery-only model needs to be compared with the battery-SC model during long term usage [164, 165].

For future study, because a functional HESS power management needs multiple input signals to operate, machine learning methods can be utilized for continuous improvement. For instance, reinforcement algorithms like DPG, DDPG and PPO have gained wide attention [166, 167], and the continuously signals from HESS can guarantee the data acquisition for training.

2.8 A case analysis of a specific EREV

A case analysis is conducted in this section to extend the overview depth of the EREV structure. Chevrolet Volt is selected in this case as it is one of the most representative EREVs that first came out to the market for over a decade. Its concept prototype, see Figure 2.11, was first unveiled in 2007.

Figure 2.11 The concept model of the Chevrolet Volt [168].

The first-generation Chevrolet Volt was installed with a 16-kWh battery pack, an APU with a 63kW engine and a 55kW ISG that guaranteed a maximum travel distance of 620 km [169-171]. The second generation has a slightly larger battery pack, a new coupling planetary gear and a more compact power coupling system, which extends the travel distance to 680 km [171]. The traction motor can produce 111 kW of power and it can operate in a pure-electric mode [172].

2.8.1 Validation and on-road testing

Governments and agencies have put forward various kinds of on-road testing for the Chevrolet Volt to identify the potential and applicability of this EREV model. The testing subjects are the travel range and energy consumption. The maximum pure electric drive range of the Chevrolet Volt is close to 55 km [169], which concerns how the energy management strategy will bring the APU to use for longer travel distance. In 2013, Idaho National Laboratory had conducted a thorough driving and charging investigation for 923 test targets that travelled a total distance of 7.6 million km [170]. The average travel distance of the studied group is driven 65.5 km per day and charged 1.46 times per day. Accordingly, if we assume the Chevrolet Volt leaves the carport with a fully charged battery, it has the potential to drive 73% of the average distance in EV mode.

When the battery soc of the Chevrolet Volt drops below 0.17, the APU is turned on for extend-range mode [110]. For the default APU charging strategy, the Chevrolet Volt will acquire its power mainly from the APU, and the remaining energy will be used to charge the battery to a higher level [173]. For the second generation of the Chevrolet Volt, a new extended-range mode is available thanks to the new planetary system. The planetary connects the engine and the ISG to increase the powertrain

power output. Model validation in [110] showed that the engine would only be cut off fuel when the vehicle speed exceeds 65 km, and the purpose was to avoid high energy-consuming for restarting the engine and raise it to a higher speed. The result also showed the engine only operated from 25 to 35 kW during the experiment.

Operating temperature is a crucial aspect that affects the energy efficiency of the EREV [174, 175]. Some recent studies conducted road tests at low temperatures to study the impact on the Chevrolet Volt. In [174], the Chevrolet Volt was tested in Idaho state for the cold climate effect, and the engineers found out the APU was forced to operate in any circumstance when the ambient temperature was lower than -2.8 ºC, regarding the battery SOC condition. They also found out that the vehicle climate control system was turned on to raise the cabin temperature, which caused the fuel consumption to drop to 47 mpg (5L/100km) when the average temperature was -26.1ºC. The study from Environment Canada [175] mentioned that the consumed energy used to heat the cabin in winter is significantly higher than colling down the cabin in summer. According to the CD on-road results, heating the cabin consumed 4.3 kW at 1.6 ºC, and it only consumed 1.4 kW at 36 ºC in another driving cycle. In addition, the pure-electric distance was studied with both the APU and the cabin conditioning turned off. The energy-distance data in seasons is shared in Figure 2.12 [175]. Results showed that the minimum distance at -5 ºC is 41 km, which was radically shorter than the maximum distance of 103 km at 27 ºC.

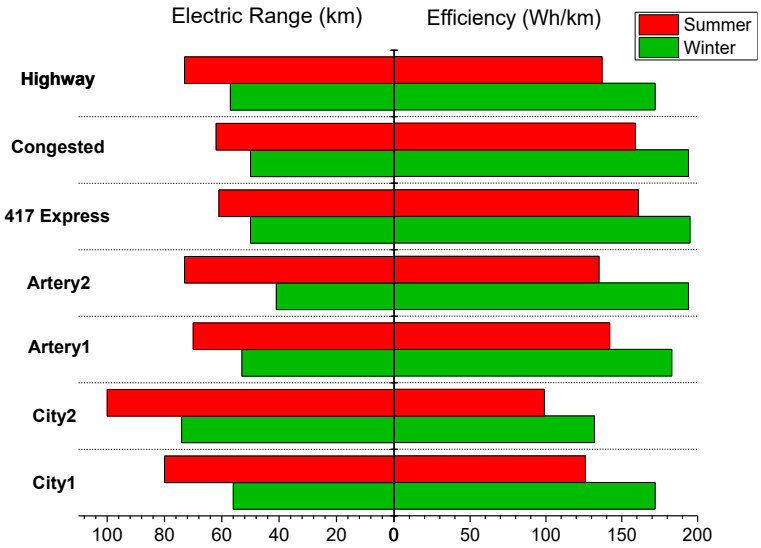

Figure 2.12 Average travel distance and Wh/km in different seasons.

2.8.2 Energy management studies applied on Chevrolet Volt

Gonder et al. [173] from the national renewable energy laboratory of the United States and General Motors designed a model to predict the fuel/electricity consumption rate of the Chevrolet Volt using the real-world driving profile. Micro trip characteristic data such as average speed, acceleration were calculated and used to estimate the energy use. The authors also carried out a green routing analysis to search for the most energy-efficient route from a large number of available route options. A fuel-optimal APU charging strategy for the Chevrolet Volt was tested against the default charging strategy. Its result has shown that 25% of the fuel consumption was reduced over 35 km [173]. In Ref. [176], a HIL test was conducted with the Chevrolet Volt model to verify the robustness of the controller. The result demonstrated the effectiveness of both the controller and the mathematical model. Liu et al [170] applied a reinforcement learning algorithm to the Chevrolet Volt model. The proposed Heuristic Planning method utilized the Dyna-H algorithm to search for the optimal fuel saving under the vehicle powertrain

framework. The result showed an overall advantage compared with Q learning and Dyna, and indicated a potential to apply in real-time simulation.

2.9 Economic, Fuel Cost and performance trade-off

2.9.1 Parts prices comparison

To better understand performance/economic trade-off, a general price comparison of EREV components is included while satisfying the optimization goals. Basic parameters, characteristics and energy consumption of Li-ion battery, SC and fuel cell power unit are summarized and compared in Table 2.4.

Li-ion battery is now the most suited energy storage for electric vehicles because of its energy and power sufficiency [177]. As shown in Figure 2.13, the market price of Li-ion battery was $1500/kWh in 2007, over $1000/kWh in 2010 and went down quickly to $176/kWh by 2018 [178, 179]. Pouch cell battery pack is widely employed for commercial use by car companies from the United States, Europe, China and Japan. In addition, 18650 and 21700 are the two iconic types of cylindrical battery cells used by Tesla, Inc, and they are usually installed into battery packs in series and in parallel. The market price of a single 18650 battery cell is between 5-8 US dollars.

Table 2.4 General price and performance comparison of energy sources.

Energy Component	Power density (W/kg)	Specific Energy (Wh/kg)	Lifespan (cycles)	Efficiency (%)	Market Price (US $/kW)	Market Price (US $/kWh)	Literatures
Li-ion	1000-3000	180-300	2000	85-95	100-150	176	[54, 143, 179]
SC	10,000-14,000	4.1-6.0	1M	>95	33.5-44.6	6000	[57, 60, 140, 180]
PEMFC	1000-1600	-	2500-5000hrs	45-66	40-53	-	[64, 108, 109, 181, 182]

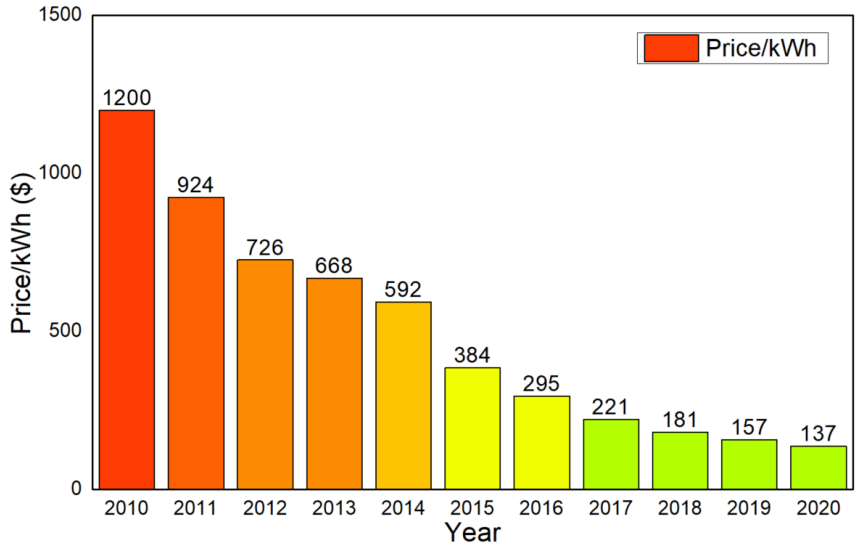

Figure 2.13 The average market price growth of Li-ion battery cells [179].

The SC characteristic is different from that of a battery. It has an extreme power density of 10-14 kW/kg [140, 180], but its low energy storage ability and its comparatively high price make it infeasible as the sole source of energy storage. However, because of the fleeting raw material market value, the past cost analyses for various HESS constructions are slowly outdated [135, 137, 178, 183]. As shown in Table 2.5, the lowest per-kilowatt price in 2018 is $33.5/kW, which is much cheaper than its price in the early twenty-first century. Therefore, although it is still expensive compared to the Li-ion batteries, it is now more affordable to combine a small size SC with the battery pack to protect battery SOH [57, 184].

Table 2.5 TCO comparison of market competitors (US $).

Vehicle Type	Retail Price	Maintenance cost	Fuel cost	TCO	Literature
ICEV(Audi A4)	36,000	12,287.6	13,719.9	62007.5	[186, 187, 189, 195]
BEV (Tesla Model 3)	46,000	4,038.9	5,523.8	55,562.7	[130] [76, 190]
EREV (BMW i3)	48,300	3,936.3	9,387.9	61,624.2	[191, 192]
FCEV(Toyota Mirai)	58,365	6,988.9	32,793.1	98,147	[5, 109, 193, 194]

2.9.2 Comparison of vehicle total cost of ownership

In order to evaluate the general vehicle expense, a concept called total cost of ownership (TCO) is presented in [196]. TCO includes the retail vehicle price and

operating cost. Conventional vehicle, BEV, EREV and fuel cell models are selected for TCO comparison. Four specific vehicle models are chosen from the U.S. market, and they are presupposed with a total travel distance of 250,000 km [197, 198]. Their investment, maintenance, and fuel (electricity) costs are listed in Table. 3.4. Gasoline, diesel and hydrogen are considered the primary fuels for EREV. According to the market, the average U.S. retail price of gasoline in 2019 is approximately 2.76 USD per gallon (around 0.966 USD/kg) [187, 188], whilst the price of hydrogen is 13.99 dollars per kg [199]. In addition, the lifespan of a fuel cell (2500-5000hrs) is much shorter than that of an engine [64, 181], showing its structure and technical design need to be improved for more extended commercial use.

From Table. 3.4, we can observe that Tesla Model 3 has the lowest TCO thanks to its low maintenance cost and pure electric consumption. It is also worth mentioning that the TCO of the BMW i3 is lower than the Audi A4, although its retail price is 34% higher on the contrary. In addition, the TCO for Toyota Mirai is significantly above average because of the high hydrogen price. The Hydrogen price is expected to go down in the near future, while Toyota in the United States offers complimentary hydrogen for three years. The EREV fuel cost can be even lower if the car itself is frequently used for short-distance drives and is charged properly during night time. In conclusion, EREV is the compromise option between ICEV and BEV, and it is perfectly suitable for all ranges of driving. The comparatively low maintenance cost and higher drive range give it a high potential to compete for a bigger market share.

2.10 Chapter summary

This chapter has provided a brief introduction of EREV structure, and summarized various APU charging strategies. Furthermore, the power management for HESS is also introduced as a relatively new area of study which can work in perfect unison with the APU charging control strategy. After that, a case analysis of the Chevrolet Volt is proposed to study its on-road performance and energy management development. Last, a characteristics and costs analysis of energy components and a comparison of vehicle general TCO costs are provided to evoke readers.

Chapter 3 Vehicle modelling design

3.1 Introduction

To test the feasibility and potential of the extended range structure, a detailed mid-size logistics van (ERLV) model is constructed in this chapter. The detailed mathematical model covers all powertrain components and strategy design in MATLAB/Simulink. The vehicle simulation analysis and strategy tests in the following chapters are conducted using this RELV model. The energy loss of the powertrain and battery aging prediction are also considered to achieve higher energy conversion accuracy. The requirements for the vehicle model are summarized as follows:

a. High energy conversion efficiency between the main components.

b. Sufficient constant-torque value and range from the traction motor for urban cycles with a favourable dynamic response.

c. Cargo/Curb weight higher than 0.5.

d. Pure electric drive ability over 30 km with maximum load.

e. Practicable on its emission improvement.

f. Ability to perform regenerative braking.

g. Compact sizing of the components.

h. Cost-effective.

3.2 Vehicle parameter

The powertrain of an extended range electric van mainly consists of an APU, an energy storage system (ESS), a drive motor and converters. The engine rotational speed of an EREV is no longer coupled with the vehicle velocity, because in most

cases, it only connects to an integrated starter generator (ISG) instead of the wheels. This advantage will have positive impacts on fuel economy and emission improvement [89]. The simplified ERLV topology is shown in Figure 3.1 [33].

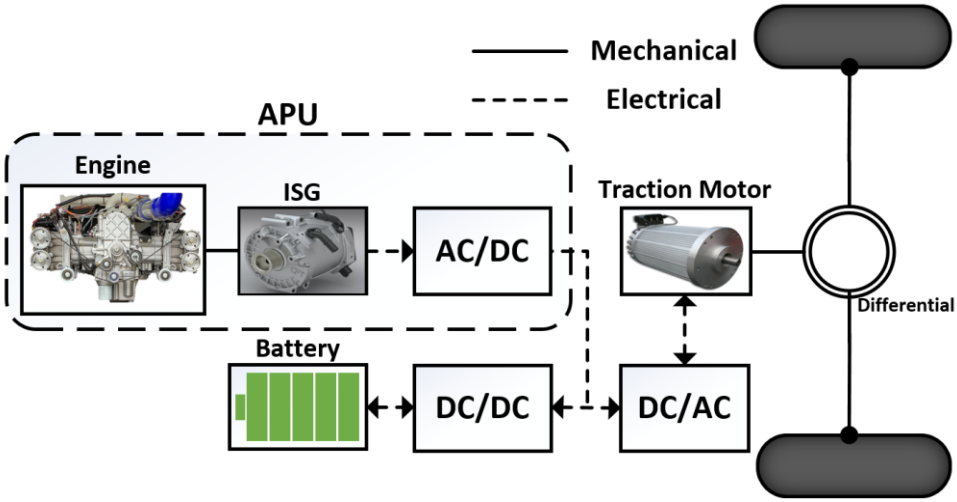

Figure 3.1 ERLV architecture.

Table 3.1 Parameters of the extended range logistics van.

Symbol	Van parameters (Unit)	Value
m_k	Vehicle mass (kg)	1800
m_c	Gross weight (kg)	3000
R	Tire radius (m)	0.31
C_d	Aerodynamic drag coefficient	0. 45
C_r	Rolling resistance coefficient	0.02
A	Vehicle frontal area (m^2)	3.32
P_{peak_Mot}	Peak power of drive motor (kW)	125
P_{eng}	Peak engine power (kW)	72
C_{bat}	Battery pack capacity (kWh)	30
V_{bat}	Battery pack terminal voltage (V)	433
C_{ft}	Fuel tank capacity (L)	40

There are two fundamental operation modes for the ERLV model: charge depleting (CD) and charge sustaining (CS). In CD mode, the ERLV will operate as a pure EV. The ESS will provide all the necessary power most of the time when the APU is turned off. However, in some aggressive driving situations, the APU may turn on to provide extra power to the motor. In addition, as the battery SOC keeps declining

to a certain level in CD mode, the APU will become operational. In this stage (CS), the APU keeps providing power to the wheel and charging the ESS, until the battery SOC climb up to a preset value.

3.3 Driving cycle

In consideration of the study object (logistics van), two driving cycles are employed in this study: CLTC-C and WLTC (class 3b). CLTC-C is an up-to-date China driving cycle for light-duty commercial vehicles. The characteristics of the electric vehicle are considered during its construction stage, which makes its speed and acceleration data more suitable and reliable than other comprehensive driving cycles. On the other hand, the WLTC is known as a worldwide driving cycle that aims to replace the NEDC, and its practicability covers all types of electric vehicles. The logistics van in this study is classified as a class 3b vehicle. In Figure 3.2 (a) and (b), both cycles are plotted with their speed data. The top speed of CLTC is 92 km/h and 40.8% of the speed data are in the low-medium speed range, while the top speed of WLTC is 97.4 km/h in its high phase.

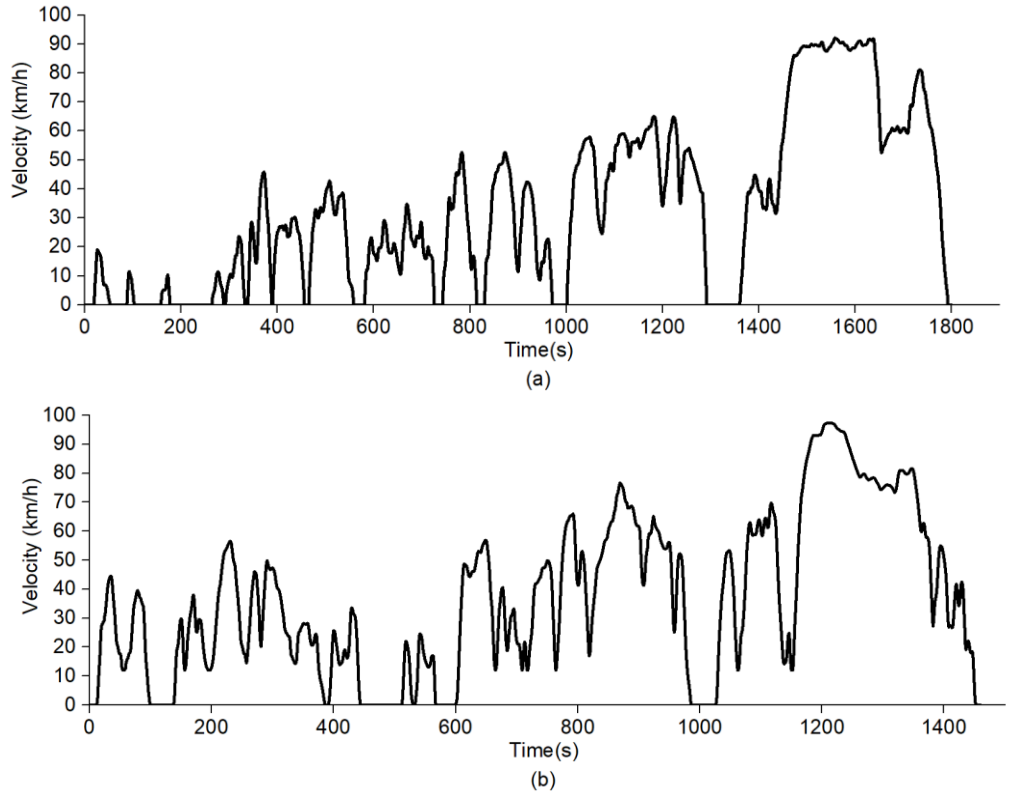

Figure 3.2 Speed profiles of (a) CLTC-C and (b) WLTC (class 3b)

The patterns of some representative driving cycles are listed and compared in Table 3.2 with the total distance, average speed, maximum speed and peak acceleration calculated. The acceleration pattern of NEDC is illogical, while its high-speed phase is not suitable for most logistics vans. Judging by the speed patterns from the table, WLTC is more aggressive than CLTC hence it has a higher performance requirement for vehicle testing.

Table 3.2 Patterns of the representative driving cycles

Driving cycle	Distance (km)	Avr. Speed (km/h)	Max. Speed (km/h)	Peak Acc (m/s^2)
CLTC-C	16.43	32.87	92	1.36
NEDC	11.01	33.6	120	1.04
FTP75	17.77	34.1	91	1.47
WLTC (3b)	15.01	37	97.4	1.75

3.4 Vehicle dynamics

The primary resistances of a running vehicle are air resistance, grade resistance and rolling resistance of the wheel. Therefore, the mathematical model of vehicle powertrain dynamics can be expressed by:

$$T_v = \left(F_w - F_{aero} - F_g - F_{rl}\right)R \tag{3.1}$$

where T_v represents the drive torque for the vehicle to accelerate, R respresents the wheel radius; $F_w, F_{aero}, F_g, F_{rl}$ are on-wheel traction force, aerodynamic drag resistance, gradient resistance and wheel rolling resistance, respectively.

The equations to calculate the vehicle resistances are:

$$F_{aero} = \frac{1}{2}\rho C_d A v^2 \tag{3.2}$$

$$F_g = m_c \, \mathrm{g} \sin\theta \tag{3.3}$$

$$F_{rl} = m_c g C_r \cos\theta \tag{3.4}$$

where m_c is the vehicle combined mass, and ρ, C_d, A, g, θ, C_r are air density, aerodynamic drag coefficient, vehicle frontal area, gravitational acceleration, incline angle and rolling resistance coefficient, respectively.

3.5 Auxiliary power unit

In the ERLV structure, the engine operation can be further optimized as it is decoupled from the wheel. In Figure 3.3, a 1.5 L turbocharged diesel engine (75 kW) is employed, and its lowest fuel rate is lower than 212g/kWh. The control strategy uses the DP algorithm to search for the best steps to maintain a high conversion efficiency based on this engine fuel consumption characteristic map. The power relation between the APU and the engine can be described as:

$$P_{APU} = P_{eng} * \eta_{ISG}(n_{ISG}, T_{ISG}) \tag{3.5}$$

where η_{ISG} is the ISG efficiency and n_{ISG}, T_{ISG} represent the transient rotational speed and the load torque of the ISG.

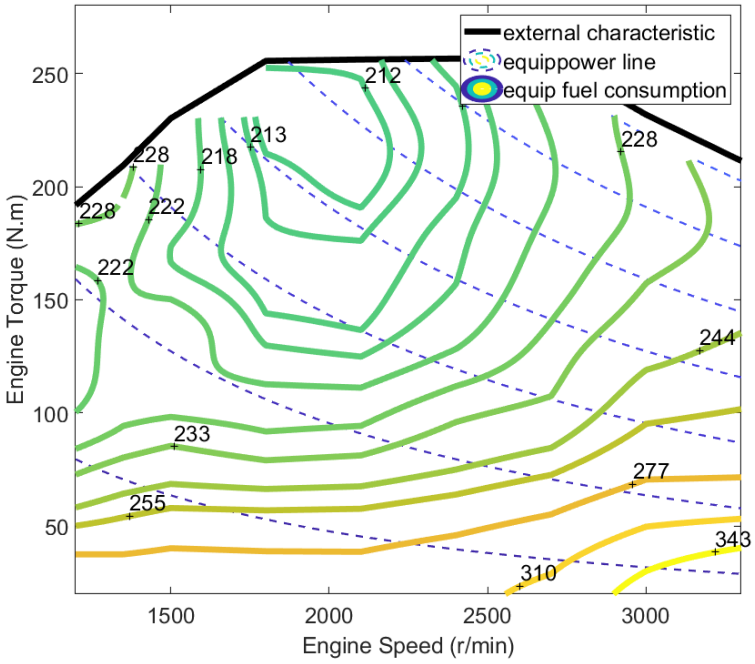

Figure 3.3 The engine efficiency map.

3.6 Traction motor

A permanent magnet synchronous motor (PMSM) is known for its compactness and high torque density, making it an excellent option for electric vehicles. Unlike induction motors, the permanent magnet inside the PMSM rotor generates a steady magnetic field by itself. By doing so, the PMSM has lower rotor inertia, a faster dynamic response, less generated heat, and most importantly, it provides higher torque density. As shown in Figure 3.4, motor UQM Powerphase 125 is selected for the Simulink model construction using its experiment data. The rated configuration is shared in Table 3.3.

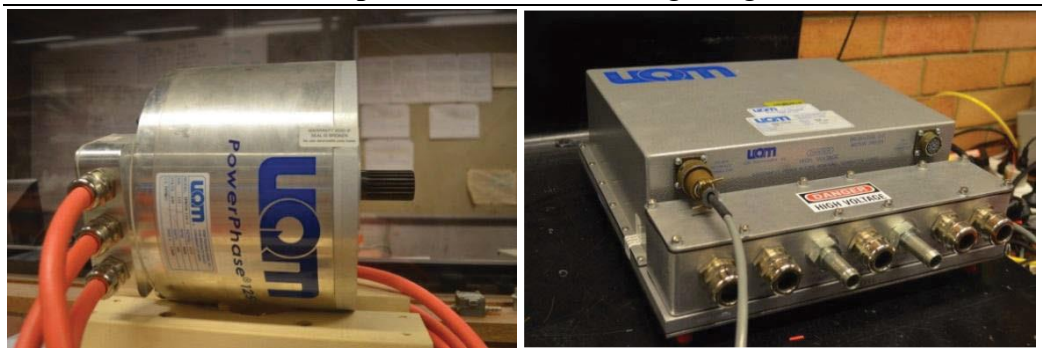

Figure 3.4 Traction motor and its controller [200].

Table 3.3 Configuration of the PMSM motor.

Motor parameters	Value	Unit
Highest efficiency	94	%
Peak torque of drive motor	300	Nm
Peak power of drive motor	125	kW
Rotational speed limit	10000	rpm
Operating voltage range	300-425	VDC
Power density	3.05	kW/kg

The power consumption can be calculated based on the equations as follows:

$$P_{mot} = \frac{T_{mot} n_{mot}}{9550} / \eta_{mot}(n_{mot}, T_{mot}) \tag{3.6}$$

$$P_{mot} + P_{acc} = P_{APU} \pm P_{bat} \tag{3.7}$$

where T_{mot}, n_{mot}, η_{mot} represent the torque, rotate speed and efficiency of the motor, while P_{mot} P_{acc}, P_{bat}, are the power of motor, accessories, battery, respectively. The drive motor efficiency map is plotted in Figure 3.5. It can be observed that APU can be used to charge the battery and supply required power at the same time. Moreover, it can work along with the battery to provide the peak power output to the vehicle.

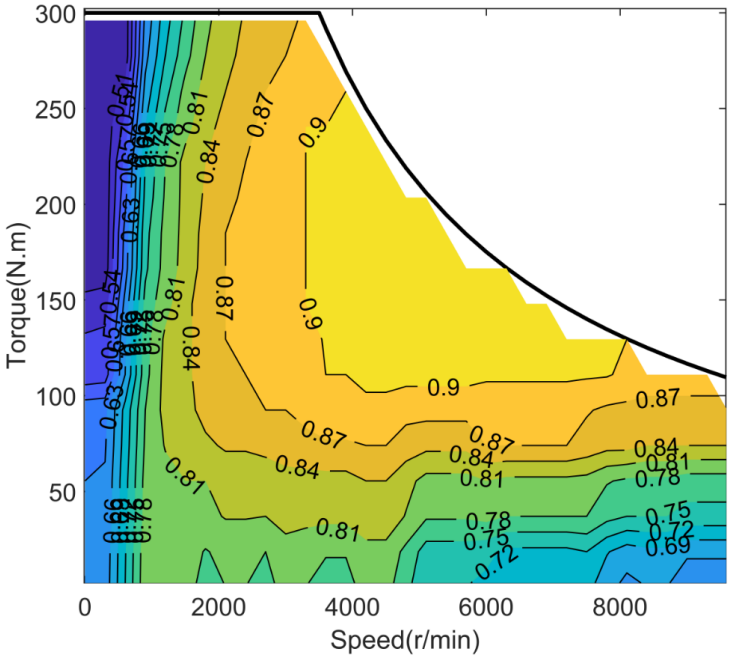

Figure 3.5 Efficiency map of the drive motor.

3.7 Battery equivalent model

The equivalent circuit model (ECM) for a lithium-ion battery is constructed with the consideration of battery loss. The battery ECM can be used to estimate battery operating conditions, improve the modelling accuracy and estimate the battery SOC [14, 201]. The battery ECM is shown in Figure 3.6. The battery model is constructed using Equation 3.8 and 3.9 to estimate the battery SOC:

$$SOC = \frac{U_{oc} - \sqrt{U_{oc}^2 - 4R_{bat}P_{bat}}}{2Q_{bat}R_{bat}} \quad 3.8$$

$$SOC = \frac{I_{bat}}{Q_{bat}} \quad 3.9$$

where U_{oc} stands for the open-circuit voltage, Q_{bat} is the total battery capacity, R_{bat}, P_{bat} and I_{bat} are the internal resistance, transient power output and the current of the battery, respectively.

The battery cell temperature is assumed to maintain at 30℃ during the simulation. The open-circuit voltage and the internal resistance variation under different SOC are demonstrated based on experimental data in Figure 3.7.

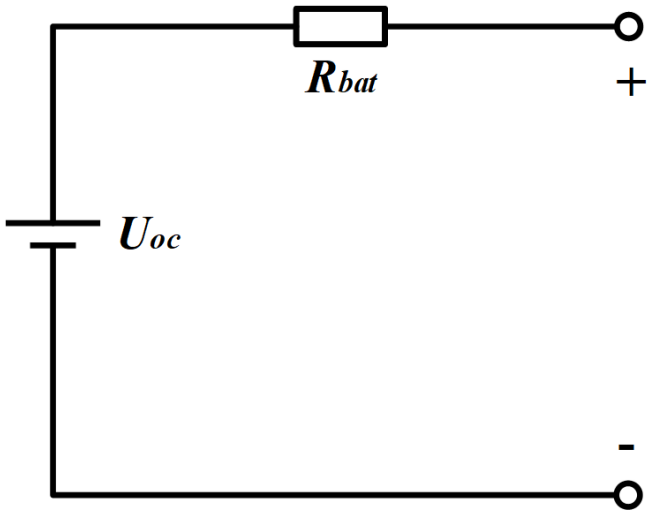

Figure 3.6 Simplified battery ECM diagram.

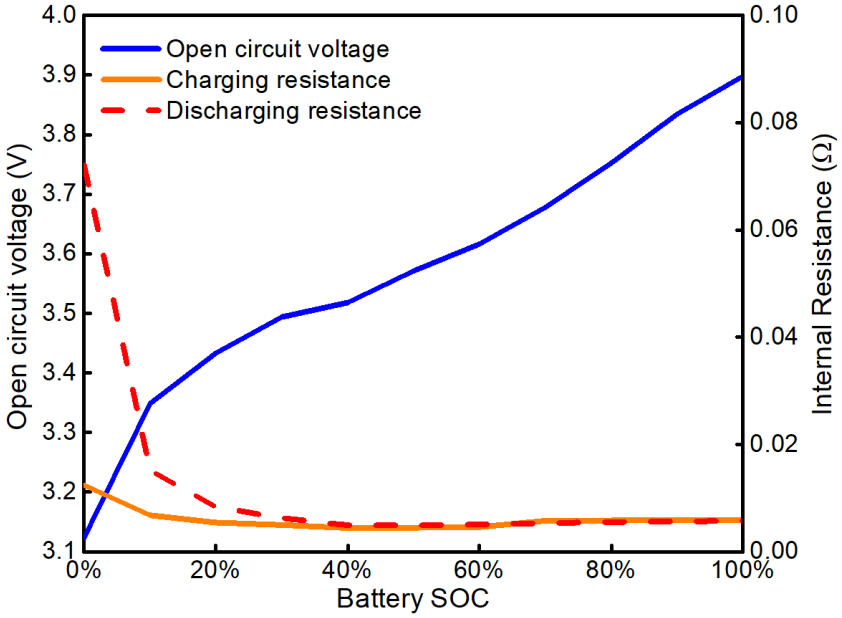

Figure 3.7 The electrical characteristics of a single battery cell.

3.8 Chapter summary

To simulate the energy consumption and performance of the platform, the mathematical model has been constructed and introduced in this chapter. The vehicle dynamics model calculates the driving resistance and internal force from the driver's command, and the power requirement goes to the main components like battery, APU and traction motor. The battery, motor and engine conversion efficiency are all taken into consideration.

Chapter 4 Investigation of energy potential and TCO for an ERLV

4.1 Introduction

During the last two decades, the logistics business has greatly expanded with the impact of the global economy and e-commerce growth. The concept of the sustainable business model has become popular, and future logistics transportation is advised to reduce carbon emissions by increasing the usage of electric logistics vehicles [202].

The total social logistics costs in China reached CNY 11.1 trillion in 2016, making China the largest logistics market in the world [203, 204]. In contrast to this, the increasing demand for logistics transportation leads to the massive discharge of air pollutants [205]. Some cities in Northern China suffer from the harmful haze with the risk of causing lung cancer [206]. Electric vehicles (EVs) can change the way how logistics businesses work. For instance, the ERLV and the BELV have on-board battery packs that can acquire electricity from the power grid and support pure-electric drive in the urban area. They are perfectly suitable for logistics dispatching from distribution centres to depots, and especially, offering a solution to complete the 'last mile' problem to customers. Thanks to the pure-electric driving range and improved powertrains, electric vehicles can significantly reduce emissions in urban areas, and even save courier companies a fortune on vehicle fuel and electricity consumption [46, 61].

The popularization of battery electric vehicles is mainly restricted by battery storage capacity, availability of charging infrastructure, battery charging speed, battery

health, and the BMS design rationality [2, 39]. A battery electric vehicle has to install a considerably larger battery than any form of the hybrid vehicle to provide a comparable driving range [60]. Using a large size battery may significantly increase the acquisition cost for urban logistics, which means the BELV is forced to charge frequently and reduce the overall transport efficiency. Therefore, the ERLV is proposed as the transition product to BELV with an effective combination of combustion engine and electric motor. It is perfect for logistics use: a logistics van requires higher drive power to carry cargo and lower running cost, and its chassis layout has sufficient space for the ERLV powertrain. In addition, the ERLV can run in pure electric mode in a decent travel distance, which guarantees minimized cost for short-range urban delivery.

The extended range system has been applied to many types of vehicles. The results from various studies proved that a small size APU could supply sufficient power for vehicle operation and reduce driver range anxiety [15, 207, 208]. Van manufacturers like Ford and LEVC announced their ERLVs to gain extra driving range with the help of a range extender [29, 209]. Studies by scholars proved that a proper APU control strategy is essential to optimize fuel consumption [36, 89, 210]. In [210], the authors compared the consumption of pure EV mode and range extend mode, and introduced an APU on/off control strategy that focused on the minimization of the purchase cost and fuel cost. In [89], trajectory optimization was adopted for a multi-point APU control strategy considering the engine emission issues. In the interest of simulation accuracy, dynamic programming (DP) is widely recognized as a promising algorithm to find the optimal fuel consumption of APU. In [83], the DP algorithm is constructed as a benchmark to compare a Neural

network control strategy, considering the vehicle remaining SOC and the distance to charging stations. However, its training driving cycle is NEDC which is no longer suitable for electric vehicles. An adaptive energy management strategy using driving pattern recognition is proposed in [71], using the results from DP as the reference. DP has the ability to search for the optimal control strategy, but its performance may differ when facing diverse traffic patterns [211].

Therefore, traffic pattern directly influences energy consumption and how the strategy operates, where scholars generated several driving cycles and classified them to train the strategy parameters [128, 207]. Recent studies prove that numerous optimization algorithms relying on the forgone driving cycle are dependable and effective [77, 83]. New and suitable driving cycles should be employed for the accuracy of the energy management study.

This chapter aims to present a thorough energy consumption and Total cost of ownership (TCO) analysis for an extended range electric van to show its energy potential. Both mathematical models of the ERLV and BELV are constructed and compared, and they adopt the same logistics van body configuration for a more accurate analysis. Their long-term battery degradation comparison is studied for the first time. Dynamic programming is adopted in the energy management strategy for energy consumption optimization, and the result reveals the optimal energy consumption for the extended range system on the logistics vehicle. Comparative results demonstrate that the ERLV has a relatively long drive distance, slower battery aging trend and cheaper TCO (6.6%) when compared to the BELV.

4.2 Optimization logic implementation

The global optimal control strategy is generally obtained by combining optimization methods and optimal control theory [6, 32]. As the key algorithm, the DP algorithm is a mathematical solution for system optimization. It breaks the complex system down into finite sub-systems recursively and searches for the optimal solutions of each sub-system. The merit of DP is to save computational load by storing the results of the sub-systems as arrays or in tables. In this case, the processor can simply read the store result to avoid recalculating when coming across the same pattern. The relationship between each connected sub-system can be described using the Bellman equation, and the calculated value can be traced back through the optimal path.

The state variable of the path is correlated with known conditions such as the control variable *u(t)* and previous state variable *x(t)*:

$$x(t) = a(x(t), u(t), t) \tag{4.1}$$

while the theory of DP is to minimize the cost function *J* given with the trajectory τ^*:

$$min\, J = \sum_{\tau=t}^{h-1} j(x(\tau), u(\tau), \tau) + \tau_h(x(\tau)) \tag{4.2}$$

where the actions in each state are defined that $u(\tau)=\{u_0, \ldots, u_{h-1}\}$.

4.3 Global optimization algorithm

In recent years, the DP algorithm based on Bellman theory has been widely applied to evaluate the theoretical optimal performance of the hybrid electric system. In this

chapter, it is used to calculate the fuel economy potential of the proposed ERLV platform under the given driving cycles.

In this test, the initial input for the ERLV platform is the speed-time driving cycle. The platform will conduct the accelerating-cruising-braking test to simulate the real-world operation. The energy saving ability of the ERLV can then be tested with the applied algorithm. According to the basic principle of DP, the giving driving cycle is first divided into N states, and each state represents a sub-system of the DP process. It contains an array of all selectable gridding SOC nodes. Then, the fuel consumption can be gathered during the state transition, and the optimal energy calculation can be performed through multi-stage decision-making. This global optimization process can be classified as the outer loop and inner loop. As seen in Figure 4.1, the outer loop is designed to search for searching optimal battery SOC trajectory of the ERLV. As the power demand from the driving cycle is already calculated through vehicle dynamics calculation, the SOC trajectory reflects a positive correlation with the APU power output. In the meantime, the key to decide the optimal SOC trajectory lies in the inner loop, where the APU is being optimized for fuel consumption improvement. The optimal engine point with the lowest fuel rate can be extracted from its constant power curve in the engine BSFC map, and later be stored in the DP database for future use. The double-loop DP framework improves the efficiency of the conventional DP method by constraining the search range of the battery SOC, and simplifies the two search processes into one.

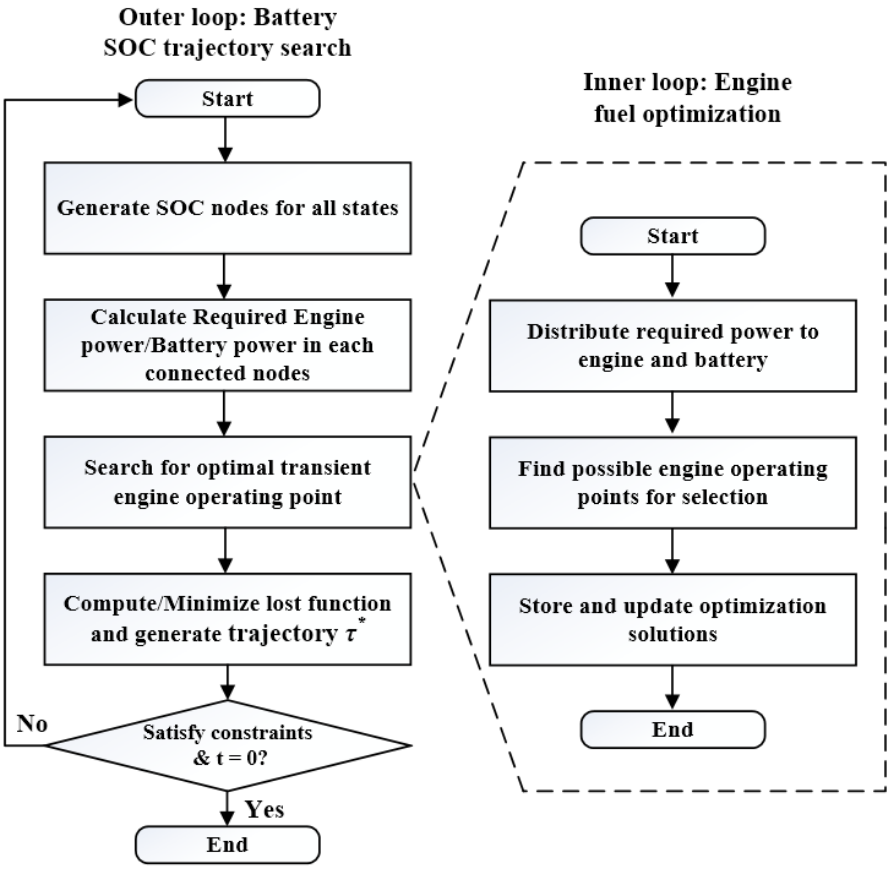

Figure 4.1 Double-loop DP flow diagram for the ERLV model.

The forward optimization process for the optimal SOC path can be applied after the completion of the reverse calculation. The objective function is as follows:

$$min\,J = \sum_{t=0}^{t=t_N} fuel\big(x(t), u(t)\big) + L_b \tag{4.3}$$

where *J* is the cost function, $fuel(x(t), u(t))$ is the fuel consumption of each step calculated from the state variable $x(t)$ and control variable $u(t)$.

With the aim of evaluating the APU fuel consumption of the ERLV, the initial and final value of the battery SOC is defined as 80% to ensure all power consumed during the cycle is converted from fuel. Penalty term L_b is added in the objective function to restrict the difference between initial and final SOC.

$$L_b = \beta(SOC_{t_N} - SOC_{t_0})^2 \tag{4.4}$$

where β is the penalty coefficient, SOC_{t_0} is the initial SOC and SOC_{t_N} is the final SOC. This concept is also illustrated using Figure 4.2, showing the logic-tree searching pattern of DP. For SOC(t) (except the final state), they are followed by plenty of possible next states $SOC_n(t+1)$ that meet the battery discharge restriction.

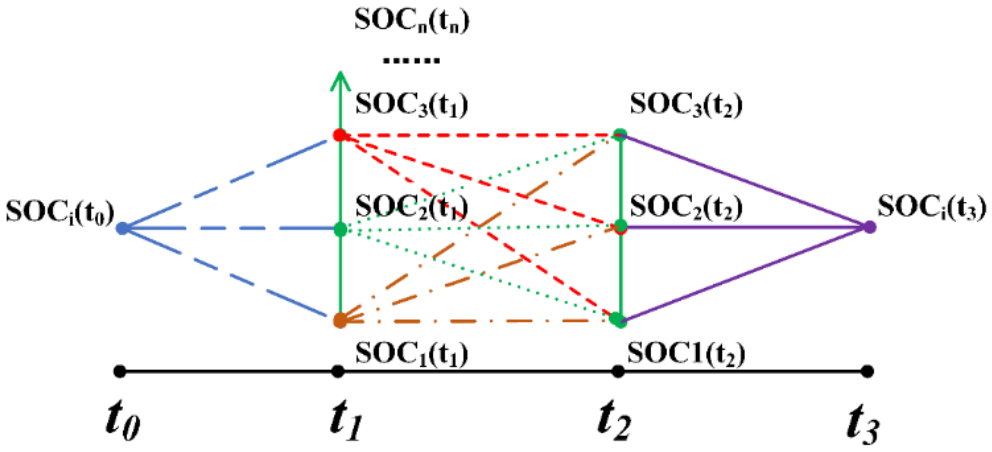

Figure 4.2 Outer layer of the DP process (possible SOC nodes search).

The time scale of the driving cycle is set to be 0.2 s for a better searching performance. The discharge rate of the battery is restricted below 6C for its state of health (SOH) protection. Therefore, the battery SOC will not fluctuate drastically during the optimization process, which means its value is constrained to only transfer to its adjacent values. Finally, the optimized fuel cost of the engine can be determined after the SOC variation pattern of a specific time step is found [34]. The accumulated fuel consumption results and the power distribution pattern are further used for energy management comparison and TCO analysis.

4.4 Battery degradation prediction

The battery state of health is a vital factor in evaluating the vehicle reliability [212]. The battery degradation models for the ERLV and BELV are constructed to test whether the battery needs to be replaced through the vehicle estimated lifespan. The

battery aging test is performed on the WLTC-3b driving cycle until the total mileage reaches 250,000 km [197, 198]. Generally, the battery temperature and the discharge rate have great influences on battery health [213]. Therefore, the battery discharge rate is included as one of the input variables in the model. In order to simulate the dynamic battery degradation with accuracy, the battery loss Q_{loss} can be estimated with a calibrated empirical formula-based Arrhenius equation according to reference [214]. It uses the Ah throughput and battery C-rate as the key variates:

$$Q_{loss} = A \cdot e^{-(\frac{E_{act} - B \cdot C_{rate}}{R \cdot T_{Bat}})} (A_h)^Z \tag{4.5}$$

where Q_{loss} is the capacity loss of the lithium-ion battery, A is the pre-exponential factor, C_{rate} is the battery discharge rate, R is the Molar gas constant (8.314J/mol/K-1), A_h is the Ah-throughput and Z is the time factor. The battery absolute temperature T_{Bat} is 308.2 K. E_{act} and B represent the activation energy and correction factor of the discharge rate, respectively. The single-step Ah-throughput can be defined as:

$$\Delta A_h = \frac{1}{3600} \int_t^{t+1} |I_{Bat}| \, dt \tag{4.6}$$

The battery of BELV in the aging test is discharged from 100% to 0% in WLTC driving cycle, and it is then assumed to be recharged to full capacity from the power grid. On the other hand, the ERLV works in a CD-CS pattern that runs 47 km in pure-electric mode, and the rest will run in sustain mode. The result from the DP shows the battery in the CS mode has 55% less Ah throughput than the CD mode, which indicates the APU operation in CD mode can slow down the battery degradation. The battery capacity Q_{loss} of the BELV and ERLV for a single WLTC

cycle is shown in Figure 4.3. The figure shows that the battery degradation in the CD mode is faster in ERLV than in BELV due to the smaller battery pack in ERLV. However, as the CS mode supports most of the driving range, it has a mitigating degradation curve which means a longer battery lifespan can be achieved. From the final mileage aging test, the battery SOH of the BELV went down with the accumulation of Q_{loss}. It gradually dropped below 0.8 when it reached 74% of the total distance (185,200 km), revealing a battery replacement is recommended [215]. On the contrary, the battery of the ERLV remains relatively steady and decreases to 0.8 with a total distance of 243,400 km, which is sufficiently close to the target mileage. The London EV Company Ltd. provided a battery warranty on its ERLV model VN5 (31 kWh battery) for up to 240,000 km [209], which is similar to this ERLV degradation result. It is worth mentioning that the impact of the ambient temperature is not considered in this battery aging test, which may negatively affect the ERLV battery lifespan due to the cold start at a low temperature. However, this will not happen to ERLV because the APU can be turned on to warm up its battery pack and vehicle cabin [174]. With the battery aging result, the TCO of the two models can be estimated.

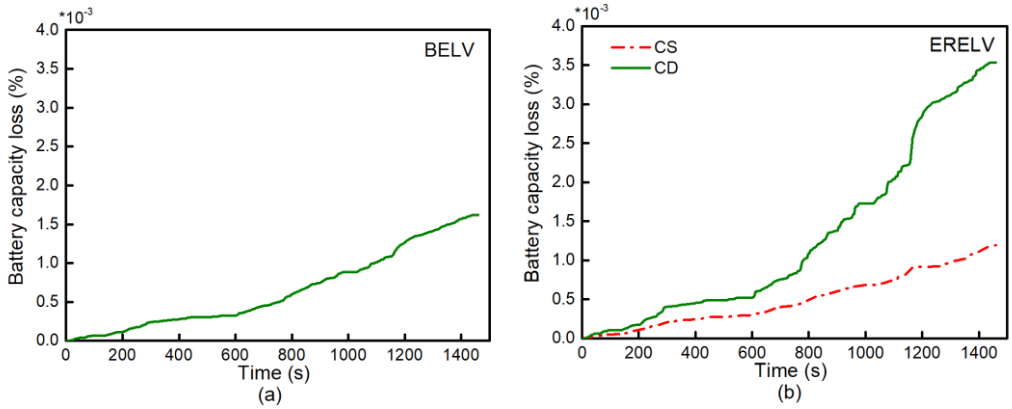

Figure 4.3 The battery capacity loss accumulation of (a) BELV and (b) ERLV in WLTC-3B

4.5 Simulation results

To analyse the APU and ESS power distribution, the power demands of the studied model should be calculated in the first place. The motor power demands of the van on CLTC-C and WLTC (class 3b) are shown in Figure 4.4 (a) and (b). As seen in the figures, WLTC has a higher power demand than CLTC, and this may lead to higher energy consumption.

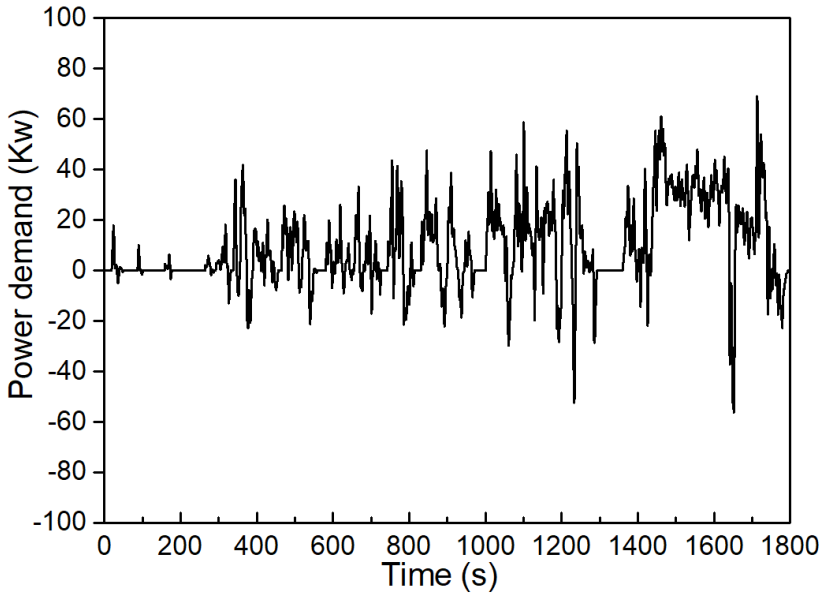

(a)

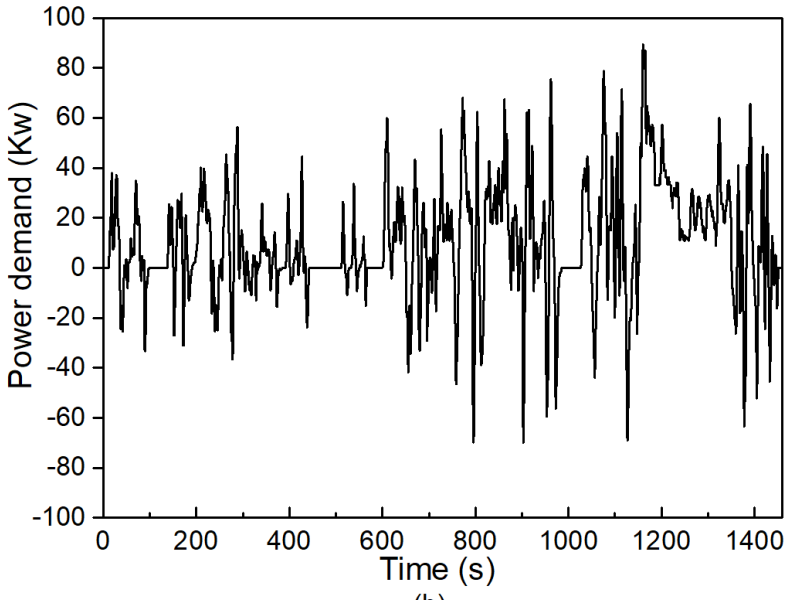

(b)

Figure 4.4 Power demands on (a) CLTC and (b)WLTC

4.5.1 Consumption comparison

After obtaining the primary power demand data, the engine of the APU is designed to operate within its optimal range for maximizing fuel conversion efficiency. To avoid frequent startup, the engine will only be turned on when the APU power demand exceeds 10 kW. After that, the engine condition is determined by its power requirement, and the DP algorithm makes sure it is running in the best fuel efficiency area. The engine optimization results are shown in Figure 4.5, where the red asterisks represent the actual engine operation points. It can be observed that most of the asterisks are located in low fuel consumption areas, verifying the rationality of the DP algorithm. In addition, there is no asterisk above the highest equivalent power line, proving the 75 kW engine can satisfy the power demand of the studied van.

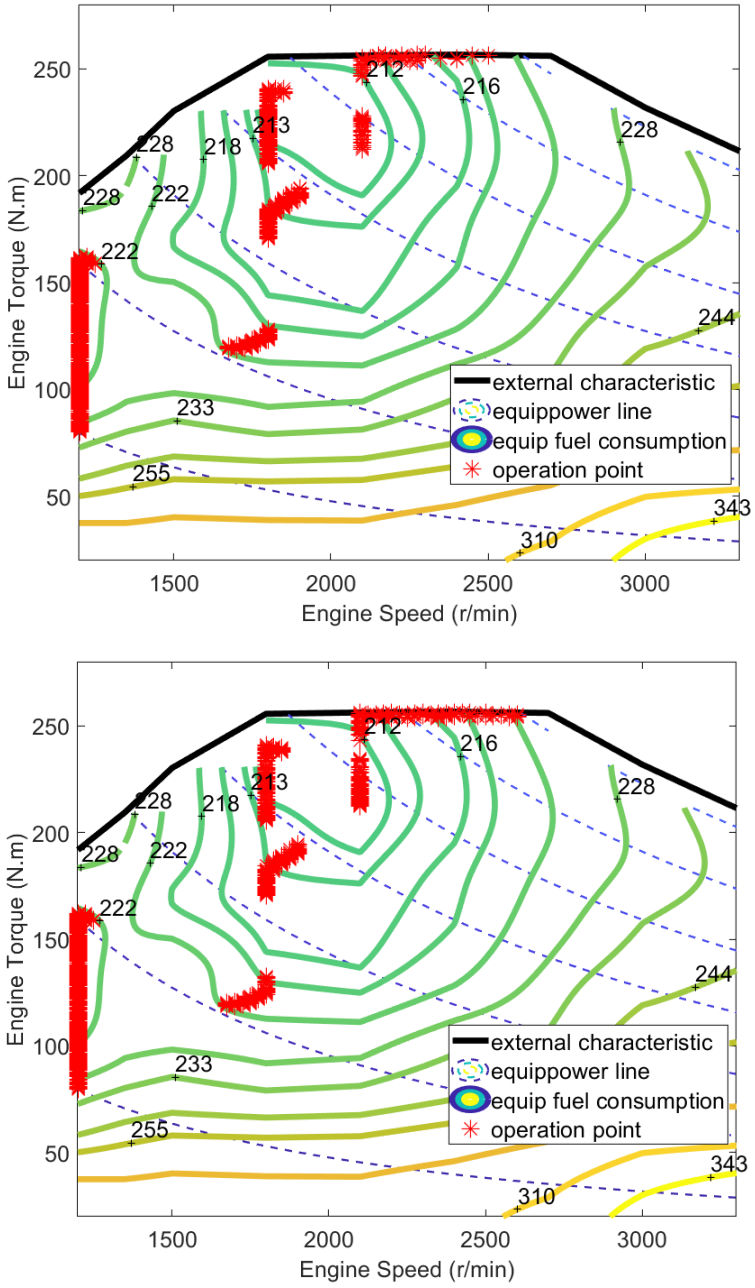

Figure 4.5 Engine operation points of CLTC (top) and WLTC

The power variation of the engine and battery are shown in Figure 4.6. It can be observed that the engine supplies power to the drive motor and battery. The regenerative braking system also takes part and handles 25% of the brake requirement to recharge the battery [216]. In some cases, when there is a high required power from the vehicle, the battery may supply power along with the engine as compensation.

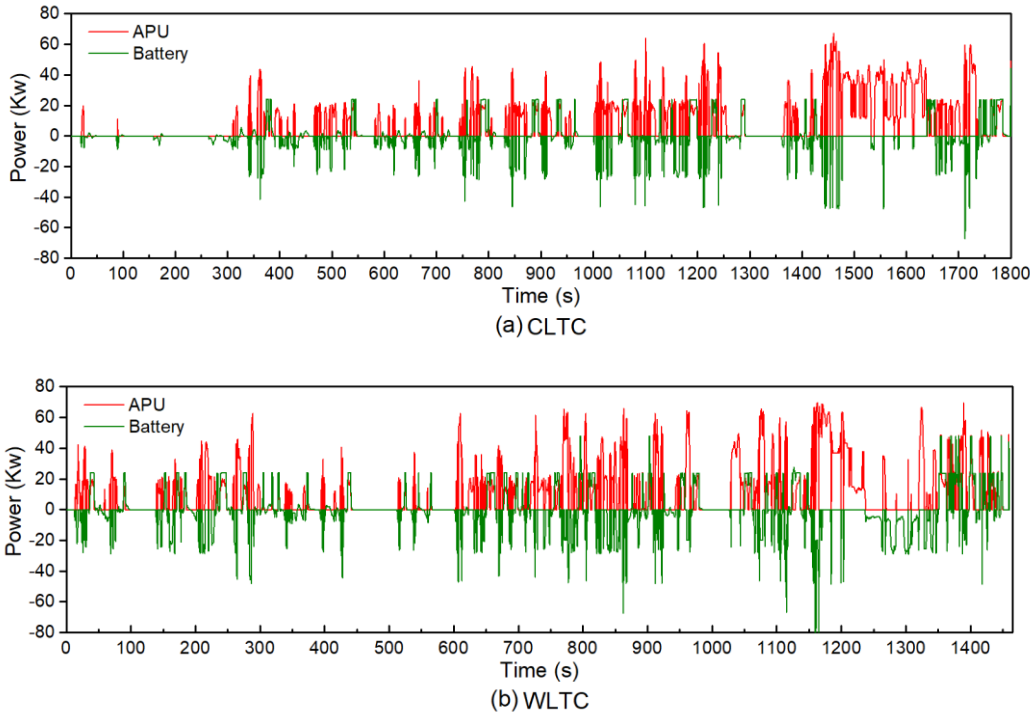

Figure 4.6 Results of engine and battery power from DP optimization

The SOC variations and accumulated fuel consumption for the two driving cycles are given in Figure 4.7 (a) and (b). For a more accurate assessment of the engine performance, both the starting and the ending values of the battery SOC are set as 0.8. The SOC variation range in CLTC is around 77.5% to 80%, while the range in WLTC is 75.5% to 80%. As for the fuel consumption, the WLTC has a more fluctuating line than CLTC, reaching a diesel consumption of 0.64 litres with 15 km travelled.

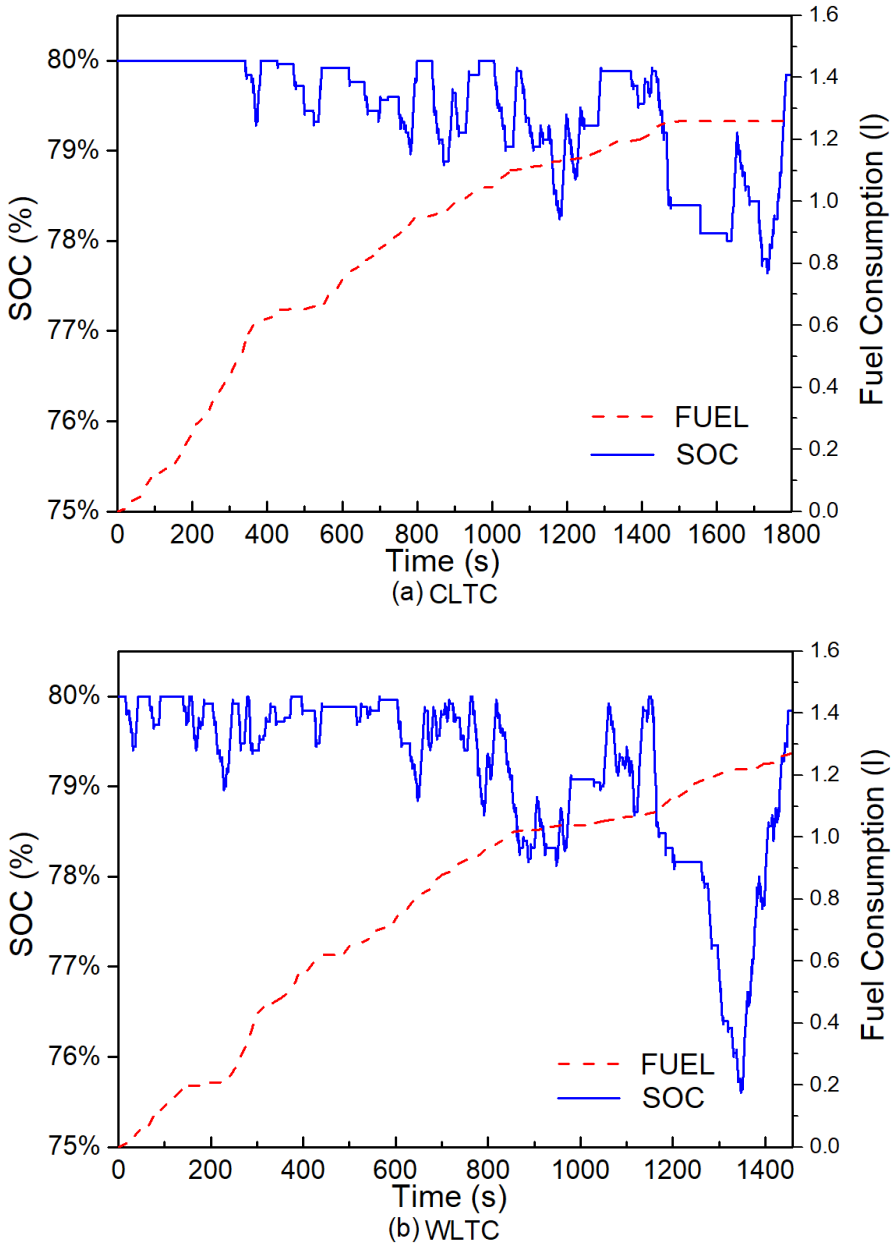

Figure 4.7 Variation of the battery SOC and fuel consumption.

A BELV mathematical model with a 60 kWh Li-ion battery is constructed as a comparison to evaluate the economic efficiency and operation cost of the ERLV model. The simulation results of both ERLV and BELV are listed in Table 4.1. The results share an expected energy consumption and driving range for these two types of vehicles with cargo fully loaded. The diesel consumption per 100 km of ERLV is only 3.81 and 4.13 litres more than that of the BELV for CLTC and WLTC,

respectively, after conversion to electrical equivalent consumption was completed. Independent data of the driving range are collected from production vehicles with similar specifications to validate the simulation result in this study. For the BELV, the Mercedes eVito has a 41 kWh battery that claims a 150 km driving range in WLTC (gross weight, 3,200 kg) [217]. For ERLV, the new Ford Transit Custom is estimated to have over 500 km driving range in NEDC [29], while the LEVC VN5 claims a 490 km driving range with a 31 kWh battery and a 1.5 L petrol engine in WLTC [209].

Table 4.1 Diesel consumption and driving rage comparison

Type	Driving Cycle	Diesel Consumption (Equivalent)	Consumption L/100km	Drive Range (km)
ERLV	CLTC-C	1.26L	7.68	572.9
	WLTC-3b	1.28L	8.46	519.3
BELV	CLTC-C	6.31kWh (0.63L)	3.87	156.3
	WLTC-3b	6.46kWh (0.65L)	4.33	139.4

* 37.6 kWh of electrical energy is equivalent to the energy of 1 gallon (3.785 litres) of Diesel [36].

4.5.2 The total cost of ownership analysis

TCO analysis is essential to further demonstrate the practical potential of ERLV and BELV in the logistics market [30, 196]. TCO includes the vehicle purchase costs and operating costs, which can be used to evaluate the economic benefits of the new technology to the potential user in the decision-making process. In this case, it helps to compare the fuel economy of different logistics vans for the companies that make a profit from providing carriage service [218, 219]. The vehicle lifetime consumptions of the two targeting vehicles were calculated using the TCO equation:

$$C_{TCO} = C_p + \sum\nolimits_{Dis} \left(C_m + C_f + C_r\right) \tag{4.7}$$

where C_{TCO} is the overall TCO, C_p is the purchase cost of the vehicle, C_m, C_f, C_r are the maintenance cost, fuel cost and the part replacement cost, respectively.

However, due to the Covid-19 pandemic and Russia-Saudi Arabia Oil Price War in March 2020, the fuel price in 2020 fluctuated widely that the diesel price varied from $3.07 per gallon to $2.37 per gallon lowest [188]. A sensitivity analysis of the diesel price is carried out for TCO calculation. On the contrary, the commercial electricity price remained relatively steady from $0.1023/kWh to $0.1107/kWh, and thus, an average price of $0.1065/kWh is selected [220]. The specific costs of TCO of the three van models are listed in Table 4.2 [178, 196, 221].

The TCO growth results of the three van models with the highest/lowest diesel price are plotted in Figure 4.8 (a)-(b). The purchase cost of the ERLV and BELV models is higher than the internal combustion logistics van (ICLV) on account of the additional expenditure for battery and electromagnetic devices [222, 223]. The operating cost consists of maintenance cost and overall fuel/electricity cost. For the maintenance cost, all models are expected to have their wheels and brake pads changed every 50,000 km [224, 225], while the engine maintenance is performed every 10,000/15,000 km for ICLV/ERLV [226, 227]. As for the fuel/electricity cost, two TCO growth trends are generated for the ERLV and ICLV from the fuel price sensitivity analysis. The highest estimated fuel cost of ICLV may increase by 22.8% of the lowest at $23,481; however, the ERLV only has a minor increment of the fuel/electricity cost toward the maximum of $16,583 thanks to its high APU fuel efficiency and the friendly grid electricity price. On the other side, the BELV has the lowest maintenance and electricity cost among all three models, but its battery is expected to be recharged over 1700 times in 250,000 km. Considering the battery aging simulation result and the real-world impact, a battery replacement for EREV is necessary [228]. The battery replacement will cost approximately $10,560

according to the average Li-ion battery market price ($176/kWh) in 2019 [54, 143, 179], which means the BELV will have the highest TCO when the fuel price is around $2.37 per gallon.

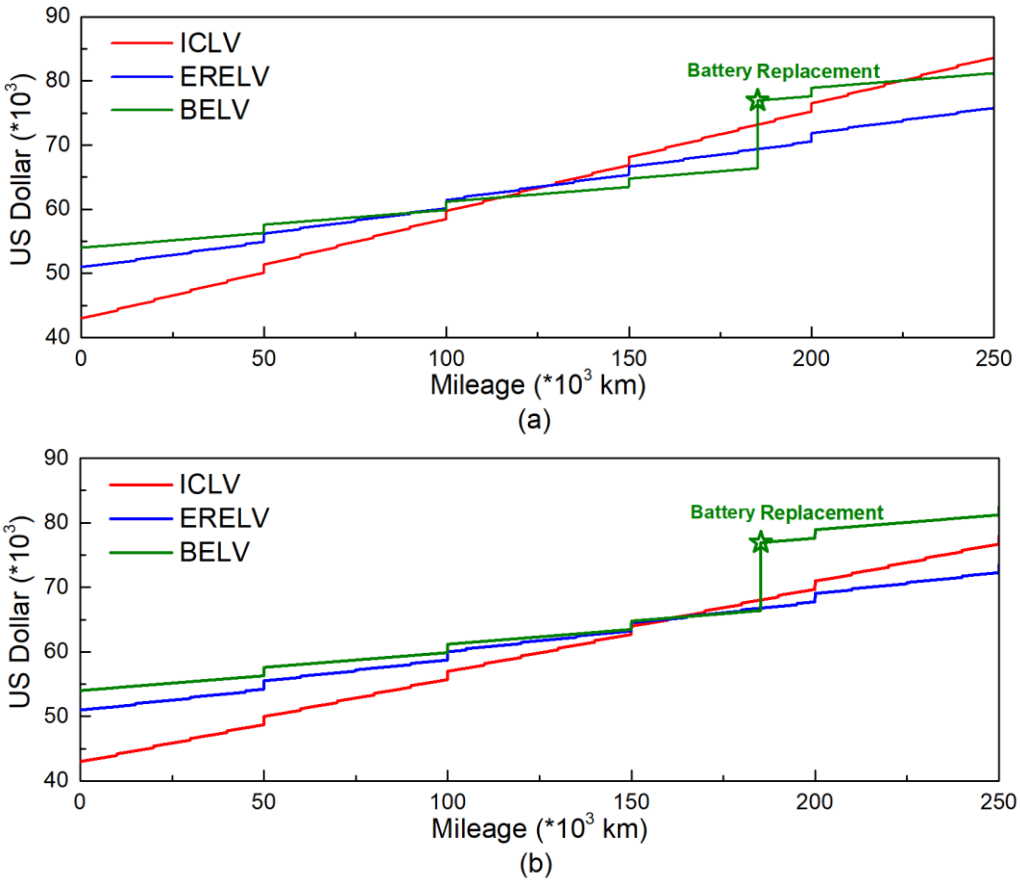

Figure 4.8 TCO growth comparisons with the highest (a) and lowest (b) diesel prices.

Table 4.2 Predicted data of TCO and energy consumption(US $).

Vehicle Type	Purchase cost	Maintenance	Battery replacement	Fuel&Elec cost	TCO
ICLV	43,000	11,500	-	23,481~30,416	77,981~84,916
BELV	54,000	6,500	10,560	11,458	82,518
ERLV	51,000	9,500	0	13,064~16,583	73,564~77,083

The fuel price fluctuation shows two interesting outcomes of the TCO between ICLV, ERLV and BELV. As mentioned above, the BELV in Figure 4.8 (b) has the highest TCO due to the high battery price. The other outcome in Figure 4.8 (a) with the highest diesel price identifies the ICLV as the most costly model for the logistics

market. The overall fuel cost of ICLV accounts for 35.8% of its TCO and causes a huge emission burden on the urban environment. In comparison, the energy costs of the BELV and ERLV are only 13.9% and 21.5%, respectively.

Considering the current logistics transportation requirement, the most suitable vehicle from above should at least satisfy both the expend and driving range requirement [216, 221]. The ICLV remains an acceptable option with its mature technology and low selling price. In terms of the ERLV and ICLV, there may be potential government policies and marketing promotions to boost their popularization. The ERLV has the lowest TCO and longest travel distance that makes it perfect for commercial use covering all travel distances. With an appropriate EMS and sizing of the APU and battery, the ERLV can inherit the advantages of the BEV and ICV with a pure-electric drive function and refuelling convenience. The BELV appeals to have the lowest maintenance and energy cost, but its battery capacity degradation will have a significant impact on the travel distance per charge in the long term [67, 211], not to mention the high battery replacement cost under heavy cycles. The battery price is expected to go down in the future, and new battery development may make BELV more competitive in the logistics market [219].

4.6 Chapter summary

This chapter has presented a thorough energy consumption and TCO analysis for an extended range electric van for short and long-term logistics tasks. The global optimization considers the joint power management of the APU and battery by locating the optimal SOC nodes in each state. The corresponding best engine fuel point under the designated battery SOC variation stage is collected, and the SOC

variation path with the lowest fuel cost through the whole driving cycle is picked as the optimal global solution. The TCO analysis comparing the three types of logistics vans is conducted as an indication for the commercial customer. Because the cost factor - fuel price is fluctuant and unpredictable, a sensitivity analysis is conducted to improve prediction accuracy.

The simulation results prove that the extended range system has the practical and economical advantage to apply on logistics vehicles. The successful deployment of the global optimization strategy keeps the engine operating in the high-efficiency range, with the engine conversion rate lower than 220g/kWh in 85% of the operating time. The optimized average fuel consumption of CLTC and WLTC reach 7.68 litres and 8.46 litres every 100 km, respectively. The following TCO study demonstrates that ERLV can provide a much longer driving range than BEV without spending too much money from the long-term perspective. The TCO of ERLV (WLTC cycle) is estimated from $73,564 to $77,083, which is the lowest among all three models.

Chapter 5 Muti-target energy management strategy of the ERLV

5.1 Introduction

Modern strategies such as model predictive control (MPC) and dynamic programming (DP) have limited practical potential because they are subject to the pre-known environment information and noise interference. Therefore, those control strategies may not be applied to real-time EMS for the target vehicle.

The RL-based algorithm, however, do not need to assume or gather any future knowledge of the environment state. In fact, it only requires datasets from the past knowledge, which fundamentally avoid the error of predicting the future states of the process [229]. RL algorithm also reduces the computational load in operation once the training is done [103]. It is known to work in the form of the Markov decision process, because its strong demand to understand the variation and relationship between states and states. The fundamental principle of the RL algorithm is to let its agent to learn an optimal, or to approximate optimal policy which can maximum the accumulated reward.

Since 2018, early energy management studies have applied some fundamental RL algorithms to the energy management study, and the Q-Learning based algorithm was the first attempt on electric vehicles fuel optimization. In Ref. [230], a speedy Q learning algorithm to control the engine throttle to improve fuel economy on a hybrid tracked vehicle. Han et al. conducted a study on using an improved double deep Q learning algorithm to reduce the impact of over-optimistic estimation on value function [73]. However, the Q-Learning based algorithms can only output

discrete action space, which is not suitable for vehicle control considering its high-dimensional action space. The Actor-Critic (AC) based algorithms are then introduced in which two neural networks are deployed for the value and policy networks. It quickly became the mainstream algorithm as it surpassed the Q-learning based algorithm in all aspects. For instance, the Deep Deterministic Policy Gradient (DDPG) algorithm is the most representative AC based algorithm enabling continuous action space [231]. Studies have proved that DDPG provided the energy management system with desired real-time control ability [232-234].

Nevertheless, the algorithms from the current studies still have unsolved issues. The DDPG can be very sensitive and unstable when interacting with a complex environment. As a deterministic policy, its exploration only relies on the noise added to the output action. However, studies found out that the AC based algorithms may get stuck into a bad solution due to pool exploration in the early stage [235, 236]. The training speed and stability are essential for the EMS; hence the current algorithm design needs to be improved for practicality. As a wide action space may result in training instability, the RL-based EMS studies above have to draw an engine optimal fuel line to limit the engine operation pattern. More importantly, the studies only constrain the battery SOC level and ignore the battery health condition, which may result in severe battery degradation in long term.

To solve these issues, this project adopts a novel AC based stochastic algorithm with maximum entropy on the APU power flow management. The algorithm is called Soft Actor-Critic (SAC) with a framework of dual critic networks and experience replay ability [85]. The policy maximizes a trade-off between the expected reward and entropy to achieve random action, which efficiently increases

the exploration in early training. The stochastic AC structure with off-policy updates provides the algorithm with stability and the ability to handle complicated tasks. Thanks to these, improvements can be made to the RL-based EMS. Compared with the existing studies, the optimization target in this work is not only limited to the fuel efficiency; the first attempt of battery charging protection in RL-based strategy is carried out by limiting the battery charging rate (C-rate) under different SOC. An improvement of the agent action space is made by introducing both engine power and speed to achieve a more linear control performance. Furthermore, to resolve the lack of exploration with the vehicle environment duing the training process, a local reset function is activated to randomize the initial battery SOC and selection of the driving cycle.

5.2 The EMS Design and requirement

The RL deployment mainly consists of three parts: environment construction, reward settings and agent programming. During each state of the training process, the agent gives out control action to the targeted system, and the system will interact with the environment and proceed to the next state according to the Markov decision process (MDP). An MDP, as shown in Figure 5.1, is a sequential decision-making process in which the action will influence not only the immediate state but also the future states and rewards. (s, a_s, p_a, r_a) are the four elements in the MDP. Element s represents the state conditions of the environment; in this study, it can contain the operating signals and data of the vehicle body. Element a_s is the action space generated from the RL agent. In each state, the agent will have one or more possible actions to pick. However, the chances of picking different actions in a certain state are not always the same. The p_a stands for the probability for the agent

to pick the corresponding action a. After selecting the action, an immediate reward r_a and new state observation s' from the environment will be fed back to the agent. The agent will keep improving the probability of the possible actions which generates better rewards r_a to maximize the accumulated rewards in each episode. The simplified flowchart of the RL interaction is also illustrated in Figure 5.2.

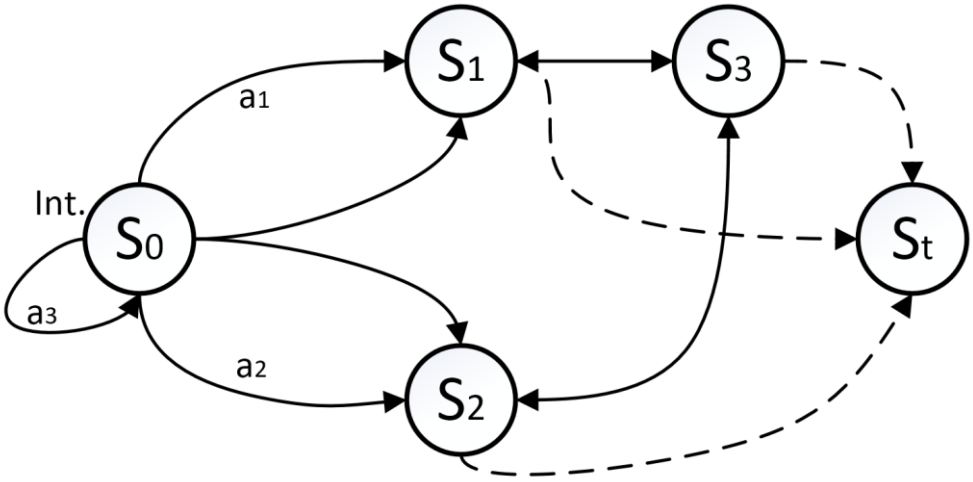

Figure 5.1 A Markov decision process diagram.

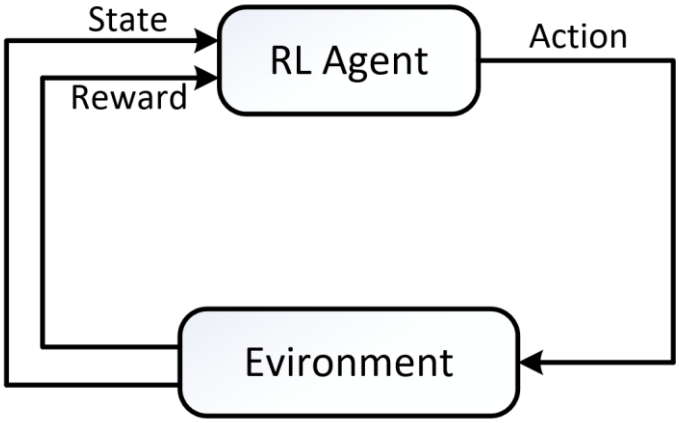

Figure 5.2 Closed-loop control in RL environment.

The RL-based ERLV platform is constructed using the Matlab 2021a version and its Simulink/Stateflow modules. The ERLV model contains an RL agent, vehicle environment and signal processing module. The upper structure is shown in Figure 5.3. The RL agent is responsible for handing out the control signals of the APU to

the vehicle environment; in this study, the two control signals are the APU output power and the corresponding engine speed. After receiving the control signals, the vehicle environment will operate according to the action space. The signals are transformed to the mathematical model where engine efficiency, fuel consumption and the ISG efficiency are being considered. After that, the generated electric power is calculated and distributed to the wheel and battery. When all simulations are cleared, the signal processing model will receive data from the vehicle components. These signals will then be treated and transferred into state reward and fed them back to the RL agent along with the vehicle state information. By repeating so, the RL agent will partially update its action pattern when a higher reward occurs.

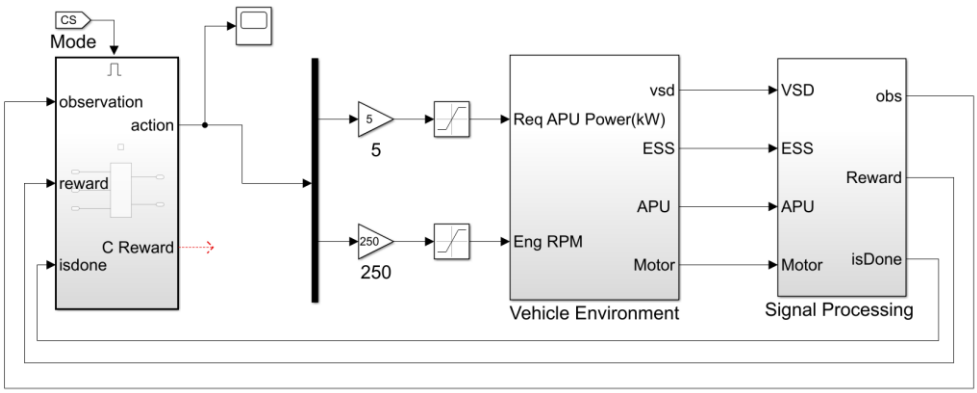

Figure 5.3 The Simulink framework of the RL-based ERLV model.

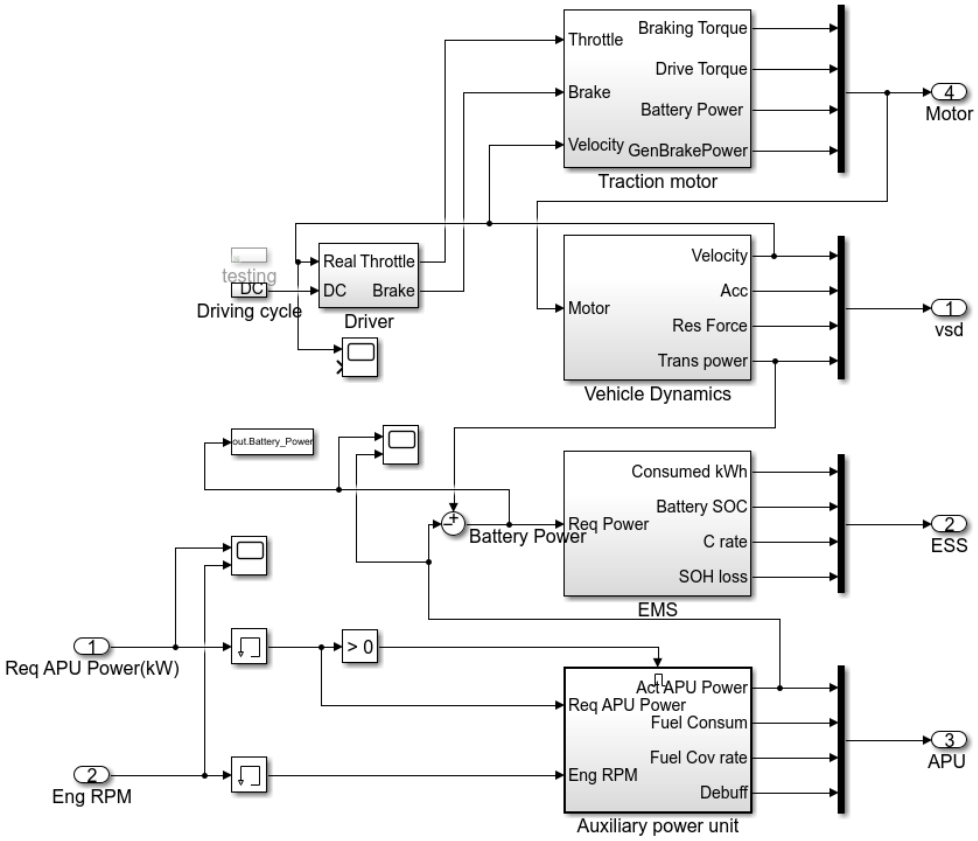

Figure 5.4 The framework of the vehicle model.

The vehicle environment model includes the models of driving cycle, driver, vehicle body, traction motor, ESS and the APU. Its framework in Matlab/Simulink is shown in Figure 5.4. The initial input to the environment are the driving cycles. The driver model has a tuned PI controller to compare the error between the current vehicle velocity with the desired velocity. It outputs a signal range of [-1, 1] for the accelerator pedal and the brake pedal to keep the vehicle up with the cycle targeting speed. The ERLV model will thereby work as a forward simulation under the control of the RL agent and the driver model.

5.2.1 Vehicle modelling for RL training

The Simulink models of the main vehicle components are explained in this section. The mathematical and physical calculations are demonstrated.

From the driver model in Figure 5.5, the velocity error with the driving cycle is being adjusted with the PI controller; and after becoming a dimensionless value, it can be transformed into the pedal signal. After that, it is handed out as the command signal for the traction motor model.

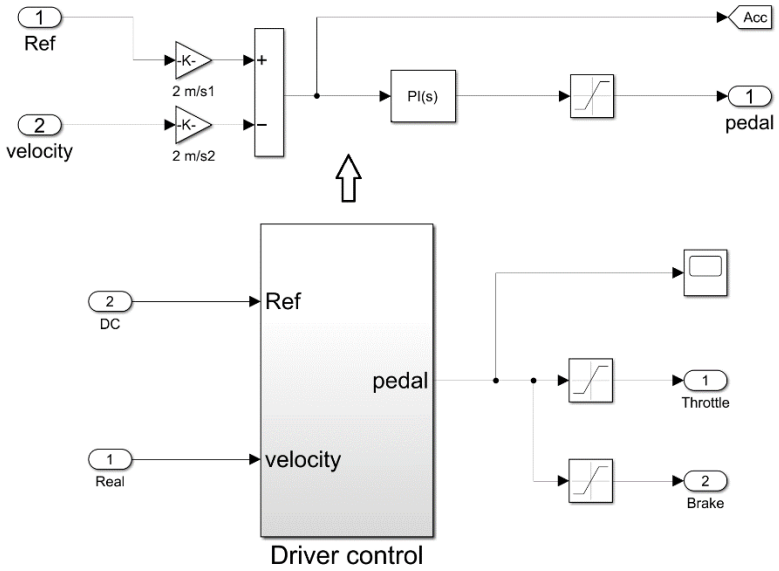

Figure 5.5 Driver model.

The driver control signal is split into throttle and brake inputs. As shown in Figure 5.6, the traction motor controller outputs torque according to the pedal movements. A constraint function relying on the Torque-Power curve map in Figure 3.5 is designed to maintain the motor torque under its limitation. The detailed energy efficiency of the motor is considered to calculate the real-time energy consumption and recycled braking energy for the EMS.

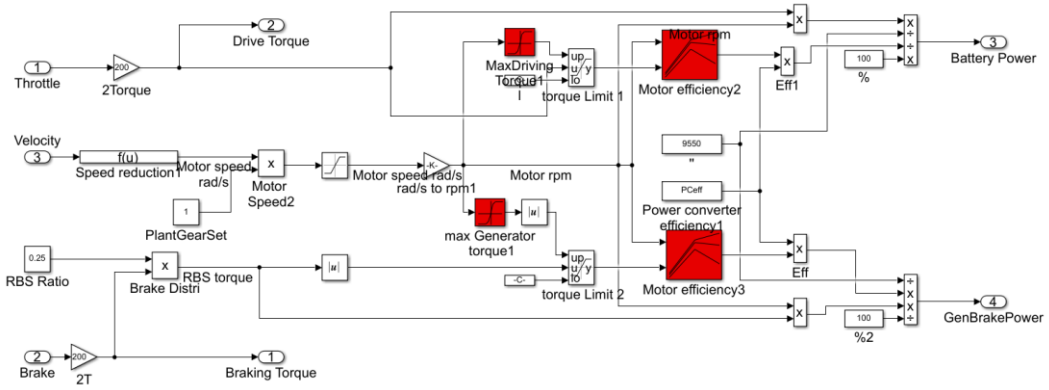

Figure 5.6 Traction motor model.

Figure 5.7 shares the simulation for vehicle body dynamics. It calculates the vehicle power consumption and its driving resistance. The logistics vehicle resistances during operation can be broken down into three forces, which are rolling resistance, aerodynamic drag resistance and grading resistance. The grading resistance is waived as the driving cycles are assumed to run on a gradeless surface. Real-time velocity of the vehicle is used to calculate the body Aerodynamic drag. After that, the model can acquire the vertical resultant force combining the wheel force from the traction motor. The operational power demand of the whole vehicle is sent to the APU and the ESS model to handle.

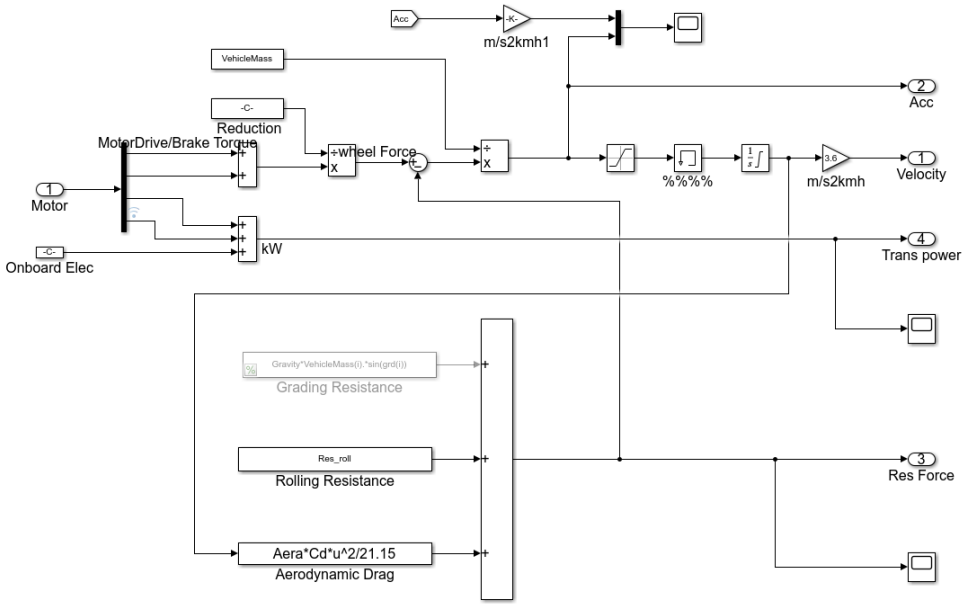

Figure 5.7 Vehicle body dynamics.

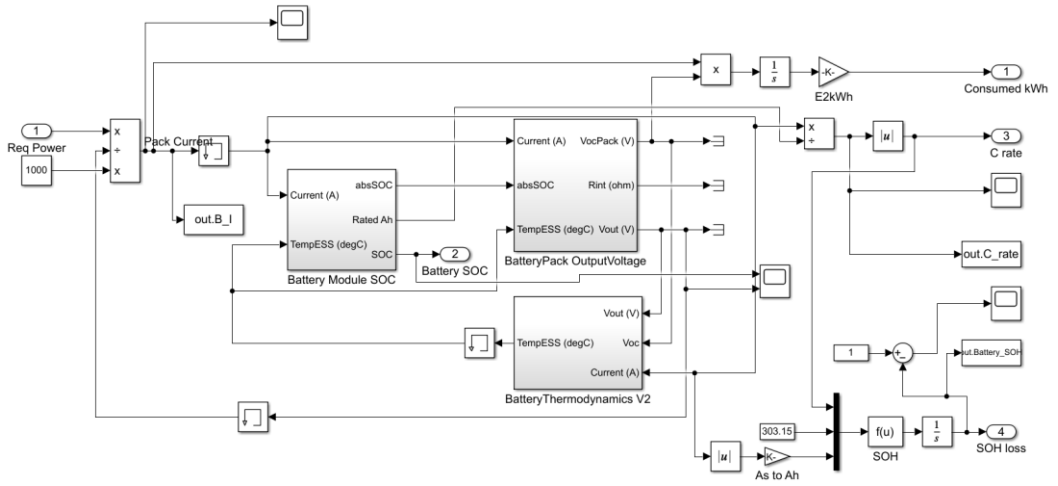

Figure 5.8 Battery model design.

A detailed EMS model (Figure 5.8) is designed using equivalent circuit model (ECM) experimental data from a lithium-ion battery. Battery ECM can be used to estimate battery operating conditions, improve the modelling accuracy and estimate the battery SOC. It considers the internal battery loss which can show how the battery cell responds to throughput in different usage scenarios. As the instant voltage of the battery pack can be predicted according to its current SOC and cell thermo conditions, the required power from the battery can be converted into current. After that, the battery pack throughput, the impact of the internal resistance according to SOC level and its temperature variation can be calculated. The transient battery discharge rate (C-rate) is provided to the RL reward calculation.

As shown in Figure 5.9, the APU model consists of the engine and an ISG. The RL agent provides the APU model with two control signals which are the required APU power and the corresponding engine speed. Consequently, the transient engine operation point can be confirmed, and the corresponding engine torque output, fuel rate and consumption are looked up according to the engine BSFC map. In the meantime, the ISG, which connects mechanically with the engine output shaft, has the same rotational speed as the engine. The generating efficiency is then acquired

and used for the EMS power flow simulation. Finally, all fuel rate, consumption and generated electric power are sent to the signal processing modal for reward calculation and fuel consumption analysis.

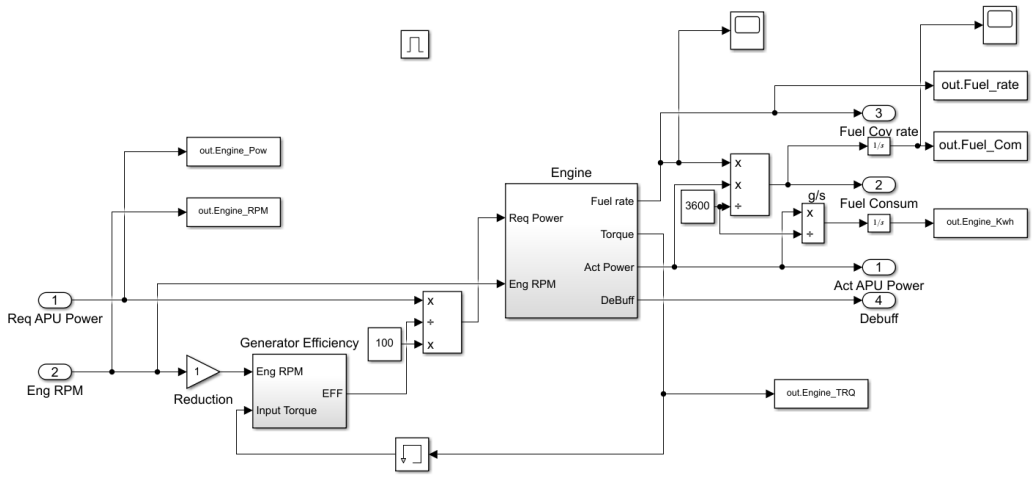

Figure 5.9 APU model.

To guarantee simulation precision, the Simulink models are subject to strict constraints. The dynamic limitation of the traction motor can be expressed by:

$$\begin{cases} -\omega_{min} \le \omega_{mot} \le \omega_{max}; \\ -P_{mot\_min} \le P_{mot}^{mode} \le P_{mot\_max}; \\ -T(\omega)_{min} \le T(\omega) \le T(\omega)_{\max}; \end{cases} \tag{5.1}$$

while

$$mode = \begin{cases} 1, P_{mot}^{mode} = T_{mot}\omega_{mot}/(9550 * \eta); \\ 0, P_{mot}^{mode} = 0; \\ -1, P_{mot}^{mode} = T_{mot}\omega_{mot}\eta/9550 \end{cases} \tag{5.2}$$

where mode stands for the traction motor operating mode, P_{mot}, T_{mot}, ω_{mot}, η are the motor power, torque, rotational speed, efficiency, respectively.

Then, the following constraints of the battery are:

$$\begin{cases} SOC_{tem}^{avl} = \dfrac{(SOC_{tem}^{abs} - SOC_{abs\_min})}{(SOC_{abs\_max} - SOC_{abs\_min})}; \\ SOC_{abs\_min} \le SOC_{abs}^{Tem} \le SOC_{abs\_max}; \\ Tem_{min} \le Tem_{bat} \le Tem_{max} \end{cases} \tag{5.3}$$

where SOC_{tem}^{avl} stands for the energy level to the available capacity, and SOC_{tem}^{abs} stands for the energy level of the absolute battery capacity. Tem_{bat} is the battery cell temperature.

The APU (engine and the ISG) is subject to:

$$\begin{cases} \omega_{idle} \le \omega_{eng} \le \omega_{max}; \\ 0 \le P_{eng} \le P_{ISG}/\eta_{ISG}; \\ T_{idle\_load} \le T(\omega)_{eng} \le T(\omega)_{\max}; \end{cases} \tag{5.4}$$

In here, the desiel engine RPM boundary is from 1200 to 3300, 1200 is the idle RPM.

5.3 Multi-target optimization and environment

A comprehensive observation of the state is required for the agent to have a clearer view of the environment [237]. The observation vector is listed in Eqation 5.5:

$$State = \{v, a_v, SOC, P_{req}, C_{rate}\} \tag{5.5}$$

which are the vehicle velocity, acceleration, battery SOC, vehicle power demand and battery discharge rate, respectively. The velocity, acceleration and power demand reflect the motion status of the vehicle, while the SOC and C_{rate} reveal the vehicle power management condition.

For ERLV charging strategy, the controlled object is the APU itself. The RL agent is programmed to output action to control the APU performance. From the existed studies [101, 104, 234], discrete values of engine power adjustment were commonly selected as their only action for the RL agent. These studies also selected an engine optimal operation curve based on specialist experience. However, when the engine follows the operation curve, both engine torque and speed will increase at the same time, which may be hard to achieve in real-world operations. An improvement is

proposed in this study by adopting continuous multi-actions in the action space. Both the engine power P_{eng} and the engine speed n_{eng} are selected as the continuous actions so that the APU can be controlled with high stability:

$$Action = \{P_{eng}, n_{eng}\} \tag{5.6}$$

with the ranges of:

$$P_{eng} \rightarrow [3, 72]\ (kW), \qquad n_{eng} \rightarrow [1200, 3300](r/min)$$

where the engine power range is from 3 kW to 72 kW, and its operating speed is from 1200 to 3300 r/min. The engine is no longer required to follow a fixed operation curve and it is allowed to explore more possible operation points under different engine speeds; and more exploration for the agent will lead to better fuel efficiency [238].

The multi-objective reward function of the RL platform consists of three elements, fuel consumption, SOC constraint and battery charge constraint.

For fuel consumption, the target is to maintain a high engine efficiency during the CS period; hence the instant fuel conversion rate (g/kWh) is selected as one of the reward variables. The SOC constraint adopts the square of the value difference between the state SOC and the desired SOC.

To take battery charging protection into consideration, a battery C-rate limitation is employed as one of the RL reward factors to extend the battery lifespan. This battery capacity fading factor K_{deg} reflects the percentage of battery degraded capacity Q_{loss} and initial capacity Q_{int} using the following equation:

$$K_{deg} = \frac{Q_{int} - Q_{deg}}{Q_{int}} \tag{5.7}$$

According to the empirical model from [239], the battery capacity degradation degree varies significantly with different SOC and C-rates. The variation of the capacity fading factor is shown in Figure 5.10.

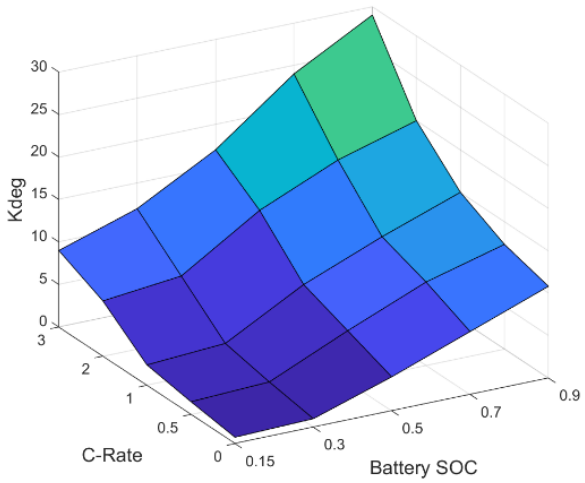

Figure 5.10 The capacity fading factor with different SOC and C-rates.

Now, combining the above elements, the immediate reward calculation can be defined as:

$$Reward = -\left\{\alpha \cdot Frate(t) + \beta \cdot \left[SOC(t) - SOC_{ref}\right]^2 + \varphi \cdot Crate \cdot K_{deg}(SOC_t, C_{rate})\right\} \quad (5.8)$$

where α, β, φ are the weights, $Frate(t)$ is the instant fuel conversion rate (minus baseline), $SOC(t)$, SOC_{ref} are the battery SOC in state (t) and target SOC, respectively. The corresponding Simulink signal route can be seen in Figure 5.11.

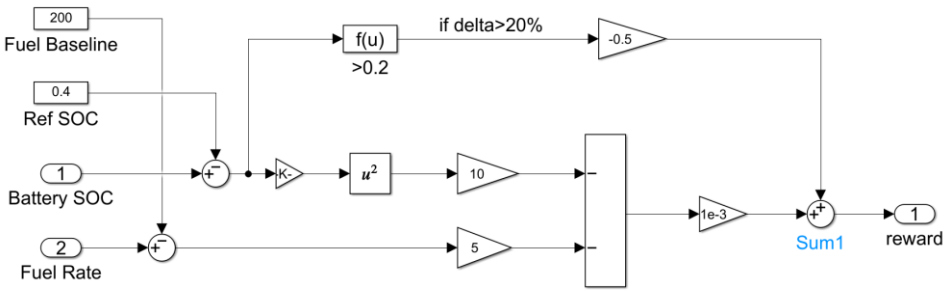

Figure 5.11 The reward calculation.

5.4 Reinforcement learning algorithm

The over-all goal of a reinforcement learning algorithm is to learn an optimal or nearly-optimal policy which can maximize the accumulated reward from the interacted environment. In other words, an optimal objective function π^* is the training target that represents the RL policy and responses to the every state signal from the environment. The agent thrives to find a balance between the exploration and exploitation in each training episodes.

In order to solve the high-dimensional problem with the state, the latest RL algorithms have combined Deep learning to improve their ability to input/output large data. This kind of improved RL algorithms is called Deep reinforcement learning. The artificial Neural network is utilized to transfer the input into labelled datasets, and in this case, it processes the vehicle states and rewards through a series of fully-connected layers and activation layers to generate an estimated value for the agent. It replaces the traditional Q-table used in Q learning.

A more matured RL structure called Actor-Critic (AC) is also utilized in this study. It combines the advantages of the Policy gradient and the function approximation. Compared with traditional actor updates of the policy gradient methods, the actor of Actor-Critic methods can be updated more efficiently by steps. A fundamental structure of AC is illustrated in Figure 5.12. It consists of two parts that are parameterized with neural networks: Actor and Critic. The Critic is used to estimate the value function of the algorithm, and it can assist the policy to learn with more accurate results. The estimated value function can be the Q value and the V value, but in an algorithm like the improved SAC, only the Q value function is estimated to lower the computational load. The Actor network, on the other hand, is used as

the policy distribution for the agent action space. It samples agent control signal(s) a' from policy $\pi_\theta(a'|s')$ to interact with the environment. After getting the reward feedback, the Critic parameter is used to update the policy parameter from the Actor network can be updated with the suggestion from the Critic.

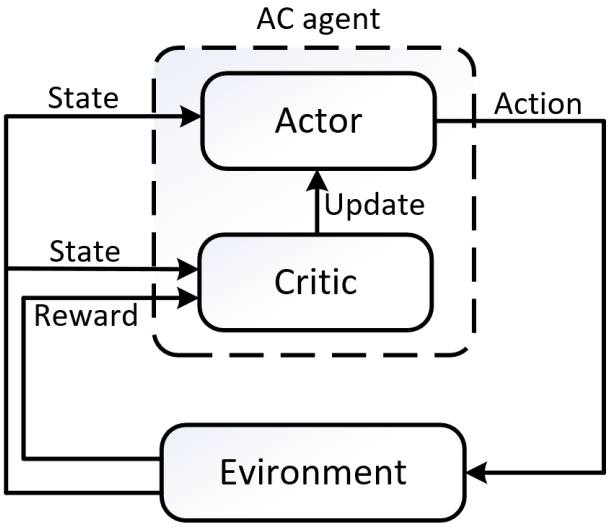

Figure 5.12 Structure of the Actor-Critic algorithm.

In the following study, two DRL algorithms using actor-critic structure are selected for the ERLV EMS, and their control results are tested and compared. The first DRL algorithm is called Deep Deterministic Policy Gradient (DDPG), which is one of the most representative and popular algorithms in the RL study. It is a deterministic algorithm combining the technologies from Deterministic Policy Gradient (DPG) and DQN (Deep Q Network), such as the ability to output continuous action spaces and high sampling efficiency with the experience replay buffer. The other algorithm is called Soft Actor-Critic (SAC) that achieves state-of-the-art performance. Unlike DDPG, it is a stochastic algorithm with off-policy learning. The improvements are made by adding entropy to the value function for better exploration; a clipped double-Q trick and target policy smoothing function guarantee the stability of the value estimation. These techniques from SAC are

especially suitable for vehicle EMS with wide action space and great uncertainty. The theoretical introduction and mathematical derivation of the two DRL algorithms are introduced in detail.

5.4.1 DDPG algorithm

DDPG is the iconic deterministic DRL algorithm with an actor-critic structure that supports continuous action spaces. DDPG is based on the previous algorithm DPG proposed in 2014 [240], and its action in each state is determined by

$$a_{\mathrm{t}} = \mu\left(s_t|\theta_\mu;\right) \tag{5.9}$$

where a_{t} is the action taken by the agent, function μ is the current optimal policy, s_t and θ_μ stand for the environment state and parameter of μ.

In order to improve the sampling efficiency and handle more complicated state observations, techniques from DQN such as experience replay buffer and target Q network are combined with DPG. There are four networks in the form of DDPG: Critic network Q_θ, Actor network μ_∂ and the two target networks Q_θ , $\mu_{\bar{\partial}}$.

The operation pattern of the DDPG algorithm is demonstrated in Figure 5.13.

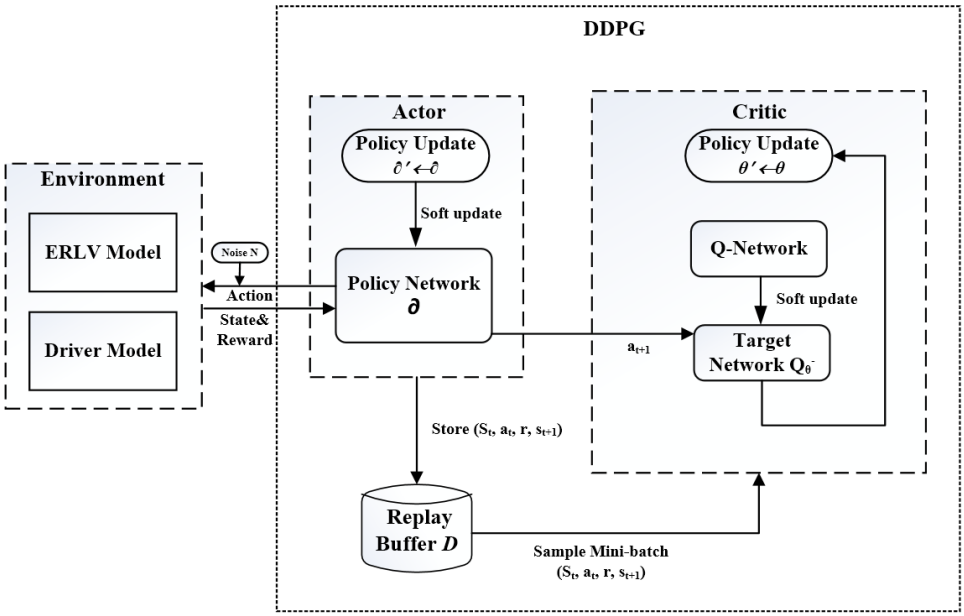

Figure 5.13 System diagram of the DDPG-based EMS.

During the agent training process, the Actor network μ_∂ generates a determined action space according to the current state. However, there is hardly any exploration for the agent to search for any better action in this state. To solve this issue, DDPG adds noise to the determined action to increase randomness. The type of noise can be Uhlenbeck-Ornstein noise, Gaussian noise or other uncorrelated random noises. It is also worth mentioning that the noise is only utilized during the training stage, only determined action from the Actor network μ_∂ is adopted during agent evaluation and testing.

The traditional Q value function can be deduced using Bellman equation after knowing the next action at state s_t:

$$Q(s_t, a_t) = E_{s_t \sim D}\left[r(s_t, a_t) + \gamma Q\left(s_{t+1}, \mu(a_{t+1})\right)\right] \tag{5.10}$$

where r is the state reward of s_t when taking action a_t. However, the Q value estimation in DDPG is operated on the Q neural network Q_θ which is similar to the DQN algorithm, and it is being trained using the experience replay technique. An objective function y_i in Equation 5.11 needs to be maximized to achieve the highest expectation of the Q value.

$$y_i = r_i + \gamma \bar{Q}\left(s_{i+1}, \bar{\mu}\left(s_{i+1}|\bar{\theta}_\mu\right)|\bar{\theta}_Q\right) \tag{5.11}$$

where i is the states sequence of the sampled minibatch and the $\bar{\theta}_Q$, $\bar{\theta}_\mu$ are the weights of the two target networks. Using the target network for estimation can help stabilize the Critic learning process.

To maximize y_i, a loss function for the Critic can be defined using the error of its squared mean:

$$J(\mathrm{Q}) = \frac{1}{N}\sum_{i}\left(y_i - Q\left(s_i, a_i|\theta_Q\right)\right)^2 \tag{5.12}$$

In the meantime, the Loss function of the Actor network can be described as:

$$J(\mu) = -\frac{1}{N}\sum_{i} Q\left(s_i, a_i|\theta_Q\right) \tag{5.13}$$

Because the data is sampled from the replay buffer, the expectation of the policy can be seen as an un-biased estimation, and the Actor network can be updated by performing gradient of θ_μ on the performance objective:

$$\nabla_{\theta_\mu} J_\beta(\mu) \approx -\frac{1}{N}\sum_{i}\left(\nabla_a Q\left(s, a|\theta_Q\right)|_{s=s_i, a=\mu(s_i)} \cdot \nabla_{\theta_\mu}\mu_\theta\left(s|\theta_\mu\right)_{s=s_i}\right) \tag{5.14}$$

where β represents the distribution function parameter, and the Q function is decomposed into the action gradient times the policy gradient by applying the chain rule.

The online Critic and Actor networks are self-updated in each gradient step using their learning rate, with the purpose of minimizing the loss function and policy gradient. The learning rate value is commonly selected from 0.1 to 10^{-5} for favourable training performance [241]. A small learning rate will bring higher training stability, but it may also lead to a longer training time.

After that, the two target networks are updated using the soft update method to stabilize the training parameters. The soft updates are performed using:

$$\begin{aligned} \bar{\theta}_Q &\leftarrow \tau\theta_Q + (1-\tau)\bar{\theta}_Q \\ \bar{\theta}_\mu &\leftarrow \tau\theta_\mu + (1-\tau)\bar{\theta}_\mu \end{aligned} \tag{5.15}$$

where τ is the smoothing factor, and the target values are constrained to change slowly according to the online values. This method significantly improves the stability of the training for unstable problems. The simplified algorithm of DDPG is listed in Table 5.1 with the hyperparameters shared in Table 5.2.

Table 5.1 DDPG Algorithm.

Algorithm 1 DDPG algorithm

Input: θ_Q, θ_{μ}

Initialize target network weights $\bar{\theta}_Q \leftarrow \theta_Q$, $\bar{\theta}_{\mu} \leftarrow \theta_{\mu}$,

Initialize replay buffer pool $D \leftarrow \emptyset$

for each iteration **do**

Initialize random noise N adding to action

Acquire initial observation s_0

for each sample step **do**

Sample action $a_t = \mu(s_t|\theta_\mu) + N_t$ from the policy with noise

Store the generated environment transition (s_t, a_t, r, s_{t+1}) in pool D

Sample random minibatch with N steps from pool D, $i \in N$

Calculate the target Q-function of the sampled minibatch: $y_i = r_i + \gamma\bar{Q}(s_{i+1}, \mu(s_{i+1}|\theta_{\mu})|\theta_Q)$

Update Critic θ_Q by minimizing the loss $J(\mathrm{Q}) = \frac{1}{N}\sum_i \left(y_i - Q(s_i, a_i|\theta_Q)\right)^2$

Update Actor θ_{μ} with policy gradient method:

$$\nabla_{\theta_\mu} J_\beta(\mu) \approx -\frac{1}{N}\sum_i \left(\nabla_a Q(s, a|\theta_Q)|_{s=s_i, a=\mu(s_i)} \cdot \nabla_{\theta_\mu}\mu_\theta(s|\theta_\mu)_{s=s_i}\right)$$

Update target networks: $\bar{\theta}_Q \leftarrow \tau\theta_Q + (1-\tau)\bar{\theta}_Q$

$\bar{\theta}_{\mu} \leftarrow \tau\theta_{\mu} + (1-\tau)\bar{\theta}_{\mu}$

end for

end for

Table 5.2 Hyperparameters of the DDPG agent.

parameters	Value	parameters	Value
Critic learn-rate	1×10^{-3}	Target smooth factor	1×10^{-3}
Actor learn-rate	1×10^{-4}	Discount factor γ	0.95
Mini-batch size	128	Sample time (s)	1
Experience buffer length	1×10^{6}	Explore noise	0.1

5.4.2 SAC algorithm

SAC algorithm is a model-free off-policy stochastic algorithm that can be used with continuous action spaces. Entropy is added to the expected return to increase stochasticity. It integrated the clipped double-Q trick and Soft Q function, which was proved to achieve a more stable estimation of the critic function [242]. The overall framework of the SAC-based EMS is present in Figure 5.14.

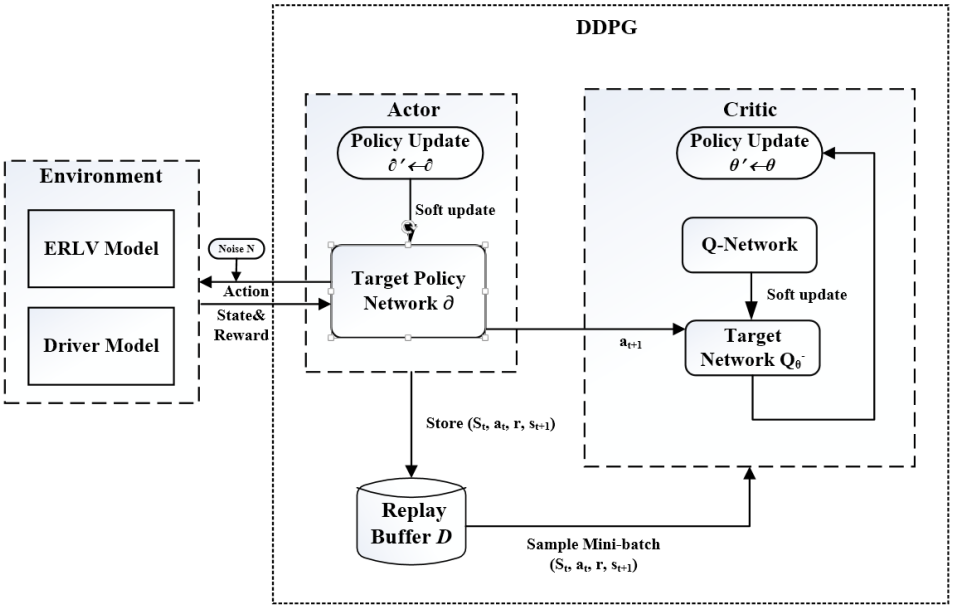

Figure 5.14 System diagram of the SAC-based EMS.

The aim of reinforcement learning is to learn a policy π that maximizes the objective in the training episode. The SAC algorithm improves the traditional objective function by adding an entropy factor with the expected reward, which forces the agent to operate randomly. Its objective function can be described as:

$$\pi^* = arg\max_{\pi} \sum_{t=0}^{K} E_{(s_t,a_t)\sim\rho_\pi}\left[r(s_t,a_t) + \alpha H(\pi(.|s_t))\right] \tag{5.16}$$

where the ρ_π is marginals of the state-action distribution, $H\big(\pi(.|s_t)\big)$ is the entropy objective regarding the policy, and α is the entropy temperature coefficient.

For the continuous domain of the algorithm, the SAC soft policy iteration should be conducted using approximations for the soft Q-value evaluation and improvement. The Q-function $Q_\theta(s_t,a_t)$ and policy $\pi_\partial(.|s_t)$ are approximated using two different neural networks. In addition, the automating adjustment of the temperature coefficient α from Ref. [236] is employed in this paper. This method improves the stability of the SAC training by varying α over the training process,

so the improved SAC algorithm only needs to optimize the Q-value function and the policy with the gradient descent method.

The policy evaluation is conducted using the soft Q-function. The soft Bellman residual can be calculated by

$$J_Q(\theta) = E_{\ s_t, a_t \sim D}\left[\frac{1}{2}(Q_\theta\ s_t, a_t\ - \left(\left(r\ s_t, a_t\ \right) + \gamma E_{s_{t+1}\sim p}[V_\theta\ s_{t+1}\ ]\right)^2\right] \quad 5.17$$

where D represents the distribution of the sampled replay buffer. The parameter $\bar{\theta}$ is acquired using the exponential moving average of the Soft Q-function [243], while $V_{\bar{\theta}}(s_{t+1})$ can be replaced and iterated using Equation 5.18

$$V_{\bar{\theta}}(s_t) = E_{a_t\sim\pi}[Q_{\bar{\theta}}(s_t, a_t) - \alpha \log \pi(a_t|s_t)] \quad (5.18)$$

where the action a_t is sampled from the policy. In here, the double-Q network framework is used to avoid overestimation that the minimum Q-function is selected for the gradient calculation.

The policy improvement is performed after evaluation with the help of the Q-value function. The exponential of a new soft Q-function is used during the policy improvement in the Kullback-Leibler (KL) divergence. The KL divergence measures the distance between the soft Q-function and $\pi_\partial(.|s_t)$, and the policy update approximation can be conducted by minimizing

$$J_\pi(\partial) = D_{\mathrm{KL}}\left[\pi_\partial(.|s_t)||\frac{exp\left(\frac{1}{\alpha}(Q_\theta(s_t,.)\right)}{Z(s_t)}\right] \quad (5.19)$$

with deformation calculation

$$J_\pi(\partial) = E_{s_t\sim D, a_t\sim\pi_\partial}\left[\log \pi_\partial(a_t|s_t) - \frac{1}{\alpha}(Q_\theta(s_t, a_t) + \log Z(s_t)\right] \quad (5.20)$$

where the partition function $Z(s_t)$ is a constant that can be ignored during the gradient step. The reparameterization trick is applied to the policy neural network, and the action of the policy can be described as

$$a_{\mathrm{t}} = y_{\partial}(\omega_t; s_t) \tag{5.21}$$

Where ω_t is the noise variable. In this case, the neural network of the policy converts the state input to an action of a Gaussian distribution with mean and standard deviation.

By combining Equation 5.20 and 5.21, the final target function of the policy can be described

$$J_{\pi}(\partial) = E_{s_t \sim D}[\alpha \log \pi_{\partial}(y_{\partial}\ \omega_t; s_t\ |s_t) - Q_{\partial}(s_t, y_{\partial}\ \omega_t; s_t\ )] \tag{5.22}$$

Finally, the SAC policy estimation and improvement can be performed using Equation 5.17 and 5.22 in each gradient step. The simplified coding of the SAC algorithm is described in Table 5.3.

Table 5.3 SAC Algorithm.

Algorithm 2 Soft Actor-Critic with Auto-tuned Entropy Weight

Input: θ_a, θ_b, ∂

Initialize target network weights $\bar{\theta}_a \leftarrow \theta_a$, $\bar{\theta}_b \leftarrow \theta_b$,

Initialize replay buffer pool $D \leftarrow \emptyset$

for each iteration **do**

for each sample step **do**

Sample action from the policy $a_t \sim \pi_\partial \ a_t|s_t$

Sample environment transition $s_{t+1} \sim p \ s_{t+1}|s_t, a_t$

Store sampled transition (s_t, a_t, r, s_{t+1}) in pool D

end for

for each gradient step **do**

Update Q-function $\theta_i \leftarrow \theta_i - \varphi_Q \widehat{\nabla}_{\theta_i} J_Q \ \theta_i \ , \ i \in \{a, b\}$

Update Policy $\partial \leftarrow \partial - \varphi_\pi \widehat{\nabla}_\partial J_\pi(\partial)$

Entropy self-adjustment $\alpha \leftarrow \alpha - \varphi \widehat{\nabla}_\alpha J(\alpha)$

Update target network $\theta_i \leftarrow \tau\theta_i + \ 1 - \tau \ \theta_i, \ i \in \{a, b\}$

end for

end for

The neural network frameworks for SAC are demonstrated in Figure 5.15, where the number of nodes in the fully connected layers decreases from 256 to 128. After multiple trial improvements on the algorithm and the NN, the hyperparameters for the SAC agent are chosen and shared in Table 5.4 to achieve a fast and stabilized performance. A single driving cycle simulation is set as a training episode until the rising battery SOC exceeds the charge-sustain threshold.

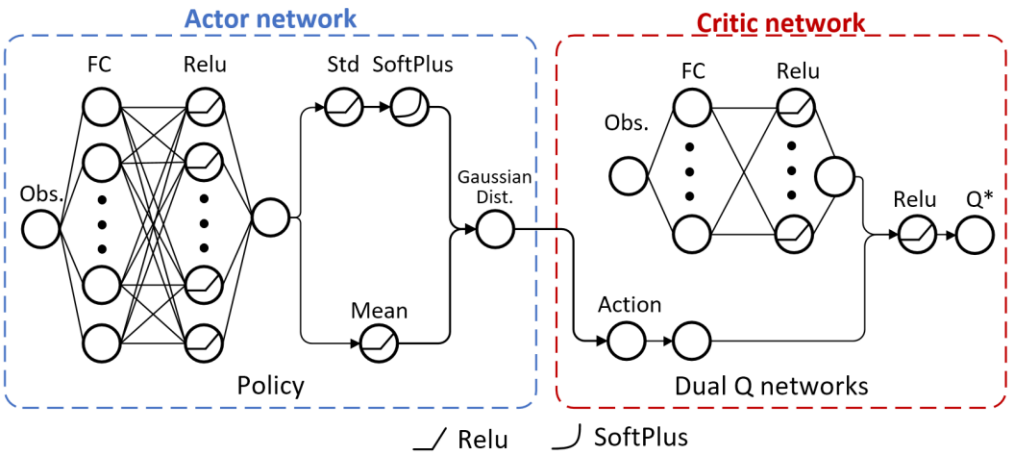

Figure 5.15 Architecture of the neural networks.

Table 5.4 Hyperparameters of the SAC agent.

parameters	Value	parameters	Value
Critic learn-rate	3×10^{-4}	Target smooth factor	1×10^{-3}
Actor learn-rate	3×10^{-4}	Discount factor γ	0.95
Entropy learn-rate	3×10^{-4}	Sample time (s)	1
Target entropy	-2	Mini-batch size	128
Initial entropy weight	0.5	Experience buffer length	1×10^{6}

5.5 Pre-training process

According to the environment design and pre-set hyperparameters of the SAC agent, the RL training process was conducted. The total RL training episode was set as 500 with 1800 steps in each episode. At the beginning of each episode, a local reset function is activated to randomize the initial battery SOC and input driving cycle to encourage agent exploration. The WLTC-3b or CLTC-C are the two random driving cycles, and the initial battery SOC is randomized within the range [0.1, 0.4]. For agent performance comparison, a DDPG agent was also trained with the same default values. In addition, the DP global optimization for the ERLV was also carried out, which is used as the benchmark to compare with the results from the two RL agents.

A converged accumulated reward suggests that the RL agent may be ready to deploy. In Figure 5.16, the visualized convergence performances of the SAC and DDPG algorithms are demonstrated. Both of the RL algorithms successfully converged within 500 episodes, but their convergence pattern diverse differently. The convergence points of SAC and DDPG were at approximately 240 and 380 episodes, proving the fast performance of SAC. For a closer look, the accumulated reward variation of the SAC quickly verged to a stable range since the beginning of the training, while the DDPG spent quite an effort to settle. It can be explained that

the DDPG needs more training episode to learn because of its poor exploration ability and instability [244]. On the contrary, the SAC algorithm improves these imperfections by adding policy uncertainty using the maximum entropy method, and the clipped double-Q trick on the soft value function mitigated the impact from over-estimation. These allow the agent to grope for the action-reward patterns in a short time.

Apart from the convergence speed, there is also a difference in the convergence quality. DDPG has the tendency to converge to a bad or non-optimal solution due to hyperparameter sensitivity; and as a deterministic policy, its exploration performance is limited by adding random noise to the action. SAC, as a stochastic policy, can guarantee more exploration of the environment. In this study, the convergence quality can be revealed by their episode reward after convergence. The SAC episode reward range was [-318, -733] while the DDPG was [-643, -950], suggesting the SAC agent has a better control quality on the ERLV charging management.

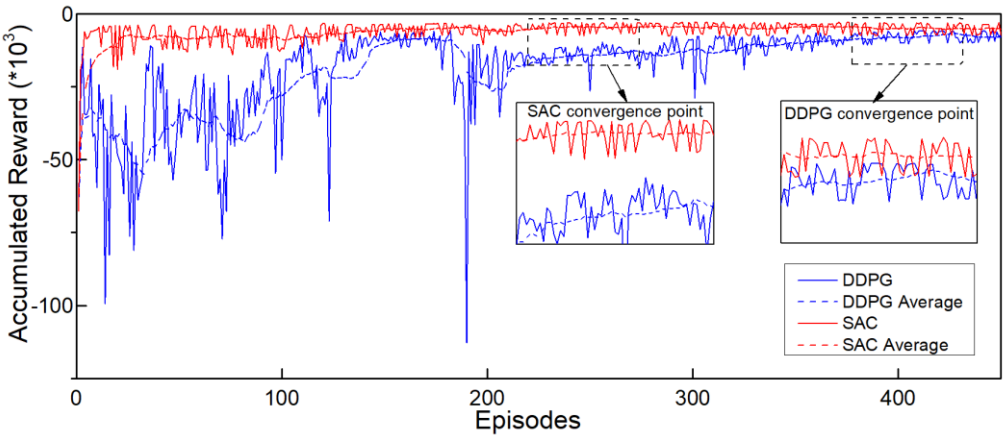

Figure 5.16 The reward convergence performance of SAC and DDPG.

5.5.1 Agent implementation

Once the qualified agents are selected, they can be used to interact with the environment for real-time performance testing. To begin with, the rationality of the APU control signal should be checked because the engine power output and rotational speed should not be fluctuating. For example, a comparison of the SAC agent control signals before and after convergence is shared in Figure 5.17. Different from the converged SAC result, the engine output power and speed from the early phase SAC agent (on the left) are unstable and disordered. Although the episode reward is not high, the control signal of this early agent is not exercisable on any engine.

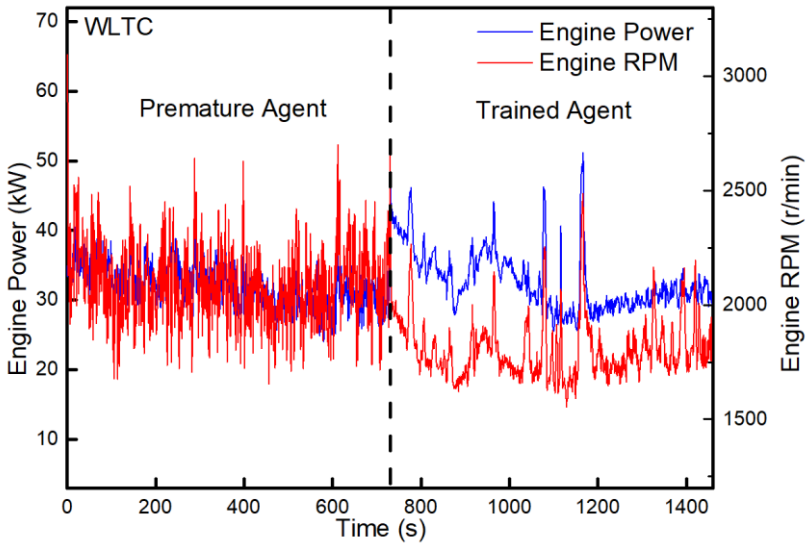

Figure 5.17 The engine operation samples of the premature/trained SAC agent.

The trained SAC agent was tested in Simulink on a Windows PC. The simulating time is approximately 6 seconds for CLTC-C (30 mins), which means the SAC agent only needs 1/300 second to process the signal and make decision in real time with an Intel I7-8750H processor (6 cores, Turbo up to 4.1 GHz).

5.6 Result analysis

After the RL training process, the converged SAC agent is examined and the power flow results of the APU and battery are shown in Figure 5.18. The engine is kept operational during the CS mode, supplying power to both the traction motor and battery. For high power demand, the battery may also work as the secondary power source to assist the APU in the CS mode. The two figures also show a negative correlation between the engine power and battery SOC; the engine power value starts from around 60 kW and it gradually drops to around 40 kW. This indicates the SAC agent is trying to quickly recharge the battery at a low SOC level as it does less harm to the battery health.

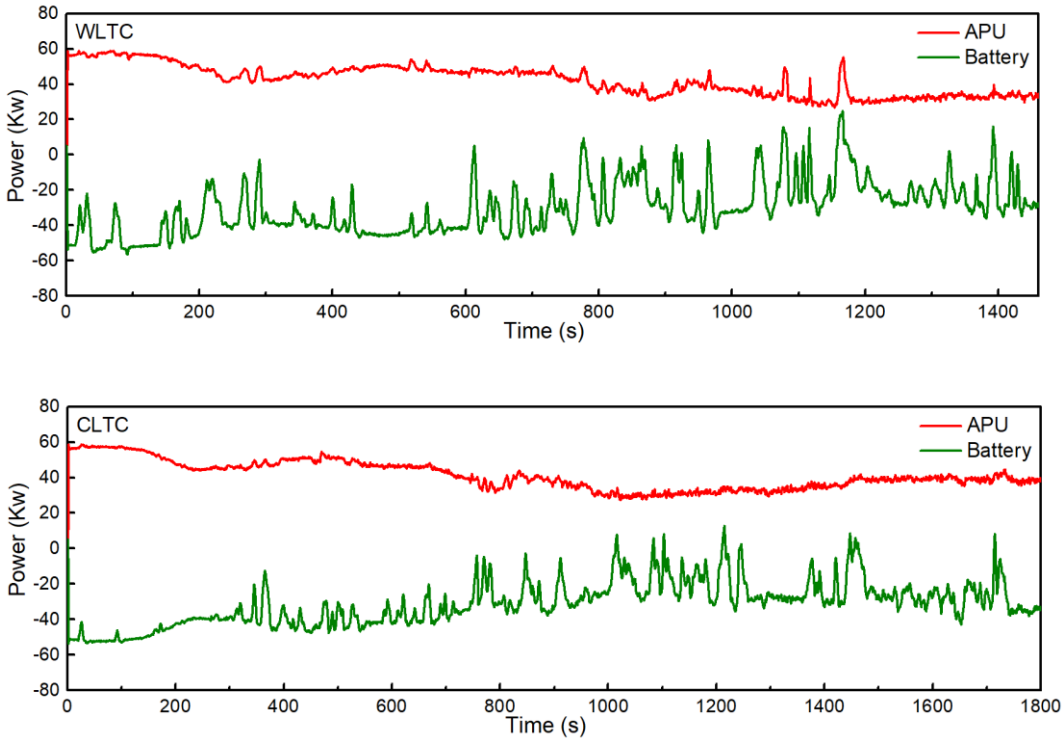

Figure 5.18 The power output of the engine and battery with the SAC agent.

After that, the conditions of the SOC trajectory, battery C-rate and fuel consumption are assessed as the quality factors of the agent performance. In Figure 5.19, the SOC trajectories of the SAC and DDPG agents during two driving cycles are plotted

against their DP results. It can be observed that both RL agents satisfied the essential requirement in the CS operation, while the SAC algorithm charges the battery more quickly to a high SOC in a short time. It is also worth mentioning that the SOC trajectories under the SAC agent's control are steeper than that of DDPG at low SOC conditions. The reason for that can be revealed by the battery C-rate in the performance tests in Figure 5.20. The battery C-rate trend using the SAC agent is more aggressive than that of DDPG at a low SOC level, showing a faster charging speed of the battery. As the battery SOC gradually goes up, the C-rate of SAC effectively reduces to alleviate battery degradation. From the above, the SAC agent outperforms DDPG by providing faster charging ability and battery protection.

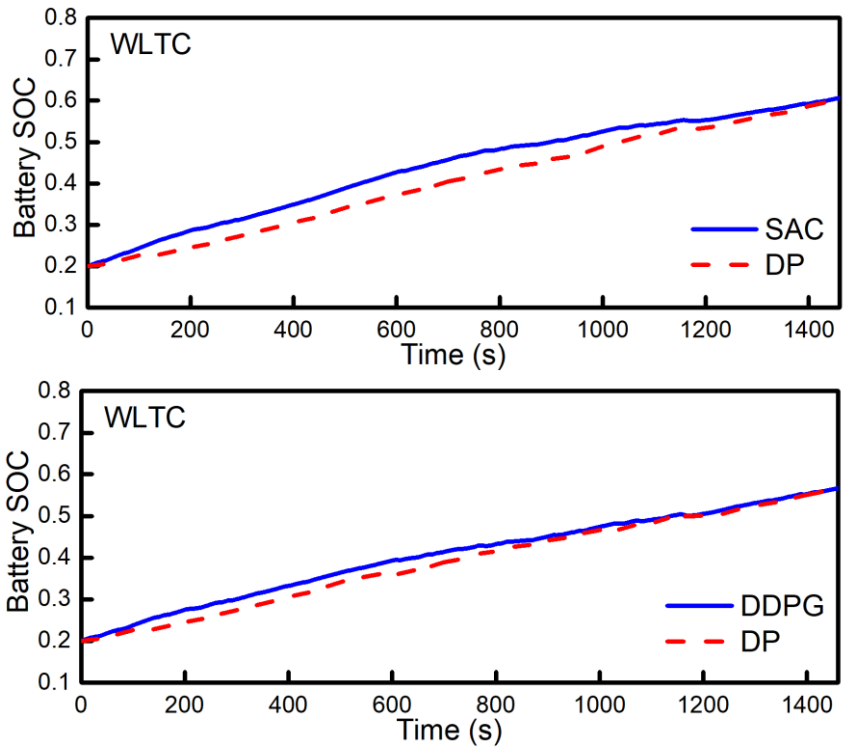

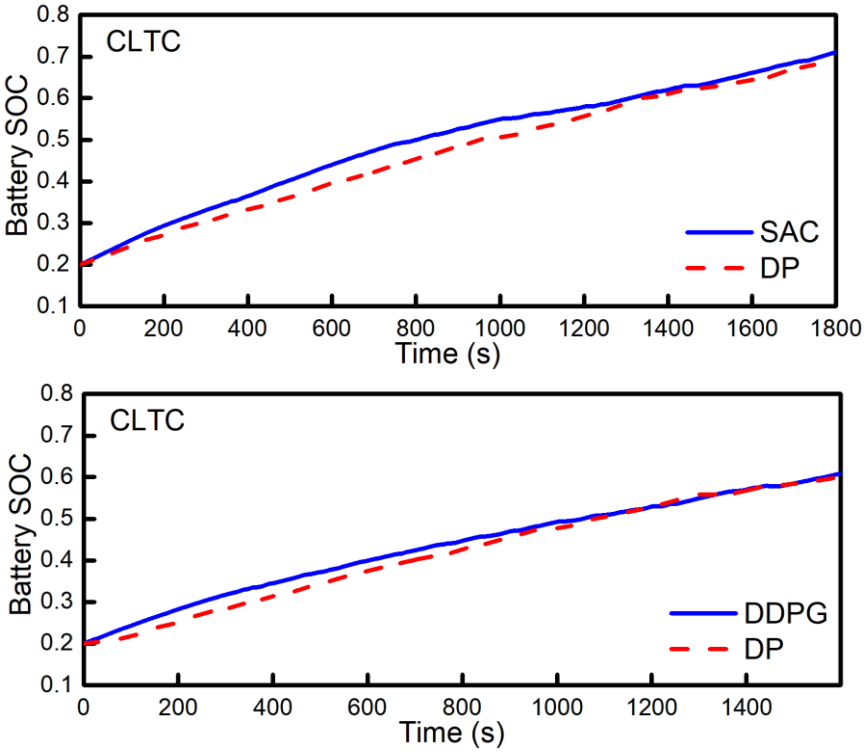

Figure 5.19 The battery SOC trajectories.

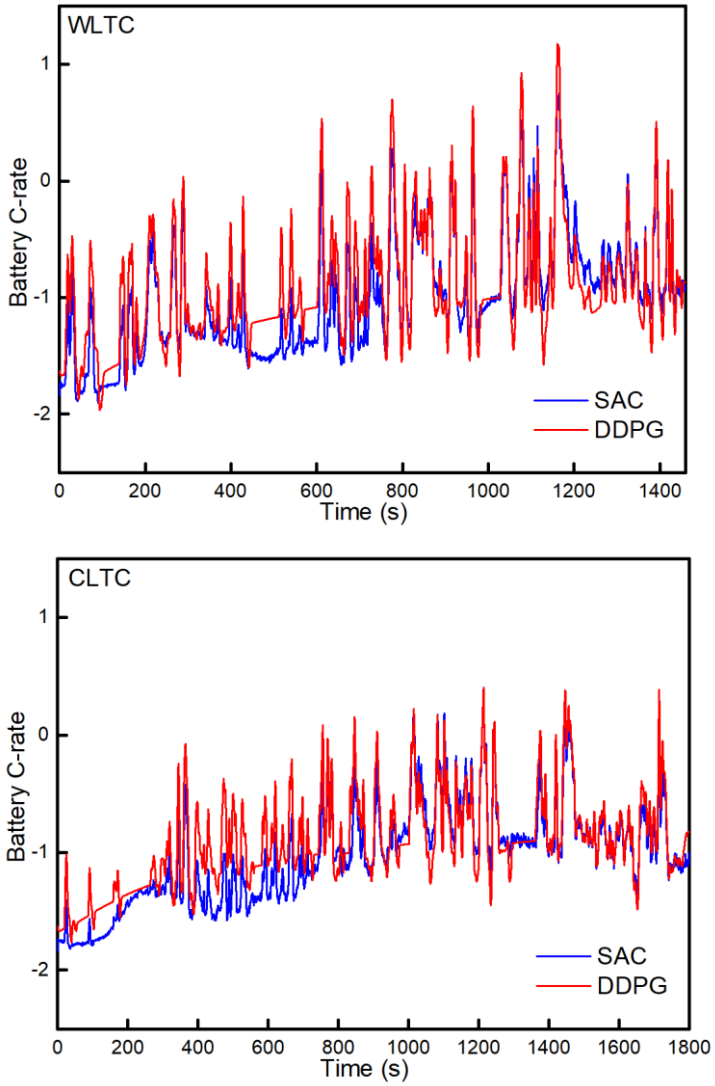

Figure 5.20 The transient battery C-rate comparisons.

The average fuel conversion rates of the SAC, DDPG and DP in WLTC are 212.9 g/kWh, 215.3 g/kWh and 212.1 g/kWh, respectively. The engine working points of SAC and DDPG are shared in Figure 5.21 for demonstration. It can be observed that most of the working points are located in the engine optimal fuel consumption areas. However, the operation points of DDPG tend to gather at the low engine speed area with larger fuel rates, which leads to higher fuel consumption. The specific fuel consumption results are shared in Table 5.5. According to the data, SAC has a 3% improvement in fuel efficiency compared with DDPG, and it achieves 95.1% and 94% of its optimal DP performance. Further analysis of

estimated fuel consumption and energy cost is shared in Table 5.6. In this case, the algorithm robustness is retested under some unfamiliar typical driving cycles. The ERLV is expected to drive 200 km per day in the analysis. The 2021 average diesel price is approximately $11.92 per litre, while the electricity price is $0.115 per kWh [188]. The electricity cost is the expense of Grid-to-Vehicle charging during night time, by which the battery is recharged from terminal SOC to full. According to the test, the average fuel consumption in 200 km using SAC and DDPG are roughly 12.82 L and 13.21, which achieves around a 3% saving on the fuel cost.

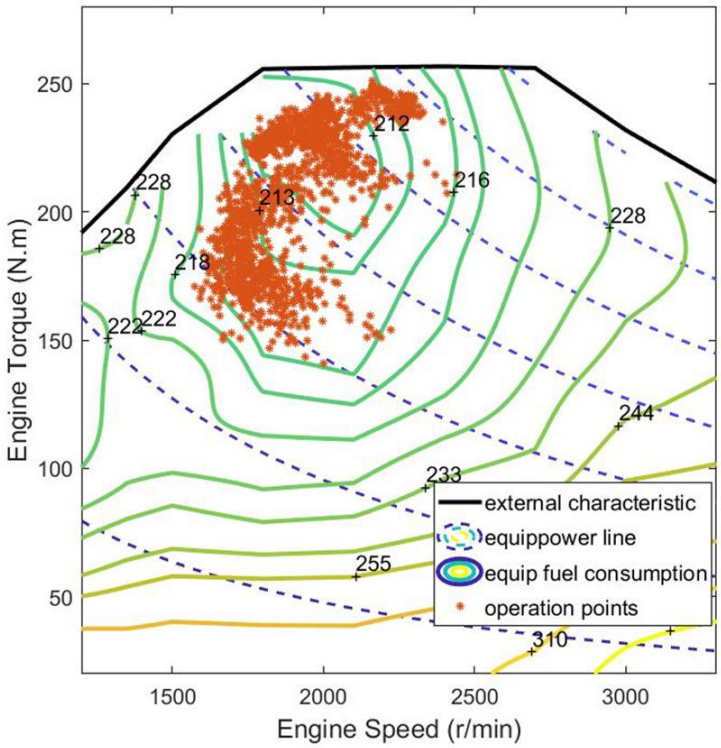

(a) SAC

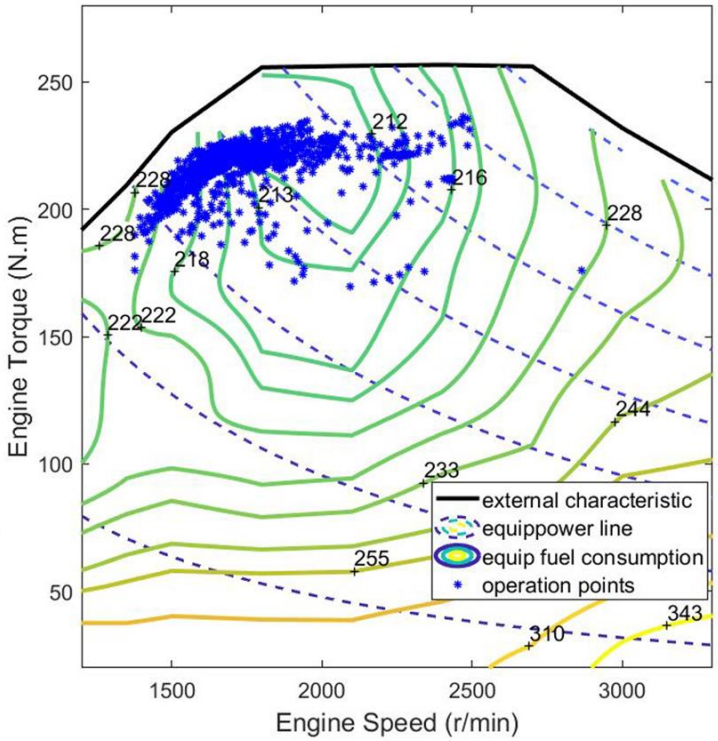

(b) DDPG

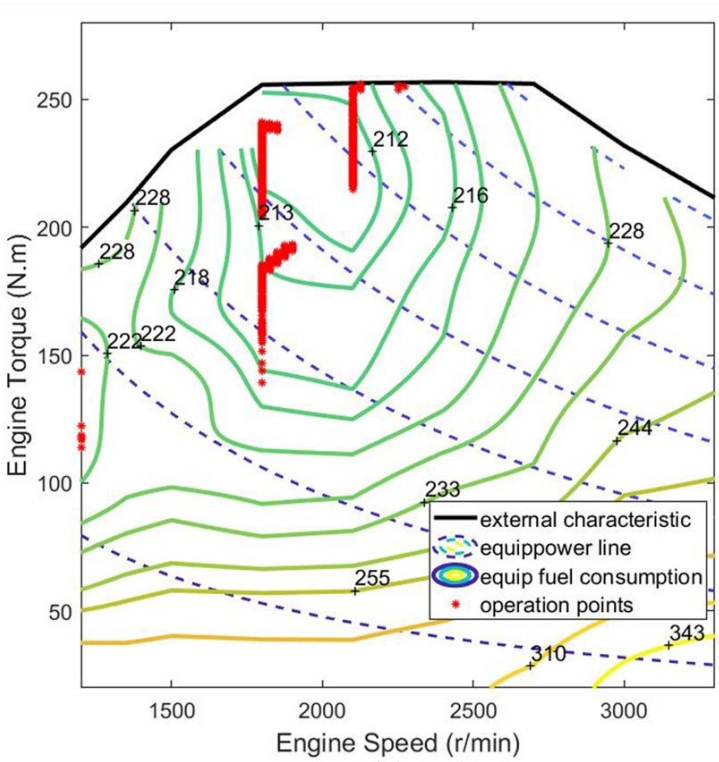

(c) DP

Figure 5.21 Engine operation points using different algorithms.

Table 5.5 Results of the fuel consumption and SOC variation.

Agent	Driving Cycle	Terminal SOC	RL Fuel Consumed (L)	DP Fuel Consumed (L)	DP Benchmark
SAC	CLTC	0.7	5.26	5	95.1%
	WLTC	0.606	4.37	4.11	94%
DDPG	CLTC	0.655	4.88	4.52	92.5%
	WLTC	0.567	4.09	3.72	90.9%

In summary, the EMS strategy itself should be robust and stable enough to interfere with the complex powertrain and road environment for real-world applications. The simulation result proves SAC a practicable solution by outrunning DDPG with faster convergence speed and higher stability to random conditions.

Table 5.6 Fuel consumption and energy cost comparison when reaching 200 km.

Driving cycle	Algorithm	Fuel cons. (L)	Terminal SOC	Fuel cost (US $)	Elec. cost (US $)
WLTC	SAC	12.42	0.45	148.05	1.94
	DDPG	13.49	0.55	160.8	1.58
CLTC	SAC	11.42	0.42	136.13	2.04
	DDPG	12.30	0.5	146.62	1.76
FTP75	SAC	13.62	0.48	162.35	1.83
	DDPG	12.89	0.35	153.65	2.29
NEDC	SAC	11.6	0.43	138.27	2.01
	DDPG	12.53	0.52	149.36	1.69
UDDS	SAC	15.07	0.57	179.63	1.51
	DDPG	14.86	0.5	177.13	1.76

5.7 Chapter summary

This chapter has proposed a self-learning APU charging control strategy for an ERLV using a state-of-the-art RL algorithm. The Soft Actor-Critic method with maximum entropy function is employed to maximize a trade-off between reward and exploration. It outputs continuous control signals of the optimized engine power and rotational speed, which is more suitable for real-world application compared with the optimal brake specific fuel consumption (BSFC) curve methods.

For the RL environment setting, the battery charging protection with C-rate limitation is deployed for the fir1st time in the RL training process to extend the battery lifespan. A reset function for the initial environment states is enabled to increase RL training randomness. The DDPG and DP algorithms are also put to use as benchmarks to compare with the performance of the proposed SAC agent.

The simulation results show a successful deployment of the RL algorithms and the construction of the RL environment. According to the training outcomes, the SAC algorithm quickly converged with a 36% efficiency boost compared with DDPG. For performance testing, SAC efficiently controls the APU to charge the battery and raised the SOC from 20% to 70% and 60% in WLTC and CLTC, with a diesel consumption of 5.26 and 4.37 litres in half an hour. For control performance comparison, SAC is proved to have a better fuel efficiency than DDPG according to the fuel map and fuel consumption results. The SAC fuel benchmarking percentage of the DP results are 95.1% and 94% in CLTC and WLTC, which are respectively 2.6% and 3.1% higher than DDPG. The charging results also show that the SAC achieves 9.9% and 10.6% faster charging speed than DDPG while having a comparable performance of the C-rate protection. The overall performance of SAC indicates itself as a preferable option for real-world applications.

Chapter 6 A case study of an ERLV with a scotch yoke boxer engine

6.1 Introduction

During the revolution of Fuel-to-electric transformation, the internal combustion engine (ICE) plays a backbone role during the midterm stage. The onboard ICE provides a stable power output that can be transformed to electricity for the ESS traction motor. To further squeeze the potential of the EREV powertrain, vehicle manufacturers and scholars have made efforts to improve and redesign specialised ICE models for HEV. Studies starting from the 21st century have proposed technologies and concepts such as the low-temperature combustion (LTC) engine, alternative fuel, modularized and lightweight engine, new expansion cycle, etc. The LTC technique can increase fuel efficiency and reduce NOx and PM emissions, but it will result in raising the amount of CO and HC. For alternative fuel applications, hydrogen, biodiesel, ethanol, and compressed natural gas are the popular substitutes for fossil fuels [25]. Alternative fuels have environment-friendly emissions that will not put public health at risk. However, it faces storage and transportation difficulties that makes itself unavailable to mass customers; it also has comparatively low energy efficiency, and the specialized engine and conversion components have poor durability. Meanwhile, the development of the modularized and lightweight engine has gained wide attention in recent years. Engines with the Atkinson cycle and Miller cycle have better fuel efficiency by adjusting the compression-expansion ratio from the Otto cycle [49]. Toyota has widely adopted this technique on Prius and Lexus CT200h by delaying the closing of the intake valve, while Volkswagen

and some other western manufacturers design their engines to close the valve earlier than the Otto cycle.

Moreover, unconventional engines with other mechanisms have been reconsidered for EREV use. Mazda announced a redesigned Wankel rotary engine especially inside an APU. The model Demio EV can extend its drive range to over 400 km in 2013 [245]. Mazda also claimed they are undergoing a project of using alternative fuels such as hydrogen and gas for the rotary engine.

In this chapter, a newly developed downsize engine prototype using a Scotch yoke mechanism is being tested for vehicle feasibility analysis. The Scotch Yoke mechanism allows the engine piston to travel in a linear motion with minimal side force. This advantage gives the piston a smoother vibration performance during the combustion cycle. From the piston motion comparison shown in Figure 6.1, the Scotch Yoke engine prototype from SYTECH does not have the unbalanced force applied on the connecting rod from the crankshaft rotary motion, which significantly mitigates the piston aging rate and engine vibration [246]. In addition, the prototype achieves lightweight by sparing the traditional crankshaft and removing the flywheel.

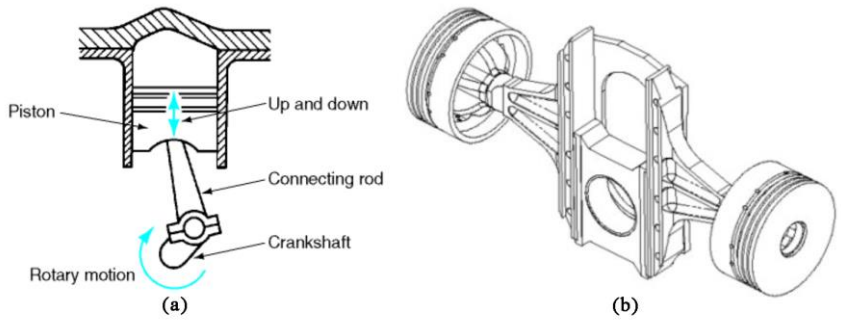

Figure 6.1 Piston motion comparison of (a) conventional; (b) Scotch Yoke.

6.2 Vehicle platform and modelling

In this chapter, the powertrain calibration and engine selection process of the ERLV is conducted. Two Scotch Yoke engine prototypes S208 and S415, as shown in Figure 6.2, are considered for future APU use. The two engines share a similar mechanism, but S208 is 800cc with two cylinders and S415 has doubled the size with four cylinders. They share a similar optimal fuel rate among 228-230 g/kWh with Ron92 fuel, and their specifications are shared in Table 6.1. The fuel rate can be further improved by applying the techniques such as turbocharging, exhaust gas recirculation, variable valve timing and direct injection.

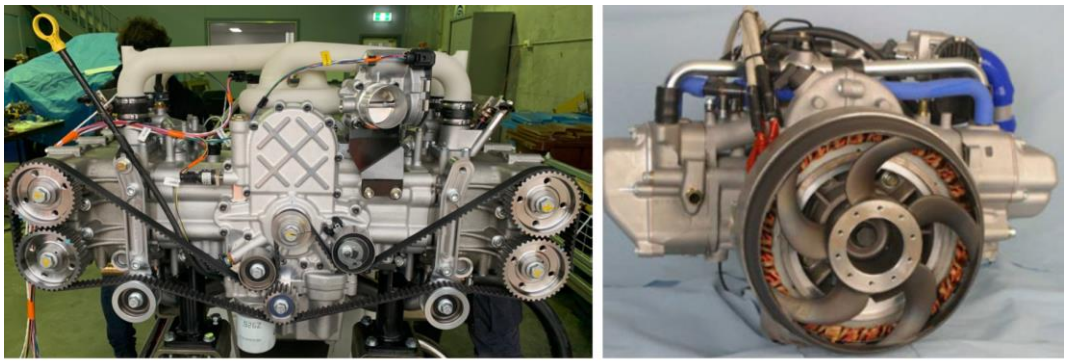

(a) (b)

Figure 6.2 Scotch Yoke engine prototypes of (a) S415; and (b) S208.

Table 6.1 Specifications of the engine prototypes.

Engine Specs.	S208	S415
Rated Power	30 kW @4500 rpm	60 kW @4500 rpm
Dry weight	39 kg	75 kg
Volume power	37.5 kW/Litre	41.2 kW/Litre
Min BSFC	230 g/kWh @3020 rpm	229 g/kWh @2950 rpm
Emission level	China 6b	China 6b

The simulation is for the sizing and applicability of the two engines for logistics transportation. The analysis of the proposed prototypes targets their engine fuel consumption performance and battery sustaining/recharging efficiency. The two

main procedures are deciding the engine operating points and deploying their charging strategies. These procedures are introduced in the following subsections.

6.2.1 Engine operating point selection

In the ERLV structure, the engine operation can be further optimized as it is decoupled from the wheel. The optimal range charging strategy is selected for the APU to maintain a low fuel consumption based on its fuel consumption characteristic map [24], and the engine can be kept on and operate in its sweet areas. The merit of doing this is that a light and down-size engine can be installed for full-time operation. This is a distinct advantage for logistics vehicles to squeeze out more space and weight.

First of all, the possible operating points of the two engines should be listed as selections. As the Scotch Yoke engines have a wide sweet range of fuel efficiency, two core operating points can be decided: the optimal fuel point that has the best fuel efficiency, and the optimal power point that has the highest and stabilized volume power (kW/L) ratio. From the studies from the previous chapters, the average range of the ERLV power demand is in the range of 30 kW to 50 kW according to the standardized driving cycles.

As shown in the partial BSFC map in Figure 6.3, the 30 kW rated power of the S208 engine satisfied the entry-level power demand of the ERLV, and its optimal power point is at around 4500 rpm with a 255g/kWh fuel rate. Thanks to the simplified Scotch yoke mechanism, S208 can maintain this high-power output for long term usage. On the other hand, S415 has doubled the engine capacity, which brings higher manufacturing costs, greater weight and internal space occupation. Its optimal fuel point lies in the RPM of 2950 with a 229g/kWh fuel rate, providing

around 45 kW power output. The two operating points aim at different optimization aspects; they are being further tested in the following subsection with the APU charging strategy applied.

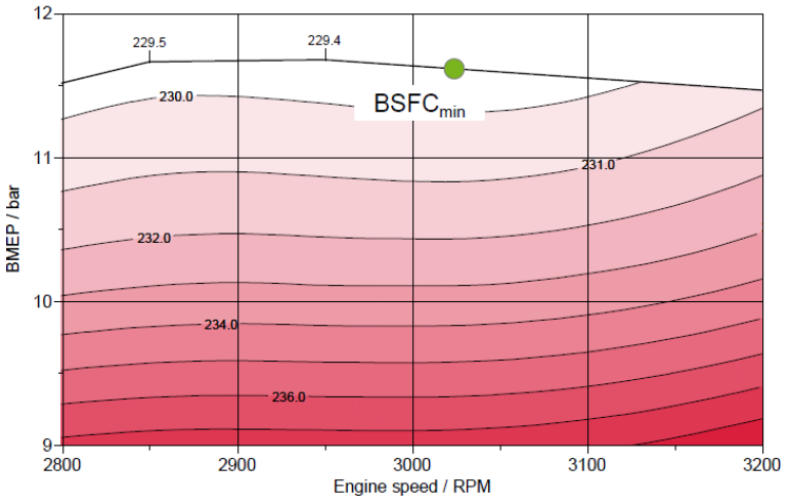

Figure 6.3 The partial BSFC map of the engine.

6.2.2 APU charging strategy design

In order to extend the lifespan of the slider block and bearing, the two Scotch Yoke engines are controlled to operate under the optimal range strategy to avoid any aggressive changes in operating conditions. Under the optimal range strategy framework, two detailed charging strategies are being tested using each engine prototype. The first charging strategy is called the CD-CS strategy. This strategy monitors the real-time SOC level and makes mode-switch decisions based on it. If the battery SOC is higher than 60%, the vehicle is set in CD mode with the APU turned off. Once the SOC drops below 40%, the vehicle will shift to CS mode for the APU to charge the battery and feed the traction motor. As the SOC slowly rises, the strategy will shift back to CD after the battery capacity reaches 60%. A simplified diagram of the strategy is illustrated in Figure 6.4.

The other deployed strategy is the sustaining strategy. Some famous EREVs adopt a similar strategy to achieve to simplify the control complexity, for example, the BMW i3 RE. This strategy normally utilizes the APU to charge the battery at a comparatively low SOC level. Unlike the CD-CS mode, the sustaining strategy only tries to maintain the minimum battery SOC level (or just slightly raise the SOC level to store some temporary energy). It is typically used to compensate for the limited pure-electric drive range, and sometimes the equipped engine has a weak power output that can not fully support the traction motor power requirement. On the contrary, a lower budget for the APU can decrease the vehicle weight and occupied space.

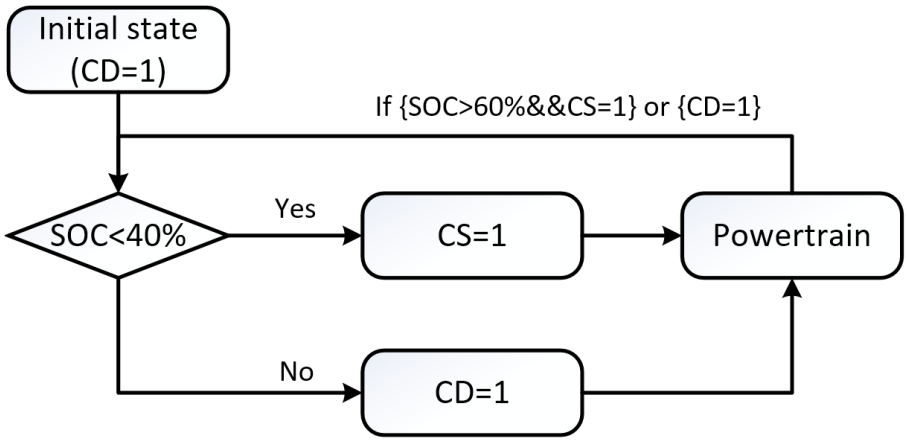

Figure 6.4 Operating logic of the CD-CS strategy.

The simulations deployment and results for the two engines using the two specific strategies are shared and discussed in the next section.

6.3 Performance and energy potential comparison

The power consumption of the ERLV consists of the driving consumption and the electrical appliance consumption. It can be calculated using the vehicle dynamics model and the equivalent electrical model. Figure 6.5 shares the transient power variation of the ERLV in WLTC and CLTC driving cycles.

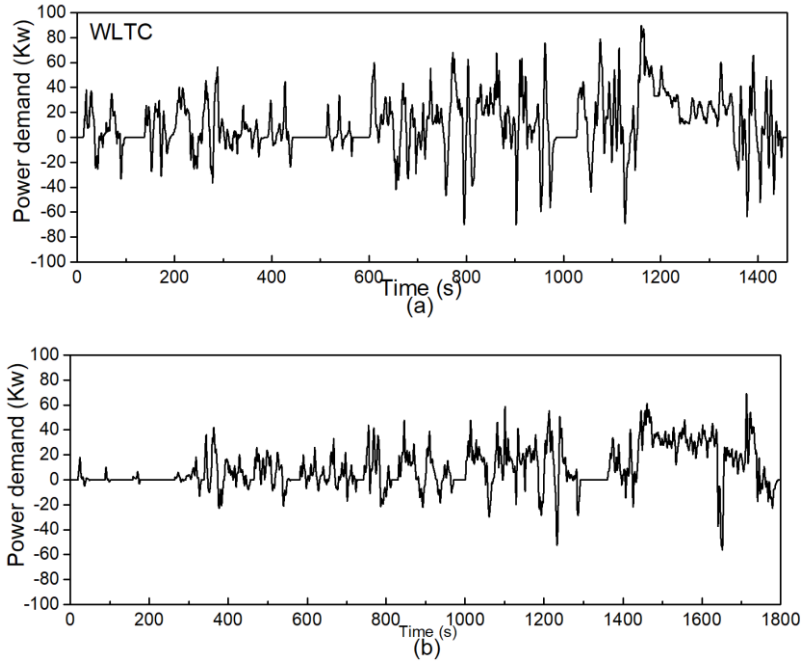

Figure 6.5 Transient power variation of the vehicle (a) WLTC; (b) CLTC

From the energy consumption simulation of the ERLV, four comparative groups are tested for each Scotch Yoke engine prototype. The simulation considers the power flow of the APU and battery output, the internal resistance of the battery and its SOC estimation, the motor efficiency and the proposed APU charging strategies. The WLTC-3b and CLTC-C for light commercial vehicles are imported as the looped inputs for the simulations for a total driving distance of 200 km. The CS-CD strategy sets its SOC range from 30% to 50%, in which the APU is operative to raise the battery SOC. On the other hand, the Sustaining strategy maintains the battery SOC in a small range when the SOC drops down to 40% from the pure-electric drive mode. It turns the APU on until approximately 1 kWh of the electric energy is charged to the battery. The below figures shared the SOC trajectories from the engine on-board simulation with the two strategies, and the orange shades stand for the operation of the APU.

Figure 6.6 demonstrates the patterns of the CS-CD and sustaining strategies operating using the 800cc S208 engine. According to the trajectory, the S208 engine satisfies the power demand for all strategies when it is operating with its rated power (30 kW, 4500rpm, 248 g/kWh). It can also be observed that the power demand from the CLTC is more mitigated compared with WLTC, causing a longer time for the engine to raise the battery SOC level. According to Table 6.2, the power demand from the CLTC is more mitigated than WLTC, as the battery provides a longer pure-electric drive range with APU remains off. In the meantime, the engine ignition frequency and operating duration in WLTC are longer than in CLTC, resulting in higher average fuel consumption of 10.2L per 100 km.

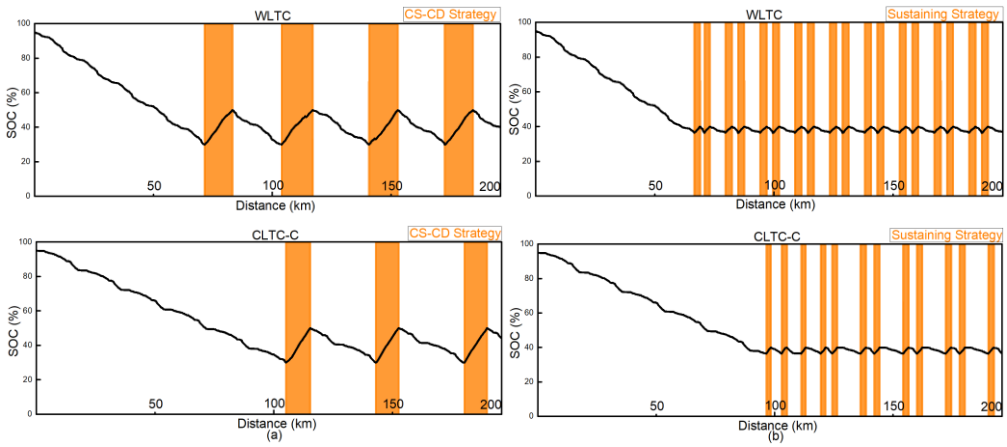

Figure 6.6 SOC variation pattern (S208 engine) using the (a) CD-CS strategy; (b) sustaining strategy.

Conversely, the S415 prototype has almost double the size of the S208, but it provides a higher output power with better fuel efficiency. Its optimal operating point outputs 45 kW with a fuel rate of 229 g/kWh, which is 50% higher than that of S208. This extra 15 kW gives the vehicle a faster-charging ability and better fuel economy. When comparing Figure 6.6 (b) and Figure 6.7 (b), however, it seems that faster charging will cause a higher starting frequency when using the sustaining strategy. Although studies have proved that frequent starting of the engine will not

do extra damage to modern engines [247], it may cause noise and vibration and bring an unpleasant driving experience to the driver. Therefore, the CS-CD strategy is more suitable for the S415 model than the Sustaining strategy when taking NVH into consideration.

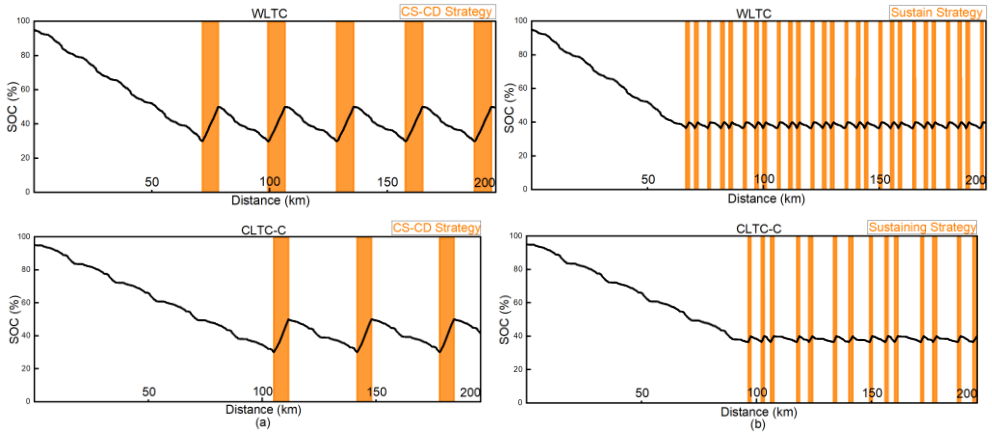

Figure 6.7 SOC variation pattern (S415 engine) using the (a) CD-CS strategy; (b) sustaining strategy.

Table 6.2 S208 energy consumption of the CS-CD&Sustaining strategy under different driving cycles.

Driving Cycle	Strategy	SOC Range	Engine on (%)	Consumption (L&kWh)	RE mode Cons. L/100 km
WLTP-3b (200 km)	CS-CD	30% to 50%	24.0%	14.0+19.8	10.2
	Sustaining	40%	25.5%	14.9+17.0	10.3
CLTC-C (200 km)	CS-CD	30% to 50%	13.6%	8.4+19.9	7.9
	Sustaining	40%	15%	15.1+16.9	7.9

Table 6.3 S415 energy consumption of the CS-CD&Sustaining strategy.

Driving Cycle	Strategy	SOC Range	Engine on (%)	Consumption (L&kWh)	RE mode Cons. L/100 km
WLTP-3b (200 km)	CS-CD	30% to 50%	17.4%	14.0+17.2	9.6
	Sustaining	40%	17.3%	13.9+17.3	9.6
CLTC-C (200 km)	CS-CD	30% to 50%	9.7%	8.3+18.4	7.4
	Sustaining	40%	10.2%	8.7+17.0	7.7

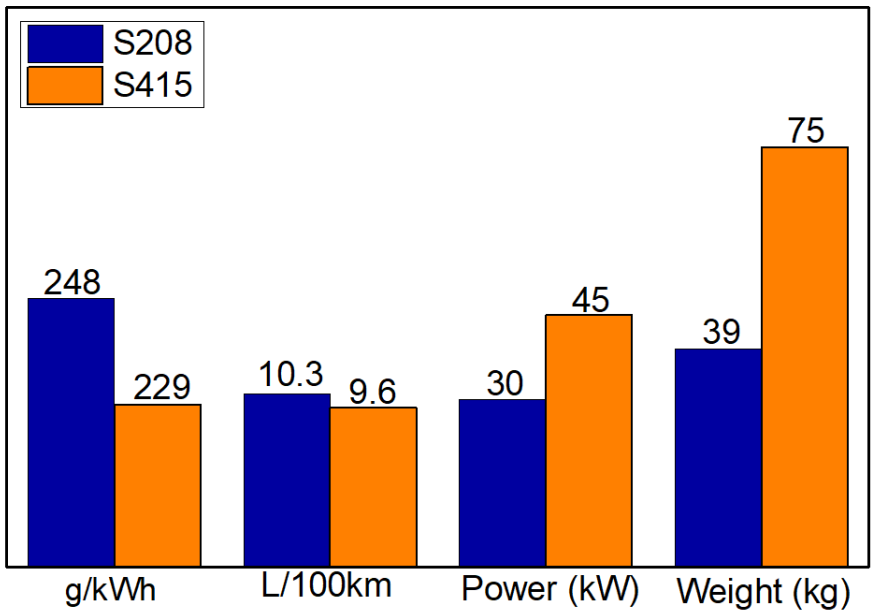

Figure 6.8 Specification comparison of the engine prototypes.

Figure 6.8 shows the comparison of the two engines regarding their efficiency, fuel rate, weight, etc. The first thing to notice is the significantly reduced engine operating time ratio. A higher power output allows S415 to remain shut down for at least 82.6% of the time, and a better fuel conversion rate brings an extra 6.8% on the fuel-saving during extend-range mode compared with S208. By comparing Table 6.2 and 6.3, the fuel consumption results suggest the Sustaining strategy is the better match for S415 to reduce starting frequency. On the contrary, the S208 has a satisfying fuel efficiency when running with its rated power; the 39 kg weight and small size make it an excellent selection for those commercial vehicles installed with a large battery pack. In general, both engine models satisfy the design criterion of the target ERLV, and vehicle manufacturers can make their own decision on the selection based on their needs. Compared to the traditional logistics van that needs to install a 2-litre engine to fulfill the power requirement, the ERLV with the downsize boxer engine can save approximately 40%-60% of the space and 35%-50% of the component weight.

6.4 Chapter summary

This chapter represents a comparative consumption analysis for an ERLV with a Scotch Yoke engine. This down-size Scotch Yoke boxer engine is selected as the ranger extender inside the vehicle APU. An analysis is conducted to excavate fuel consumption and feasibility based on the two different engine prototypes. According to the results, the two engine prototypes show some unique features in the performance, energy potential and operating pattern. The results are summarized below.

1. A higher power output allows S415 to remain shut down for at least 82.6% of the time, and a better fuel conversion rate brings an extra 6.8% on the fuel-saving during extend-range mode compared with S208.
2. Both engine models satisfy the design criterion of the target ERLV, and vehicle manufacturers can make their own decision on the selection based on their needs.

Chapter 7 Conclusions and future works

7.1 Thesis conclusions

This thesis has proposed a complete energy management study for the extended range electric vehicle, which reveals the application potential of this platform from the angles of performance and economic efficiency. The modern control algorithms are deployed and tested successfully as the EMS to achieve favourable energy efficiency.

The main work and contributions of this thesis can be summarized as follows:

1. A detailed background introduction on the EREV and its structure design is shared. The functions of key components such as the APU, battery, supercapacitor and traction motor are discussed.

It is worthwhile to systemically summarize the states estimation techniques in the hope of providing some inspiration for EMS practitioners.

2. A classification of the EREV energy management study is conducted in terms of two main aspects: APU charging control strategy and HESS power management. A wide-range literature review on the two areas is presented to establish familiarity with and understanding of current research while looking for existing gaps or drawbacks. A case analysis is also conducted based on an EREV model to share its market performance, and the economic potential of the EREV platform (including material cost and TCO) is compared against other types of vehicles.

3. Before designing and testing any EMS for the EREV, detailed models of the vehicle body and powertrain should be constructed to improve its applicability. The Battery model can be used to estimate battery SOC, capacity, cell temperature and

SOH; the APU model consists of transient Fuel-to-Watt conversion rate from the BSFC map.

4. The energy consumption and total cost of ownership analysis are conducted on a specific logistics van model. The analysis focuses on searching for the optimal energy economy of the APU and battery for short driving cycles and long term usage. A global optimization strategy using the DP algorithm is developed to search for optimal APU operation points while the battery charging rate is limited within ±6C. Minimum fuel consumption is guaranteed to show the fuel potential of this vehicle platform. In addition, a battery degradation simulation is performed to study the long term usage over the whole vehicle lifespan. The final TCO results can guide the prosumers on selecting the cost&eco-friendly logistics vehicle for future industry.

5. Further research is established on the basics of the last chapter using the same mathematical model of the ERLV. Different from the previous DP algorithm, this approach introduced the RL algorithms to achieve real-time control ability with continuous action space outputs. The state-of-the-art algorithm, SAC, is adopted with a multi-target learning framework to achieve the balance of fuel consumption, maintaining battery SOC level and battery SOH. The maximum entropy method helps the model seek better APU operation points with faster speed and wider exploration. The control performance of the algorithm beats DDPG with a 3% average boost in fuel consumption.

6. An ERLV equipped with the novel scoke yoke engine mechanism is studied, considering the energy potential and applicability. Two engine prototypes with different engine capacities are being compared with two unique APU charging

strategies. Results show that the 1.6 L engine prototype remained shut down at 82.6% of the time for over 200 km; an extra 6.8% of the fuel was saved thanks to holding the engine at its optimal fuel point. In general, both of the Scotch Yoke engines achieve high fuel efficiency with a lightweight design compared with the traditional engine, demonstrating great potential to spare more internal space and TCO spending for practical application.

7.2 Future research

In light of the favourable fuel efficiency and TCO comparison, the ERLV structure can be considered one of the possible options for the logistics market. [71] Future research topics based on what this thesis has explored are suggested as follows:

1. Engine emission simulation can be added to the system, and it can be used as one of the multi-targets to optimize the emission level. Multi-condition optimization for engine emission control is also worth studying, to distinguish the APU performance based on the operating area (rural, urban or special areas).

2. HIL and rapid prototyping tests of the EREV platform can be conducted to test the average fuel consumption and engine stability. The reliability of the RL-based strategies is expected to be verified in road tests with real-world conditions.

3. The control strategies can be redesigned for the Fuel-cell EREV platform, as the characteristics of the fuel-cell system vary considerably from those of combustion engines.

4. Combine the RL strategies with the developing autonomous driving technology through internal Ethernet to the onboard signal processing switch and controllers.

5. Deploy more advanced control strategies on the regenerative braking system and multi-speed transmission to improve the overall energy efficiency, and employ the proposed strategies to power-split or any improved hybrid vehicle type.

6. The future APU control strategy can be extended utilizing the V2X technologies. For instance, the estimated travel distance, number of the nearby petrol/charging stations, traffic conditions and driver behaviour perception can be integrated as inputs of the EMS. The above actions will bring operational flexibility to the future strategy.

7. The range extended system can be further installed on heavy vehicles, long-duty transport vehicles, agricultural vehicles and even motor-drive boats/ferries to improve their energy efficiency and exhaust emission.

Bibliography

[1] W. M. Budzianowski, "Negative carbon intensity of renewable energy technologies involving biomass or carbon dioxide as inputs," *Renewable and Sustainable Energy Reviews,* vol. 16, no. 9, pp. 6507-6521, 2012.

[2] P. K.-H. Dost, P. Spichartz, and C. Sourkounis, "Charging Behavior of Users Utilizing Battery Electric Vehicles and Extended Range Electric Vehicles Within the Scope of a Field Test," *IEEE Transactions on Industry Applications,* vol. 54, no. 1, pp. 580-590, 2018.

[3] A. Solouk, M. Shakiba-Herfeh, J. Arora, and M. Shahbakhti, "Fuel consumption assessment of an electrified powertrain with a multi-mode high-efficiency engine in various levels of hybridization," *Energy Conversion and Management,* vol. 155, pp. 100-115, 2018.

[4] I. E. Agency. (2020, 01 Jan). *Change in energy demand and renewables output*. Available: https://www.iea.org/data-and-statistics/charts/change-in-energy-demand-and-renewables-output-in-electricity-heat-and-transport-2019-to-2020

[5] R. Álvarez Fernández, S. Corbera Caraballo, F. Beltrán Cilleruelo, and J. A. Lozano, "Fuel optimization strategy for hydrogen fuel cell range extender vehicles applying genetic algorithms," *Renewable and Sustainable Energy Reviews,* vol. 81, pp. 655-668, 2018.

[6] J. Du, J. Chen, Z. Song, M. Gao, and M. Ouyang, "Design method of a power management strategy for variable battery capacities range-extended electric vehicles to improve energy efficiency and cost-effectiveness," *Energy,* vol. 121, pp. 32-42, 2017.

[7] X.-l. Wu *et al.*, "Extended-range electric vehicle-oriented thermoelectric surge control of a solid oxide fuel cell system," *Applied Energy,* vol. 263, 2020.

[8] X. Wu, X. Hu, X. Yin, Y. Peng, and V. Pickert, "Convex programming improved online power management in a range extended fuel cell electric truck," *Journal of Power Sources,* vol. 476, 2020.

[9] P. T. M. Ronald M. Dell, David A.J. Rand, P. T. M. Ronald M. Dell, David A.J. Rand,, Ed. *Towards Sustainable Road Transport*. Elsevier, 2014.

[10] W. S. Bou Nader, C. J. Mansour, and M. G. Nemer, "Optimization of a Brayton external combustion gas-turbine system for extended range electric vehicles," *Energy,* vol. 150, pp. 745-758, 2018.

[11] Z. Chen, C. C. Mi, R. Xiong, J. Xu, and C. You, "Energy management of a power-split plug-in hybrid electric vehicle based on genetic algorithm and quadratic programming," *Journal of Power Sources,* vol. 248, pp. 416-426, 2014.

[12] X. Hu, C. M. Martinez, and Y. Yang, "Charging, power management, and battery degradation mitigation in plug-in hybrid electric vehicles: A unified cost-optimal approach," *Mechanical Systems and Signal Processing,* vol. 87, pp. 4-16, 2017.

[13] Y. Yang, X. Hu, H. Pei, and Z. Peng, "Comparison of power-split and parallel hybrid powertrain architectures with a single electric machine:

Dynamic programming approach," *Applied Energy,* vol. 168, pp. 683-690, 2016.
[14] S. Xie, X. Hu, S. Qi, and K. Lang, "An artificial neural network-enhanced energy management strategy for plug-in hybrid electric vehicles," *Energy,* vol. 163, pp. 837-848, 2018.
[15] P. Chambon *et al.*, "Development of a range-extended electric vehicle powertrain for an integrated energy systems research printed utility vehicle," *Applied Energy,* vol. 191, pp. 99-110, 2017.
[16] R. Xiong, J. Cao, and Q. Yu, "Reinforcement learning-based real-time power management for hybrid energy storage system in the plug-in hybrid electric vehicle," *Applied Energy,* vol. 211, pp. 538-548, 2018.
[17] S. F. Tie and C. W. Tan, "A review of energy sources and energy management system in electric vehicles," *Renewable and Sustainable Energy Reviews,* vol. 20, pp. 82-102, 2013.
[18] J. Peng, H. He, and R. Xiong, "Study on Energy Management Strategies for Series-parallel Plug-in Hybrid Electric Buses," *Energy Procedia,* vol. 75, pp. 1926-1931, 2015.
[19] S. J. Moura, J. L. Stein, and H. K. Fathy, "Battery-Health Conscious Power Management in Plug-In Hybrid Electric Vehicles via Electrochemical Modeling and Stochastic Control," *IEEE Transactions on Control Systems Technology,* vol. 21, no. 3, pp. 679-694, 2013.
[20] S. Di Cairano, W. Liang, I. V. Kolmanovsky, M. L. Kuang, and A. M. Phillips, "Power Smoothing Energy Management and Its Application to a Series Hybrid Powertrain," *IEEE Transactions on Control Systems Technology,* vol. 21, no. 6, pp. 2091-2103, 2013.
[21] M. Ye, X. Song, R. Xiong, and F. Sun, "A Novel Dynamic Performance Analysis and Evaluation Model of Series-Parallel Connected Battery Pack for Electric Vehicles," *IEEE Access,* vol. 7, pp. 14256-14265, 2019.
[22] S. Zhou, P. Walker, and N. Zhang, "Parametric design and regenerative braking control of a parallel hydraulic hybrid vehicle," *Mechanism and Machine Theory,* vol. 146, 2020.
[23] Z. Yuan, L. Teng, S. Fengchun, and H. Peng, "Comparative Study of Dynamic Programming and Pontryagin's Minimum Principle on Energy Management for a Parallel Hybrid Electric Vehicle," *Energies,* vol. 6, no. 4, pp. 2305-2318, 2013.
[24] B. Xiao, J. Ruan, W. Yang, P. D. Walker, and N. Zhang, "A review of pivotal energy management strategies for extended range electric vehicles," *Renewable and Sustainable Energy Reviews,* 2021.
[25] A. Solouk *et al.*, "Fuel Economy Benefits of Integrating a Multi-Mode Low Temperature Combustion (LTC) Engine in a Series Extended Range Electric Powertrain," presented at the SAE Technical Paper Series, 2016.
[26] L. Xu, J. Li, J. Hua, X. Li, and M. Ouyang, "Optimal vehicle control strategy of a fuel cell/battery hybrid city bus," *International Journal of Hydrogen Energy,* vol. 34, no. 17, pp. 7323-7333, 2009.
[27] D. Cesiel and C. Zhu, "A Closer Look at the On-Board Charger: The development of the second-generation module for the Chevrolet Volt," *IEEE Electrification Magazine,* vol. 5, no. 1, pp. 36-42, 2017.

[28] J. Jeong, W. Lee, N. Kim, K. Stutenberg, and A. Rousseau, "Control Analysis and Model Validation for BMW i3 Range Extender," presented at the SAE Technical Paper Series, 2017.
[29] Ford. (2019, 04 May). *NEW FORD TRANSIT AND TOURNEO CUSTOM*. Available: https://media.ford.com/content/fordmedia/feu/en/news/2019/09/23/New-Ford-Transit-and-Tourneo-Custom-Plug-In-Hybrids-Deliver-Zero-Emission-Driving.html
[30] M. Redelbach, E. D. Özdemir, and H. E. Friedrich, "Optimizing battery sizes of plug-in hybrid and extended range electric vehicles for different user types," *Energy Policy,* vol. 73, pp. 158-168, 2014.
[31] M. F. M. Sabri, K. A. Danapalasingam, and M. F. Rahmat, "A review on hybrid electric vehicles architecture and energy management strategies," *Renewable and Sustainable Energy Reviews,* vol. 53, pp. 1433-1442, 2016.
[32] J. Li, X. Jin, and R. Xiong, "Multi-objective optimization study of energy management strategy and economic analysis for a range-extended electric bus," *Applied Energy,* vol. 194, pp. 798-807, 2017.
[33] M. Yao, B. Zhu, and N. Zhang, "Adaptive real-time optimal control for energy management strategy of extended range electric vehicle," *Energy Conversion and Management,* 2021.
[34] J. Li, Y. Wang, J. Chen, and X. Zhang, "Study on energy management strategy and dynamic modeling for auxiliary power units in range-extended electric vehicles," *Applied Energy,* vol. 194, pp. 363-375, 2017.
[35] M. Rodrigues, S. King, D. Scott, and D. Wang, "Advanced Energy Management Strategies for Range Extended Electric Vehicle," 2015. Available: https://doi.org/10.4271/2015-26-0121
[36] H. Zhang, L. Fu, J. Song, and Q. J. E. P. Yang, "Power Energy Management and Control Strategy Study for Extended-range Auxiliary Power Unit," vol. 104, pp. 32-37, 2016.
[37] Y. L. Guo, X. D. Wang, and J. Long, "The Study on 45KW Range Extended Electric Vehicle Auxiliary Power Unit," in *Applied Mechanics and Materials*, 2014, vol. 556, pp. 2128-2132: Trans Tech Publ.
[38] B.-C. Chen, Y.-Y. Wu, and H.-C. Tsai, "Design and analysis of power management strategy for range extended electric vehicle using dynamic programming
" *Applied Energy,* vol. 113, pp. 1764-1774, 2014/01/01/ 2014.
[39] L. Zhang, X. Hu, Z. Wang, F. Sun, and D. G. Dorrell, "A review of supercapacitor modeling, estimation, and applications: A control/management perspective," *Renewable and Sustainable Energy Reviews,* vol. 81, pp. 1868-1878, 2018.
[40] S. Zhang, R. Xiong, and F. Sun, "Model predictive control for power management in a plug-in hybrid electric vehicle with a hybrid energy storage system," *Applied Energy,* vol. 185, pp.
1654-1662, 2017.
[41] S. Nazari, J. B. Siegel, and A. Stefanopoulou, "Optimal Energy Management for a Mild Hybrid Vehicle with Electric and Hybrid Engine

Boosting Systems," *IEEE Transactions on Vehicular Technology,* pp. 1-1, 2019.
[42] H. H. Eldeeb, A. T. Elsayed, C. R. Lashway, and O. Mohammed, "Hybrid Energy Storage Sizing and Power Splitting Optimization for Plug-In Electric Vehicles," *IEEE Transactions on Industry Applications,* vol. 55, no. 3, pp. 2252-2262, 2019.
[43] J. Bauman and M. Kazerani, "An Analytical Optimization Method for Improved Fuel Cell–Battery–Ultracapacitor Powertrain," *IEEE Transactions on Vehicular Technology,* vol. 58, no. 7, pp. 3186-3197, 2009.
[44] P. Bentley, D. A. Stone, and N. Schofield, "The parallel combination of a VRLA cell and supercapacitor for use as a hybrid vehicle peak power buffer," *Journal of Power Sources,* vol. 147, no. 1-2, pp. 288-294, 2005.
[45] J. Moreno, M. E. Ortuzar, and J. W. Dixon, "Energy-management system for a hybrid electric vehicle, using ultracapacitors and neural networks," *IEEE Transactions on Industrial Electronics,* vol. 53, no. 2, pp. 614-623, 2006.
[46] C. H. Hubert Friedl, Gerald Teuschl, "Range Extender Technology for Electric Vehicles," presented at the 2018 5th International Conference on Electric Vehicular Technology (ICEVT), 2018.
[47] J. Andert, K. Herold, R. Savelsberg, and M. Pischinger, "NVH Optimization of Range Extender Engines by Electric Torque Profile Shaping," *IEEE Transactions on Control Systems Technology,* vol. 25, no. 4, pp. 1465-1472, 2017.
[48] M. Borghi, E. Mattarelli, J. Muscoloni, C. A. Rinaldini, T. Savioli, and B. Zardin, "Design and experimental development of a compact and efficient range extender engine," *Applied Energy,* vol. 202, pp. 507-526, 2017.
[49] R. D. Reitz and G. Duraisamy, "Review of high efficiency and clean reactivity controlled compression ignition (RCCI) combustion in internal combustion engines," *Progress in Energy and Combustion Science,* vol. 46, pp. 12-71, 2015.
[50] L. Y. Richard Tamba. (2019, 01. 12). *FIRST FIRING OF 415B TC ENGINE*. Available: https://www.sytechpowertrain.com/newsinfo/569412.html
[51] R. Guo, M.-j. Wang, and C. Cao, "Gas torque compensation control for range extender start-stop vibration reduction in electric vehicle," *Proceedings of the Institution of Mechanical Engineers, Part I: Journal of Systems and Control Engineering,* vol. 231, no. 7, pp. 567-581, 2017.
[52] Y. Qin *et al.*, "Noise and vibration suppression in hybrid electric vehicles: State of the art and challenges," *Renewable and Sustainable Energy Reviews,* vol. 124, 2020.
[53] Mazda. (2018, 09.01). *Mazda rotary engine to return as EV range-extender*. Available: https://www.mazda-press.com/eu/news/2018/mazda-rotary-engine-to-return-as-ev-range-extender-/
[54] M. A. Cusenza, S. Bobba, F. Ardente, M. Cellura, and F. Di Persio, "Energy and environmental assessment of a traction lithium-ion battery pack for plug-in hybrid electric vehicles," *J Clean Prod,* vol. 215, pp. 634-649, Apr 1 2019.

[55] F. V. Conte, "Battery and battery management for hybrid electric vehicles: a review," *e & i Elektrotechnik und Informationstechnik,* vol. 123, no. 10, pp. 424-431, 2006.
[56] L. Lu, X. Han, J. Li, J. Hua, and M. Ouyang, "A review on the key issues for lithium-ion battery management in electric vehicles," *Journal of Power Sources,* vol. 226, pp. 272-288, 2013.
[57] W. Zuo, R. Li, C. Zhou, Y. Li, J. Xia, and J. Liu, "Battery-Supercapacitor Hybrid Devices: Recent Progress and Future Prospects," *Adv Sci (Weinh),* vol. 4, no. 7, p. 1600539, Jul 2017.
[58] Y. S. W. K.T Chau, C.C Chan, "An overview of energy sources for electric vehicles," *Energy Conversion & Management* pp. 1021-1039, 1999.
[59] L. Sun and N. Zhang, "Design, implementation and characterization of a novel bi-directional energy conversion system on DC motor drive using super-capacitors," *Applied Energy,* vol. 153, pp. 101-111, 2015.
[60] L. Kouchachvili, W. Yaïci, and E. Entchev, "Hybrid battery/supercapacitor energy storage system for the electric vehicles," *Journal of Power Sources,* vol. 374, pp. 237-248, 2018.
[61] B. Xiao, H. Lu, H. Wang, J. Ruan, and N. Zhang, "Enhanced Regenerative Braking Strategies for Electric Vehicles: Dynamic Performance and Potential Analysis," *Energies,* vol. 10, no. 11, 2017.
[62] Maxwell. (2021, 01, March). *Ultracapacitor Overview*. Available: https://maxwell.com/products/ultracapacitors/
[63] Z. Song *et al.*, "Multi-objective optimization of a semi-active battery/supercapacitor energy storage system for electric vehicles," *Applied Energy,* vol. 135, pp. 212-224, 2014.
[64] T. Li, L. Huang, and H. Liu, "Energy management and economic analysis for a fuel cell supercapacitor excavator," *Energy,* vol. 172, pp. 840-851, 2019.
[65] F. Zhang, X. Hu, R. Langari, and D. Cao, "Energy management strategies of connected HEVs and PHEVs: Recent progress and outlook," *Progress in Energy and Combustion Science,* vol. 73, pp. 235-256, 2019.
[66] S. Eckroad and B. Radimer, "REVIEW OF ENGINEERING DESIGN CONSIDERATIONS FOR BATTERY ENERGY MANAGEMENT-SYSTEMS," (in English), *Ieee Transactions on Energy Conversion,* Article vol. 6, no. 2, pp. 303-309, Jun 1991.
[67] H. He, R. Xiong, K. Zhao, and Z. Liu, "Energy management strategy research on a hybrid power system by hardware-in-loop experiments," *Applied Energy,* vol. 112, pp. 1311-1317, 2013.
[68] M. A. Hannan, M. S. H. Lipu, A. Hussain, and A. Mohamed, "A review of lithium-ion battery state of charge estimation and management system in electric vehicle applications: Challenges and recommendations," *Renewable and Sustainable Energy Reviews,* vol. 78, pp. 834-854, 2017.
[69] Y. Xing, E. W. M. Ma, K. L. Tsui, and M. Pecht, "Battery Management Systems in Electric and Hybrid Vehicles," *Energies,* vol. 4, no. 11, pp. 1840-1857, 2011.

[70] J.-S. WON, R. LANGARI, and M. J. I. t. o. c. s. t. EHSANI, "An energy management and charge sustaining strategy for a parallel hybrid vehicle with CVT," vol. 13, no. 2, pp. 313-320, 2005.
[71] S. Zhang and R. Xiong, "Adaptive energy management of a plug-in hybrid electric vehicle based on driving pattern recognition and dynamic programming," *Applied Energy,* vol. 155, pp. 68-78, 2015.
[72] Y. Yan, Q. Li, W. Chen, B. Su, J. Liu, and L. Ma, "Optimal Energy Management and Control in Multimode Equivalent Energy Consumption of Fuel Cell/Supercapacitor of Hybrid Electric Tram," *IEEE Transactions on Industrial Electronics,* vol. 66, no. 8, pp. 6065-6076, 2019.
[73] X. Han, H. He, J. Wu, J. Peng, and Y. Li, "Energy management based on reinforcement learning with double deep Q-learning for a hybrid electric tracked vehicle," *Applied Energy,* vol. 254, 2019.
[74] M. G. Simoes, B. Blunier, and A. Miraoui, "Fuzzy-Based Energy Management Control: Design of a Battery Auxiliary Power Unit for Remote Applications," *IEEE Industry Applications Magazine,* vol. 20, no. 4, pp. 41-49, 2014.
[75] Q. LI, W. CHEN, Y. LI, S. LIU, and J. HUANG, "Energy management strategy for fuel cell/battery/ultracapacitor hybrid vehicle based on fuzzy logic," *International Journal of Electrical Power & Energy Systems,* vol. 43, no. 1, pp. 514-525, 2012.
[76] M. N. Nic Lutsey, "Update on electric vehicle costs in the United States through 2030," *INTERNATIONAL COUNCIL ON CLEAN TRANSPORTATION,* vol. 06, 2019.
[77] S. Di Cairano, D. Bernardini, A. Bemporad, and I. V. Kolmanovsky, "Stochastic MPC With Learning for Driver-Predictive Vehicle Control and its Application to HEV Energy Management," *IEEE Transactions on Control Systems Technology,* vol. 22, no. 3, pp. 1018-1031, 2014.
[78] J. Zhao, Y. Ma, Z. Zhang, S. Wang, and S. Wang, "Optimization and matching for range-extenders of electric vehicles with artificial neural network and genetic algorithm," *Energy Conversion and Management,* vol. 184, pp. 709-725, 2019.
[79] H. A. Borhan, A. Vahidi, A. M. Phillips, M. L. Kuang, and I. V. Kolmanovsky, "Predictive energy management of a power-split hybrid electric vehicle," in *2009 American control conference*, 2009, pp. 3970-3976: IEEE.
[80] H. BORHAN, A. VAHIDI, A. M. PHILLIPS, M. L. KUANG, I. V. KOLMANOVSKY, and S. D. CAIRANO, "MPC-Based Energy Management of a Power-Split Hybrid Electric Vehicle," *IEEE Transactions on Control Systems Technology,* vol. 20, no. 3, pp. 593-603, 2012.
[81] X. Hu, C. Zou, X. Tang, T. Liu, and L. Hu, "Cost-Optimal Energy Management of Hybrid Electric Vehicles Using Fuel Cell/Battery Health-Aware Predictive Control," *IEEE Transactions on Power Electronics,* vol. 35, no. 1, pp. 382-392, 2020.
[82] W. Gao, "Performance Comparison of a Fuel Cell-Battery Hybrid Powertrain and a Fuel Cell-Ultracapacitor Hybrid Powertrain," *IEEE Transactions on Vehicular Technology,* vol. 54, no. 3, pp. 846-855, 2005.

[83] L. Xi, X. Zhang, C. Sun, Z. Wang, X. Hou, and J. Zhang, "Intelligent Energy Management Control for Extended Range Electric Vehicles Based on Dynamic Programming and Neural Network," *Energies,* vol. 10, no. 11, 2017.
[84] E. Chemali, P. J. Kollmeyer, M. Preindl, and A. Emadi, "State-of-charge estimation of Li-ion batteries using deep neural networks: A machine learning approach," *Journal of Power Sources,* vol. 400, pp. 242-255, 2018.
[85] T. Haarnoja, A. Zhou, P. Abbeel, and S. Levine, "Soft actor-critic: Off-policy maximum entropy deep reinforcement learning with a stochastic actor," in *International conference on machine learning*, 2018, pp. 1861-1870: PMLR.
[86] F. R. Salmasi, "Control Strategies for Hybrid Electric Vehicles: Evolution, Classification, Comparison, and Future Trends," *IEEE Transactions on Vehicular Technology,* vol. 56, no. 5, pp. 2393-2404, 2007.
[87] H. He, R. Xiong, H. Guo, and S. Li, "Comparison study on the battery models used for the energy management of batteries in electric vehicles," *Energy Conversion and Management,* vol. 64, pp. 113-121, 2012.
[88] Y. Huang *et al.*, "A review of power management strategies and component sizing methods for hybrid vehicles," *Renewable and Sustainable Energy Reviews,* vol. 96, pp. 132-144, 2018.
[89] X. Zhang, Z. Wu, X. Hu, W. Qian, and Z. Li, "Trajectory Optimization-Based Auxiliary Power Unit Control Strategy for an Extended Range Electric Vehicle," *IEEE Transactions on Vehicular Technology* vol. 66, no. 12, pp. 10866-10874, 2017.
[90] T. Ray and P. Saini, "Engineering design optimization using a swarm with an intelligent information sharing among individuals," *Engineering Optimization,* vol. 33, no. 6, pp. 735-748, 2001.
[91] Y. Huang, H. Wang, A. Khajepour, H. He, and J. Ji, "Model predictive control power management strategies for HEVs: A review," *Journal of Power Sources,* vol. 341, pp. 91-106, 2017.
[92] H. Wu, P. Walker, J. Wu, J. Liang, J. Ruan, and N. Zhang, "Energy management and shifting stability control for a novel dual input clutchless transmission system," *Mechanism and Machine Theory,* vol. 135, pp. 298-321, 2019.
[93] H. Yang, Y. Zhang, P. D. Walker, J. Liang, N. Zhang, and B. Xia, "Speed sensorless model predictive current control with ability to start a free running induction motor," *IET Electric Power Applications,* vol. 11, no. 5, pp. 893-901, 2017.
[94] W. Yang, J. Liang, J. Yang, and N. Zhang, "Investigation of a Novel Coaxial Power-Split Hybrid Powertrain for Mining Trucks," *Energies,* vol. 11, no. 1, 2018.
[95] X. Li *et al.*, "Online management of lithium-ion battery based on time-triggered controller area network for fuel-cell hybrid vehicle applications," *Journal of Power Sources,* vol. 195, no. 10, pp. 3338-3343, 2010.
[96] N. Murgovski, L. M. Johannesson, and J. Sjoberg, "Engine On/Off Control for Dimensioning Hybrid Electric Powertrains via Convex Optimization,"

IEEE Transactions on Vehicular Technology, vol. 62, no. 7, pp. 2949-2962, 2013.
[97] B.-H. Nguyen, R. German, J. P. F. Trovao, and A. Bouscayrol, "Real-Time Energy Management of Battery/Supercapacitor Electric Vehicles Based on an Adaptation of Pontryagin's Minimum Principle," *IEEE Transactions on Vehicular Technology,* vol. 68, no. 1, pp. 203-212, 2019.
[98] S. Xie, X. Hu, Z. Xin, and J. Brighton, "Pontryagin's Minimum Principle based model predictive control of energy management for a plug-in hybrid electric bus," *Applied Energy,* vol. 236, pp. 893-905, 2019.
[99] R. Xiong, Y. Duan, J. Cao, and Q. Yu, "Battery and ultracapacitor in-the-loop approach to validate a real-time power management method for an all-climate electric vehicle," *Applied Energy,* vol. 217, pp. 153-165, 2018.
[100] M. Mohebbi, M. Charkhgard, and M. Farrokhi, "Optimal neuro-fuzzy control of parallel hybrid electric vehicles," in *2005 IEEE Vehicle Power and Propulsion Conference*, 2005, pp. 26-30: IEEE.
[101] J. Wu, H. He, J. Peng, Y. Li, and Z. Li, "Continuous reinforcement learning of energy management with deep Q network for a power split hybrid electric bus," *Applied Energy,* vol. 222, pp. 799-811, 2018.
[102] X. Qi, Y. Luo, G. Wu, K. Boriboonsomsin, and M. Barth, "Deep reinforcement learning enabled self-learning control for energy efficient driving," *Transportation Research Part C: Emerging Technologies,* vol. 99, pp. 67-81, 2019.
[103] X. Hu, T. Liu, X. Qi, and M. Barth, "Reinforcement Learning for Hybrid and Plug-In Hybrid Electric Vehicle Energy Management: Recent Advances and Prospects," *IEEE Industrial Electronics Magazine,* vol. 13, no. 3, pp. 16-25, 2019.
[104] X. Tang, J. Chen, T. Liu, Y. Qin, and D. Cao, "Distributed Deep Reinforcement Learning-Based Energy and Emission Management Strategy for Hybrid Electric Vehicles," *IEEE Transactions on Vehicular Technology,* pp. 1-1, 2021.
[105] C. Berner *et al.*, "Dota 2 with large scale deep reinforcement learning," 2019.
[106] N. O'Connell, A. Röll, R. Lechner, T. Luo, and M. Brautsch, "PODE-blend as pilot fuel in a biomethane dual fuel engine: Experimental analysis of performance, combustion and emissions characteristics," *Renewable Energy,* vol. 143, pp. 101-111, 2019.
[107] A. K. Agarwal, A. P. Singh, and R. K. Maurya, "Evolution, challenges and path forward for low temperature combustion engines," *Progress in Energy and Combustion Science,* vol. 61, pp. 1-56, 2017.
[108] Z. Salameh, "Energy Storage," in *Renewable Energy System Design*, 2014, pp. 201-298.
[109] A. N. Laboratory, "Toyota Mirai Testing," 2018, Available: https://www.hydrogen.energy.gov/pdfs/progress18/tahi_lohse-busch_2018.pdf.
[110] J. Jeong, S. Choi, N. Kim, H. Lee, K. Stutenberg, and A. Rousseau, "Model Validation of the Chevrolet Volt 2016," presented at the SAE Technical Paper Series, 2018.

[111] C. A. Ramos-Paja, C. Bordons, A. Romero, R. Giral, and L. Martinez-Salamero, "Minimum Fuel Consumption Strategy for PEM Fuel Cells," *IEEE Transactions on Industrial Electronics,* vol. 56, no. 3, pp. 685-696, 2009.
[112] X. Han, F. Li, T. Zhang, T. Zhang, and K. Song, "Economic energy management strategy design and simulation for a dual-stack fuel cell electric vehicle," *International Journal of Hydrogen Energy,* vol. 42, no. 16, pp. 11584-11595, 2017.
[113] S. Ahmadi, S. M. T. Bathaee, and A. H. Hosseinpour, "Improving fuel economy and performance of a fuel-cell hybrid electric vehicle (fuel-cell, battery, and ultra-capacitor) using optimized energy management strategy," *Energy Conversion and Management,* vol. 160, pp. 74-84, 2018.
[114] N. Bizon, "Real-time optimization strategy for fuel cell hybrid power sources with load-following control of the fuel or air flow," *Energy Conversion and Management,* vol. 157, pp. 13-27, 2018.
[115] L. Barelli, G. Bidini, and A. Ottaviano, "Optimization of a PEMFC/battery pack power system for a bus application," *Applied Energy,* vol. 97, pp. 777-784, 2012.
[116] X. Zhang, Z. Wu, X. Hu, W. Qian, and Z. J. I. T. o. V. T. Li, "Trajectory Optimization-Based Auxiliary Power Unit Control Strategy for an Extended Range Electric Vehicle," vol. 66, no. 12, pp. 10866-10874, 2017.
[117] X. Ba, Y. Guo, J. Zhu, and C. Zhang, "An Equivalent Circuit Model for Predicting the Core Loss in a Claw-Pole Permanent Magnet Motor With Soft Magnetic Composite Core," *IEEE Transactions on Magnetics,* vol. 54, no. 11, pp. 1-6, 2018.
[118] M. Zandi, A. Payman, J.-P. Martin, S. Pierfederici, B. Davat, and F. Meibody-Tabar, "Energy Management of a Fuel Cell/Supercapacitor/Battery Power Source for Electric Vehicular Applications," *IEEE Transactions on Vehicular Technology,* vol. 60, no. 2, pp. 433-443, 2011.
[119] X. Zhao and S. Niu, "Design and Optimization of a Novel Slot-PM-Assisted Variable Flux Reluctance Generator for Hybrid Electric Vehicles," *IEEE Transactions on Energy Conversion,* vol. 33, no. 4, pp. 2102-2111, 2018.
[120] H. Wang, Y. Huang, A. Khajepour, A. Soltani, and D. Cao, "Cyber-Physical Predictive Energy Management for Through-The-Road Hybrid Vehicles," *IEEE Transactions on Vehicular Technology,* pp. 1-1, 2019.
[121] B.-C. Chen, Y.-Y. Wu, and H.-C. Tsai, "Design and analysis of power management strategy for range extended electric vehicle using dynamic programming," *Applied Energy,* vol. 113, pp. 1764-1774, 2014.
[122] S. R. Matthias Rogge, Dirk Uwe Sauer, "Operating Strategies for a Range Extender used in Battery Electric Vehicles," *2013 IEEE Vehicle Power and Propulsion Conference (VPPC),* 2013.
[123] G. Fiengo, L. Glielmo, and F. Vasca, "Control of Auxiliary Power Unit for Hybrid Electric Vehicles," *IEEE Transactions on Control Systems Technology,* vol. 15, no. 6, pp. 1122-1130, 2007.
[124] J. Hu, G. Zu, Y. I. Han, and S. Nie, "PARAMETERS DESIGN AND CONTROL STRATEGY OPTIMISATION FOR RANGE-EXTENDED

ELECTRIC VEHICLE," *Journal of the Balkan Tribological Association,* Article vol. 22, no. 3A-II, pp. 3496-3512, 2016.
[125] Y. H. Hung, C. H. Wu, C. Y. Lin, and Y. M. Tung, "System Dynamics Analysis and Mode-Switch Control for a 3-Mode Range-Extender Electric Vehicle," (in English), *Applied Mechanics and Materials,* vol. 459, p. 361, Oct 2013
2014-02-06 2013.
[126] M. U. Karaoğlan, N. S. Kuralay, and C. O. Colpan, "Investigation of the effects of battery types and power management algorithms on drive cycle simulation for a range-extended electric vehicle powertrain," *International Journal of Green Energy,* vol. 16, no. 1, pp. 1-11, 2018.
[127] G.-S. Lee, D.-H. Kim, J.-H. Han, M.-H. Hwang, and H.-R. Cha, "Optimal Operating Point Determination Method Design for Range-Extended Electric Vehicles Based on Real Driving Tests," *Energies,* vol. 12, no. 5, 2019.
[128] H. Liu, C. Wang, X. Zhao, and C. Guo, "An Adaptive-Equivalent Consumption Minimum Strategy for an Extended-Range Electric Bus Based on Target Driving Cycle Generation," *Energies,* vol. 11, no. 7, 2018.
[129] R. Verma and P. A. Lakshminiarayanan, "A case study on the application of a genetic algorithm for optimization of engine parameters," *Proceedings of the Institution of Mechanical Engineers, Part D: Journal of Automobile Engineering,* vol. 220, no. 4, pp. 471-479, 2006.
[130] L. Sun, P. Walker, K. Feng, and N. Zhang, "Multi-objective component sizing for a battery-supercapacitor power supply considering the use of a power converter," *Energy,* vol. 142, pp. 436-446, 2018.
[131] N. Nitta, F. Wu, J. T. Lee, and G. Yushin, "Li-ion battery materials: present and future," *Materials Today,* vol. 18, no. 5, pp. 252-264, 2015.
[132] M. J. Kellaway, P. Jennings, D. Stone, E. Crowe, and A. Cooper, "Early results from a systems approach to improving the performance and lifetime of lead acid batteries," *Journal of Power Sources,* vol. 116, no. 1-2, pp. 110-117, 2003.
[133] Q. Cai, D. J. L. Brett, D. Browning, and N. P. Brandon, "A sizing-design methodology for hybrid fuel cell power systems and its application to an unmanned underwater vehicle," *Journal of Power Sources,* vol. 195, no. 19, pp. 6559-6569, 2010.
[134] R. E. Araujo, R. de Castro, C. Pinto, P. Melo, and D. Freitas, "Combined Sizing and Energy Management in EVs With Batteries and Supercapacitors," *IEEE Transactions on Vehicular Technology,* vol. 63, no. 7, pp. 3062-3076, 2014.
[135] C. Xiang, Y. Wang, S. Hu, and W. Wang, "A New Topology and Control Strategy for a Hybrid Battery-Ultracapacitor Energy Storage System," *Energies,* vol. 7, no. 5, pp. 2874-2896, 2014.
[136] I. Aharon and A. Kuperman, "Topological Overview of Powertrains for Battery-Powered Vehicles With Range Extenders," *IEEE Transactions on Power Electronics,* vol. 26, no. 3, pp. 868-876, 2011.

[137] C. Raga, A. Barrado, H. Miniguano, A. Lazaro, I. Quesada, and A. Martin-Lozano, "Analysis and Sizing of Power Distribution Architectures Applied to Fuel Cell Based Vehicles," *Energies,* vol. 11, no. 10, 2018.
[138] J. A. P. J. Lopes, P. A. V. Ferreira, "Optimal Sizing of Batteries and Ultracapacitors for Fuel Cell Electric Vehicles," *IECON 2011 - 37th Annual Conference of the IEEE Industrial Electronics Society, Melbourne, VIC,* pp. 4603-4608, 2011.
[139] Z. Hu *et al.*, "Multi-objective energy management optimization and parameter sizing for proton exchange membrane hybrid fuel cell vehicles," *Energy Conversion and Management,* vol. 129, pp. 108-121, 2016.
[140] A. F. Burke, "Batteries and Ultracapacitors for Electric, Hybrid, and Fuel Cell Vehicles," *Proceedings of the IEEE,* vol. 95, no. 4, pp. 806-820, 2007.
[141] L. Wang, E. G. Collins, and H. Li, "Optimal Design and Real-Time Control for Energy Management in Electric Vehicles," *IEEE Transactions on Vehicular Technology,* vol. 60, no. 4, pp. 1419-1429, 2011.
[142] N. R. R. Sadoun, P. Bartholomeüs, B. Barbedette and P. Le Moigne, ""Influence of the drive cycles on the sizing of hybrid storage system battery-supercapacitor supplying an electric vehicle,"" *IECON 2011 - 37th Annual Conference of the IEEE Industrial Electronics Society,* pp. 4106-4112, 2011.
[143] A. Ostadi and M. Kazerani, "Optimal Sizing of the Battery Unit in a Plug-in Electric Vehicle," *IEEE Transactions on Vehicular Technology,* vol. 63, no. 7, pp. 3077-3084, 2014.
[144] Z. Song, H. Hofmann, J. Li, X. Han, and M. Ouyang, "Optimization for a hybrid energy storage system in electric vehicles using dynamic programing approach," *Applied Energy,* vol. 139, pp. 151-162, 2015.
[145] N. R. R. Sadoun, P. Bartholomeüs, B. Barbedette and P. Le Moigne, "Influence of the drive cycles on the sizing of hybrid storage system battery-supercapacitor supplying an electric vehicle," *IECON 2011 - 37th Annual Conference of the IEEE Industrial Electronics Society, Melbourne, VIC,* pp. 4106-4112, 2011.
[146] S. W. a. X. G. Tongzhen Wei, "Performance analysis and comparision of ultracapacitor based regenerative braking system," *2009 4th IEEE Conference on Industrial Electronics and Applications,* pp. 3405-3410, 2009.
[147] K. F. Li Sun, Chris Chapman, Nong Zhang, "An Adaptive Power-Split Strategy for Battery–Supercapacitor Powertrain—Design, Simulation, and Experiment," *IEEE TRANSACTIONS ON POWER ELECTRONICS,* vol. 32, no. 12, pp. 9364-9375, 2017.
[148] L. Gao, R. A. Dougal, and S. Liu, "Power Enhancement of an Actively Controlled Battery/Ultracapacitor Hybrid," *IEEE Transactions on Power Electronics,* vol. 20, no. 1, pp. 236-243, 2005.
[149] M. Ortuzar, J. Moreno, and J. Dixon, "Ultracapacitor-Based Auxiliary Energy System for an Electric Vehicle: Implementation and Evaluation," *IEEE Transactions on Industrial Electronics,* vol. 54, no. 4, pp. 2147-2156, 2007.

[150] H. Jung, H. Wang, and T. Hu, "Control design for robust tracking and smooth transition in power systems with battery/supercapacitor hybrid energy storage devices," *Journal of Power Sources,* vol. 267, pp. 566-575, 2014.
[151] M.-E. Choi, S.-W. Kim, and S.-W. Seo, "Energy Management Optimization in a Battery/Supercapacitor Hybrid Energy Storage System," *IEEE Transactions on Smart Grid,* vol. 3, no. 1, pp. 463-472, 2012.
[152] W. Yang, J. Ruan, J. Yang, and N. Zhang, "Investigation of integrated uninterrupted dual input transmission and hybrid energy storage system for electric vehicles," *Applied Energy,* vol. 262, 2020.
[153] J. Wang *et al.*, "Cycle-life model for graphite-LiFePO4 cells," *Journal of Power Sources,* vol. 196, no. 8, pp. 3942-3948, 2011.
[154] S. M. Lukic, S. G. Wirasingha, F. Rodriguez, J. Cao, A. Emadi, and Ieee, *Power management of an ultracapacitor/battery hybrid energy storage system in an HEV* (2006 Ieee Vehicle Power and Propulsion Conference). New York: Ieee, 2006, pp. 179-184.
[155] S. M. Lukic, C. Jian, R. C. Bansal, F. Rodriguez, and A. Emadi, "Energy Storage Systems for Automotive Applications," *IEEE Transactions on Industrial Electronics,* vol. 55, no. 6, pp. 2258-2267, 2008.
[156] D. W. Corson, "High power battery systems for hybrid vehicles," *Journal of Power Sources,* vol. 105, pp. 110-113, 2002.
[157] J. Bauman and M. Kazerani, "A Comparative Study of Fuel-Cell–Battery, Fuel-Cell–Ultracapacitor, and Fuel-Cell–Battery–Ultracapacitor Vehicles," *IEEE Transactions on Vehicular Technology,* vol. 57, no. 2, pp. 760-769, 2008.
[158] L. Zhang *et al.*, "Hybrid electrochemical energy storage systems: An overview for smart grid and electrified vehicle applications," *Renewable and Sustainable Energy Reviews,* vol. 139, 2021.
[159] Z. Song *et al.*, "Simultaneous Identification and Control for Hybrid Energy Storage System Using Model Predictive Control and Active Signal Injection," *IEEE Transactions on Industrial Electronics,* vol. 67, no. 11, pp. 9768-9778, 2020.
[160] B. Wang, J. Xu, B. Cao, and X. Zhou, "A novel multimode hybrid energy storage system and its energy management strategy for electric vehicles," *Journal of Power Sources,* vol. 281, pp. 432-443, 2015.
[161] M.-E. Choi, J.-S. Lee, and S.-W. Seo, "Real-Time Optimization for Power Management Systems of a Battery/Supercapacitor Hybrid Energy Storage System in Electric Vehicles," *IEEE Transactions on Vehicular Technology,* vol. 63, no. 8, pp. 3600-3611, 2014.
[162] J. R. Miller, "Electrochemical capacitor thermal management issues at high-rate cycling," *Electrochimica Acta,* vol. 52, no. 4, pp. 1703-1708, 2006.
[163] Y. Dandeville, P. Guillemet, Y. Scudeller, O. Crosnier, L. Athouel, and T. Brousse, "Measuring time-dependent heat profiles of aqueous electrochemical capacitors under cycling," *Thermochimica Acta,* vol. 526, no. 1-2, pp. 1-8, 2011.

[164] A. Manthiram, Y. Fu, S.-H. Chung, C. Zu, and Y.-S. Su, "Rechargeable Lithium–Sulfur Batteries," *Chemical Reviews,* vol. 114, no. 23, pp. 11751-11787, 2014/12/10 2014.
[165] A. Eftekhari, "The rise of lithium–selenium batteries," *Sustainable Energy & Fuels,* 10.1039/C6SE00094K vol. 1, no. 1, pp. 14-29, 2017.
[166] R. Lian, H. Tan, J. Peng, Q. Li, and Y. Wu, "Cross-Type Transfer for Deep Reinforcement Learning Based Hybrid Electric Vehicle Energy Management," *IEEE Transactions on Vehicular Technology,* vol. 69, no. 8, pp. 8367-8380, 2020.
[167] B. Xu *et al.*, "Ensemble Reinforcement Learning-Based Supervisory Control of Hybrid Electric Vehicle for Fuel Economy Improvement," *IEEE Transactions on Transportation Electrification,* vol. 6, no. 2, pp. 717-727, 2020.
[168] Wikipedia, "Chevy Volt Concept NAIAS 2007," C. V. C. N. 2007, Ed., ed. https://en.wikipedia.org/wiki/File:Chevy_Volt_Concept_NAIAS_2007_02.jpg, 2007.
[169] U. S. D. o. Energy, "2013 Chevrolet Volt Fuel Economy," https://www.fueleconomy.gov/feg/Find.do?action=sbs&id=32655&id=33900&id=352462014, Accessed on: 03-10-2021.
[170] J. Smart, W. Powell, and S. Schey, "Extended Range Electric Vehicle Driving and Charging Behavior Observed Early in the EV Project," presented at the SAE Technical Paper Series, 2013.
[171] S. M. N. H. M. Anwar, M. Teimor, M. Korich and M. B. Hayes, "Development of a power dense and environmentally robust traction power inverter for the second-generatio chevrolet VOLT extended-range EV," *2015 IEEE Energy Conversion Congress and Exposition (ECCE),* pp. 6006-6013, 2015.
[172] T. Liu, X. Hu, W. Hu, and Y. Zou, "A Heuristic Planning Reinforcement Learning-Based Energy Management for Power-Split Plug-in Hybrid Electric Vehicles," *IEEE Transactions on Industrial Informatics,* vol. 15, no. 12, pp. 6436-6445, 2019.
[173] G. Jeffrey, W. Eric, and R. Sai, "Connectivity-Enhanced Route Selection and Adaptive Control for the Chevrolet Volt," *Journal of Traffic and Transportation Engineering,* vol. 4, no. 1, 2016.
[174] J. Smart, "Advanced Vehicle Testing Activity – Cold Weather On-road Testing of a 2012 Chevrolet Volt," Idaho National Laboratory, http://avt.inl.gov2014.
[175] A. J. C. A. LOISELLE-LAPOINTE, H. RIBBERINK, "CHEVROLET VOLT ON-ROAD TEST PROGRAMS IN CANADA PART 1: EFFECTS OF DRIVE CYCLE, AMBIENT TEMPERATURE AND ACCESSORY USAGE ON ENERGY CONSUMPTION AND ALL-ELECTRIC RANGE," *International Journal of Automotive Technology,* vol. 18, no. 1, pp. 103-115, 2017.
[176] A. S. Abdelrahman, K. S. Algarny, and M. Z. Youssef, "A Novel Platform for Powertrain Modeling of Electric Cars With Experimental Validation Using Real-Time Hardware in the Loop (HIL): A Case Study of GM Second

Generation Chevrolet Volt," *IEEE Transactions on Power Electronics,* vol. 33, no. 11, pp. 9762-9771, 2018.
[177] X. Li, Z. Wang, and L. Zhang, "Co-estimation of capacity and state-of-charge for lithium-ion batteries in electric vehicles," *Energy,* vol. 174, pp. 33-44, 2019.
[178] A. Khaligh and L. Zhihao, "Battery, Ultracapacitor, Fuel Cell, and Hybrid Energy Storage Systems for Electric, Hybrid Electric, Fuel Cell, and Plug-In Hybrid Electric Vehicles: State of the Art," *IEEE Transactions on Vehicular Technology,* vol. 59, no. 6, pp. 2806-2814, 2010.
[179] Bloomberg. (2019, July 11). *Electric Vehicle Outlook 2019*. Available: https://about.bnef.com/electric-vehicle-outlook/#toc-viewreport
[180] Maxwell. (2018, July 22). *K2 ULTRACAPACITORS - 2.7V SERIES product specifications - Maxwell Technologies*. Available: www.maxwell.com/images/documents/k2series_ds_10153704.pdf
[181] (2017). *Hydrogen and Fuel Cells Overview*. Available: https://www.energy.gov/sites/prod/files/2017/06/f34/fcto-h2-fc-overview-dla-worldwide-energy-conf-2017-satyapal.pdf
[182] Y. Haseli, "Maximum conversion efficiency of hydrogen fuel cells," *International Journal of Hydrogen Energy,* vol. 43, no. 18, pp. 9015-9021, 2018.
[183] S. Kim and P. H. Chou, "Size and Topology Optimization for Supercapacitor-Based Sub-Watt Energy Harvesters," *IEEE Transactions on Power Electronics,* vol. 28, no. 4, pp. 2068-2080, 2013.
[184] V. R. a. A. R. Y. Kim, "Design and Management of Battery-Supercapacitor Hybrid Electrical Energy Storage Systems for Regulation Services," *IEEE Transactions on Multi-Scale Computing Systems,* vol. 3, pp. 12-24, 2017.
[185] (2019, Jun 26, 2019). *Fuel Cell Power Module for Heavy Duty Motive Applications*. Available: http://ballard.com/docs/default-source/motive-modules-documents/fcvelocity_md_low_res.pdf
[186] U. S. d. o. energy. (2018, 09.11). *EPA Fuel Economy of 2018 Audi A4*. Available: https://www.fueleconomy.gov/feg/Find.do?action=sbs&id=39327
[187] U. S. d. o. energy. (2019, September 20). *National Average Price* Available: https://afdc.energy.gov/fuels/prices.html
[188] U. S. E. I. Administration. (2021, September 5). *Gasoline and Diesel Fuel Update*. Available: https://www.eia.gov/petroleum/gasdiesel/
[189] S. R. Department. (2017, 22.07). *Average car operating costs in the United States in 2017*
y. Available: https://www.statista.com/statistics/624068/average-car-operating-costs-in-the-united-states/
[190] U. S. d. o. energy. (2018, 08.11). *EPA Fuel Economy of 2018 Tesla Model 3*. Available: https://www.fueleconomy.gov/feg/Find.do?action=sbs&id=41056
[191] U. S. d. o. energy. (2018, 08.11). *EPA Fuel Economy of 2018BMW i3*. Available: https://www.fueleconomy.gov/feg/Find.do?action=sbs&id=39834

[192] BMW. (2019, 03.11). *BMW i3 Maintenance Cost and Schedule Guide*. Available: https://www.bmwux.com/bmw-maintenance-warranty-guide/bmw-i3-maintenance/
[193] TOYOTA. (2019, 07.11). *MIRAI- Pricing and Financing*. Available: https://ssl.toyota.com/mirai/faq.html
[194] TOYOTA. (2019, 09.11). *2017 Mirai Product Information*. Available: https://ssl.toyota.com/mirai/assets/core/Docs/Mirai%20Specs.pdf
[195] U. S. E. I. Administration. (2019, September 5). *Gasoline and Diesel Fuel Update*. Available: https://www.eia.gov/petroleum/gasdiesel/
[196] A. Babin, N. Rizoug, T. Mesbahi, D. Boscher, Z. Hamdoun, and C. Larouci, "Total Cost of Ownership Improvement of Commercial Electric Vehicles Using Battery Sizing and Intelligent Charge Method," *IEEE Transactions on Industry Applications,* vol. 54, no. 2, pp. 1691-1700, 2018.
[197] N. C. f. S. a. Analysis, "VEHICLE SURVIVABILITY AND TRAVEL MILEAGE SCHEDULES," U.S. Department of Transportation, United State.2006.
[198] N. News, "What's the life expectancy of my car," 2006, Available: https://www.nbcnews.com/id/wbna12040753#.W5FuNOhKiM8, Accessed on: 01-Mar-2021.
[199] (2015). *Joint Agency Staff Report on Assembly Bill 8: Assessment of Time and Cost Needed to Attain 100 Hydrogen Refueling Stations in California*. Available: https://ww2.energy.ca.gov/2015publications/CEC-600-2015-016/CEC-600-2015-016.pdf
[200] J. Ruan, "Design and Verification of Novel Powertrain Management for Multi-Geared Battery Electric Vehicles," PhD, Faculty of Engineering and Information Technology, University of Technology Sydney, 2016.
[201] C. Zhang, W. Allafi, Q. Dinh, P. Ascencio, and J. Marco, "Online estimation of battery equivalent circuit model parameters and state of charge using decoupled least squares technique," *Energy,* vol. 142, pp. 678-688, 2018.
[202] S. Nosratabadi, A. Mosavi, S. Shamshirband, E. Kazimieras Zavadskas, A. Rakotonirainy, and K. W. Chau, "Sustainable Business Models: A Review," *Sustainability,* vol. 11, no. 6, 2019.
[203] Kastone. (2017, 09 May). *2017 Global Smart Logistics Summit*. Available: http://www.kastone.com.cn/en/case/large/1111.html
[204] ChinaGoAbroad. (2017, 05 May). *A look into the world's largest logistics market - China*. Available: http://www.chinagoabroad.com/en/article/28072
[205] J. Keirstead, M. Jennings, and A. Sivakumar, "A review of urban energy system models: Approaches, challenges and opportunities," *Renewable and Sustainable Energy Reviews,* vol. 16, no. 6, pp. 3847-3866, 2012.
[206] W. J. Guan, X. Y. Zheng, K. F. Chung, and N. S. Zhong, "Impact of air pollution on the burden of chronic respiratory diseases in China: time for urgent action," (in English), *Lancet,* Review vol. 388, no. 10054, pp. 1939-1951, Oct 2016.
[207] M. Montazeri-Gh and M. Mahmoodi-K, "Optimized predictive energy management of plug-in hybrid electric vehicle based on traffic condition," *Journal of Cleaner Production,* vol. 139, pp. 935-948, 2016.

[208] M. Montazeri-Gh and M. Mahmoodi-k, "Development a new power management strategy for power split hybrid electric vehicles," *Transportation Research Part D: Transport and Environment,* vol. 37, pp. 79-96, 2015.
[209] LEVC. (2020, 02-April). *MEET THE STREETWISE VN5 ELECTRIC VAN*.
[210] J. Guanetti, S. Formentin, and S. M. Savaresi, "Energy Management System for an Electric Vehicle With a Rental Range Extender: A Least Costly Approach," *IEEE Transactions on Intelligent Transportation Systems,* vol. 17, no. 11, pp. 3022-3034, 2016.
[211] S. Zhang, R. Xiong, and J. Cao, "Battery durability and longevity based power management for plug-in hybrid electric vehicle with hybrid energy storage system," *Applied Energy,* vol. 179, pp. 316-328, 2016.
[212] J. Tian, R. Xiong, and W. Shen, "State-of-Health Estimation Based on Differential Temperature for Lithium Ion Batteries," *IEEE Transactions on Power Electronics,* vol. 35, no. 10, pp. 10363-10373, 2020.
[213] J. Tian, R. Xiong, W. Shen, and F. Sun, "Electrode ageing estimation and open circuit voltage reconstruction for lithium ion batteries," *Energy Storage Materials,* vol. 37, pp. 283-295, 2021.
[214] M. Schimpe, M. E. von Kuepach, M. Naumann, H. C. Hesse, K. Smith, and A. Jossen, "Comprehensive Modeling of Temperature-Dependent Degradation Mechanisms in Lithium Iron Phosphate Batteries," *Journal of The Electrochemical Society,* vol. 165, no. 2, pp. A181-A193, 2018.
[215] Y. Ma, Y. Chen, X. Zhou, and H. Chen, "Remaining Useful Life Prediction of Lithium-Ion Battery Based on Gauss–Hermite Particle Filter," *IEEE Transactions on Control Systems Technology,* vol. 27, no. 4, pp. 1788-1795, 2019.
[216] J. Ruan, P. D. Walker, P. A. Watterson, and N. Zhang, "The dynamic performance and economic benefit of a blended braking system in a multi-speed battery electric vehicle," *Applied Energy,* vol. 183, pp. 1240-1258, 2016.
[217] Mercedes-Benz. (2020). *The eVito panel van: your holistic solution for electromobility*. Available: https://www.mercedes-benz.ie/vans/en/vito/e-vito-panel-van
[218] A. Mahmoudzadeh Andwari, A. Pesiridis, S. Rajoo, R. Martinez-Botas, and V. Esfahanian, "A review of Battery Electric Vehicle technology and readiness levels," *Renewable and Sustainable Energy Reviews,* vol. 78, pp. 414-430, 2017.
[219] J. Hagman, S. Ritzén, J. J. Stier, and Y. Susilo, "Total cost of ownership and its potential implications for battery electric vehicle diffusion," *Research in Transportation Business & Management,* vol. 18, pp. 11-17, 2016.
[220] U. S. E. I. Administration, "SHORT-TERM ENERGY OUTLOOK," U.S. Energy Information Administration, https://www.eia.gov/outlooks/steo/report/electricity.php2020.
[221] Ö. Simsekoglu and A. Nayum, "Predictors of intention to buy a battery electric vehicle among conventional car drivers," *Transportation Research Part F: Traffic Psychology and Behaviour,* vol. 60, pp. 1-10, 2019.

[222] Volkswagen. (2019, 03-09). *The new ABT eTransporter 6.1*. Available: https://www.volkswagen-vans.co.uk/en/electric-vans/abt-etransporter-6-1.html
[223] Ford. (2020, 09-09). *2020 TRANSIT PASSENGER VAN XLT*. Available: https://www.ford.com/trucks/transit-passenger-van-wagon/models/transit-xlt/
[224] AUTOACCESSORIESGARAGE. (2018, 23-05-2020). *Brakes FAQs (i.e. How Long do Brake Pads & Rotors Last?)*. Available: https://www.autoaccessoriesgarage.com/Brakes/FAQ
[225] L. B. Shi, F. Wang, L. Ma, Q. Y. Liu, J. Guo, and W. J. Wang, "Study of the friction and vibration characteristics of the braking disc/pad interface under dry and wet conditions," *Tribology International,* vol. 127, pp. 533-544, 2018.
[226] R. Sharma, C. Manzie, M. Bessede, R. H. Crawford, and M. J. Brear, "Conventional, hybrid and electric vehicles for Australian driving conditions. Part 2: Life cycle CO2-e emissions," *Transportation Research Part C: Emerging Technologies,* vol. 28, pp. 63-73, 2013.
[227] Ford. Oil Change-Vehicle service [Online]. Available: https://www.me.ford.com/en/omn/ownersite/basic-maintenance/oil-change/#:~:text=Ford%20Motor%20Company%20generally%20recommends,oil%20and%20filter%20more%20frequently.
[228] S. Ebbesen, P. Elbert, and L. Guzzella, "Battery State-of-Health Perceptive Energy Management for Hybrid Electric Vehicles," *IEEE Transactions on Vehicular Technology,* vol. 61, no. 7, pp. 2893-2900, 2012.
[229] H. He, S. Quan, F. Sun, and Y.-X. Wang, "Model Predictive Control With Lifetime Constraints Based Energy Management Strategy for Proton Exchange Membrane Fuel Cell Hybrid Power Systems," *IEEE Transactions on Industrial Electronics,* vol. 67, no. 10, pp. 9012-9023, 2020.
[230] T. Liu, B. Wang, and C. Yang, "Online Markov Chain-based energy management for a hybrid tracked vehicle with speedy Q-learning," *Energy,* vol. 160, pp. 544-555, 2018.
[231] T. P. Lillicrap *et al.*, "Continuous control with deep reinforcement learning," 2015.
[232] Y. Wu, H. Tan, J. Peng, H. Zhang, and H. He, "Deep reinforcement learning of energy management with continuous control strategy and traffic information for a series-parallel plug-in hybrid electric bus," *Applied Energy,* vol. 247, pp. 454-466, 2019.
[233] Y. Li, H. He, A. Khajepour, H. Wang, and J. Peng, "Energy management for a power-split hybrid electric bus via deep reinforcement learning with terrain information," *Applied Energy,* vol. 255, 2019.
[234] R. Lian, J. Peng, Y. Wu, H. Tan, and H. Zhang, "Rule-interposing deep reinforcement learning based energy management strategy for power-split hybrid electric vehicle," *Energy,* vol. 197, 2020.
[235] G. Matheron, N. Perrin, and O. J. a. p. a. Sigaud, "The problem with DDPG: understanding failures in deterministic environments with sparse rewards," 2019.
[236] T. Haarnoja *et al.*, "Soft actor-critic algorithms and applications," 2018.

[237] S. Sun, J. Zhang, J. Bi, and Y. Wang, "A Machine Learning Method for Predicting Driving Range of Battery Electric Vehicles," *Journal of Advanced Transportation,* vol. 2019, pp. 1-14, 2019.
[238] J. K. Tim de Bruin, Karl Tuyls, Robert Babuˇska, "The importance of experience replay database composition in deep reinforcement learning," *In Deep reinforcement learning workshop, NIPS,* 2015.
[239] E. Wikner and T. Thiringer, "Extending Battery Lifetime by Avoiding High SOC," *Applied Sciences,* vol. 8, no. 10, 2018.
[240] G. L. David Silver, Nicolas Heess, Thomas Degris, Daan Wierstra, Martin Riedmiller, "Deterministic Policy Gradient Algorithms," *Proceedings of the 31 st International Conference on Machine Learning,* no. JMLR: W&CP volume 32., 2014.
[241] W. Zhang, J. Wang, Y. Liu, G. Gao, S. Liang, and H. Ma, "Reinforcement learning-based intelligent energy management architecture for hybrid construction machinery," *Applied Energy,* vol. 275, 2020.
[242] S. Fujimoto, H. Hoof, and D. Meger, "Addressing function approximation error in actor-critic methods," in *International Conference on Machine Learning*, 2018, pp. 1587-1596: PMLR.
[243] V. Mnih *et al.*, "Human-level control through deep reinforcement learning," vol. 518, no. 7540, pp. 529-533, 2015.
[244] J. R. Vázquez-Canteli and Z. Nagy, "Reinforcement learning for demand response: A review of algorithms and modeling techniques," *Applied Energy,* vol. 235, pp. 1072-1089, 2019.
[245] Mazda. (2020, 01 March). *Entering a New Era and Looking Further into the Future*. Available: https://www.mazda.com/en/innovation/stories/rotary/newera/
[246] V. Arakelian, J.-P. Le Baron, and M. Mkrtchyan, "Design of Scotch yoke mechanisms with improved driving dynamics," vol. 230, no. 4, pp. 379-386, 2016.
[247] J. Bishop, A. Nedungadi, G. Ostrowski, B. Surampudi, P. Armiroli, and E. Taspinar, "An engine start/stop system for improved fuel economy," SAE technical paper0148-7191, 2007.